

APPLICATIONS OF BROADBAND POLARIZATION-INSENSITIVE FIBER OPTICAL PARAMETRIC AMPLIFIERS

MARIA BASTAMOVA

Doctor of Philosophy

ASTON UNIVERSITY

October 2024

©Mariia Bastamova, 2024

Mariia Bastamova asserts her moral right to be identified as the author of this thesis

This copy of the thesis has been supplied on condition that anyone who consults it is understood to recognize that its copyright belongs to its author and that no quotation from the thesis and no information derived from it may be published without appropriate permission or acknowledgement.

Aston University

APPLICATIONS OF BROADBAND POLARIZATION- INSENSITIVE FIBER OPTICAL PARAMETRIC AMPLIFIERS

Bastamova Mariia

Doctor of Philosophy

2024

Summary

This thesis explores a major challenge in the development of fiber optical parametric amplifiers (FOPAs) in optical communication systems: the mitigation of stimulated Brillouin scattering (SBS). The research focuses on pump phase modulation as an effective SBS suppression technique for FOPAs, particularly in the amplification of QAM signals within state-of-the-art polarization-insensitive FOPA architectures. Both single-polarization and polarization-insensitive FOPAs are studied to evaluate the impact of pump phase modulation on signal degradation, as an induced phase noise, which negatively affects signal OSNR and pathways to minimize this impact.

A numerical and experimental study was conducted to evaluate the required optical signal-to-noise ratio (OSNR) and the performance of various phase modulation schemes on the impact of pump phase modulation on QAM signals. The key findings reveal that the pump phase modulation-induced signal phase noise is proportional to the pump bandwidth and the effect of pump phase modulation on signals is more complex in polarization-insensitive FOPAs compared to single-polarization FOPAs. It can be minimized by optimizing pump phase modulation by using a higher number of sine tones with smaller spacing between them, which results in a denser, bandwidth efficient pump spectrum, allowing for effective SBS mitigation while keeping the total pump bandwidth narrow. Nearly complete cancellation of this impact is possible by employing features of polarization diversity schemes.

The key results provide the optimization enabled a new record in long-haul transmission experiments, where polarization-insensitive FOPAs were used as in-line amplifiers. In these experiments, a data transmission at distance of 539 km below BER of 0.02 was achieved for a 200G PDM-16-QAM signal, maintaining a net FOPA gain of 25 dB.

Keywords: stimulated Brillouin scattering, SBS mitigation, pump phase modulation, pump dithering, QAM signal amplification, fiber optical communications.

ACKNOWLEDGEMENTS

I would like to express my deepest gratitude to my supervisor, Professor Andrew Ellis, for providing me with the opportunity to work at the Aston Institute of Photonic Technologies, and for his continuous support, guidance, and belief in me. I am also sincerely thankful to my co-supervisor, Professor Nick Doran, for his mentorship and positive encouragement throughout my research.

Special thanks to Dr. Vladimir Gordienko for teaching me so much in simulations, lab work, writing, and beyond, and for his constant guidance, patience, and kindness. His enormous assistance has been invaluable.

I would also like to thank Professor Stylianos Sygletos for the successful collaboration and for teaching me how to work with coherent transmitters, receivers, and DSP. My gratitude also goes to Dr. Sonia Boscolo for her engagement and for bringing us together for insightful discussions.

My sincere thanks to Furukawa Electric, particularly Dr. Shigehiro Takasaka and Dr. Ryuichi Sugizaki, for providing the fiber that made my experiments so successful. I also extend my appreciation to Dr. Charles Laperle of Ciena for providing the technical support and transponders, which played a crucial role in my work.

I would like to acknowledge Dr. Florent Bessin for his contributions to the success of my experimental work, Dr. Aleksandr Donodin for his assistance in the lab and his guidance in understanding optical transmission experiments. Special thanks to Dr. Mingming Tan and Dini Pratiwi for teaching me how to work with the recirculation loop, and to Mohammed Patel and Dr. Yiming Li for their help with electronics and their support in my experiments.

I am grateful to Dr. Pedro Freire, Sasipim Srivallapanondh, Dr. Stepan Bogdanov, and Dr. Diana Galiakhmetova for their help and advice in the day-to-day life of a PhD student.

Lastly, my heartfelt thanks go to my mother, who has always been there to support me during the dark moments.

LIST OF CONTENTS

ACKNOWLEDGEMENTS.....	3
LIST OF CONTENTS	4
LIST OF ABBREVIATIONS	7
NOMENCLATURE	9
LIST OF FIGURES.....	12
LIST OF TABLES	18
LIST OF PUBLICATIONS.....	19
Peer-reviewed	19
Conference proceedings.....	19
1 INTRODUCTION.....	21
1.1 Motivation.....	21
1.2 Thesis structure.....	25
2 STATE-OF-THE-ART.....	27
2.1 Theoretical Foundations and Design Principles of FOPA.....	27
2.2 FOPA in optical communications.....	30
2.3 Polarization-insensitive FOPA	34
2.4 Nonlinear crosstalk in FOPA.....	36
2.5 Stimulated Brillouin scattering in FOPA.....	39
2.5.1 SBS phenomenon in optical fibers.....	39
2.5.2 Concept of the SBS threshold	40
2.5.3 SBS mitigation principles	43
2.5.4 Fibers with a nonuniform core diameter and co-doping in the fiber core.....	43
2.5.5 Fibers with a nonuniform strain and temperature distribution.....	45
2.5.6 Fibers divided by optical isolators	46
2.5.7 Fibers with fiber Bragg gratings	46
2.5.8 Pump phase modulation with sine tones	46

2.5.9 Alternative phase modulation	49
2.5.10 Summary on SBS mitigation principles for state-of-the-art FOPA design	52
2.5.11 Impact of pump phase modulation on FOPA performance	53
3 IMPACT OF PUMP PHASE MODULATION ON QAM SIGNALS AMPLIFICATION BY FOPA.....	59
3.1 Comparative analysis of pump phase modulation techniques	59
3.2 Impact of pump phase modulation on QAM signals in FOPA.....	63
3.2.1 Instantaneous pump frequency modulation and FOPA gain modulation	63
3.2.2 Induced phase noise in QAM signals due to pump phase modulation.....	66
3.2.3 Calculation of BER for QAM signals with induced phase noise.....	68
3.3 Impact of pump phase modulation in polarization-insensitive FOPA.....	71
3.4 Employment of polarization diversity architecture to mitigate an impact of pump phase modulation in FOPA.....	74
3.5 Summary.....	81
4 EXPERIMENTAL STUDY OF PUMP PHASE MODULATION IN LOOPED PI-FOPA.....	83
4.1 SBS suppression effectiveness of pump phase modulation with different multi-sinusoidal waveforms	83
4.1.1 Experimental setup.....	83
4.1.2 Measurement of phase modulated pump spectra	85
4.1.3 Measurement of SBS threshold increase.....	87
4.2 Impact of pump phase modulation with different multi-sinusoidal waveforms on a coherently detected 16QAM signal	89
4.2.1 Methodology of rOSNR measurements	89
4.2.2 Evaluation of rOSNR penalty with Real-World receivers	91
4.2.3 The rOSNR penalty as a function of pump bandwidth	93
4.2.4 rOSNR penalty as a function of the pump modulation base tone frequency	95
4.2.5 rOSNR penalty distribution across the FOPA gain spectrum	96

4.3 Summary.....	97
5 PERFORMANCE EVALUATION OF PI-FOPA IN RECIRCULATION LOOP ENVIRONMENT	99
5.1 WDM transmission using recirculation loop with MZ-FOPA	99
5.1.1 Experimental setup.....	99
5.1.2 Results and Discussion	101
5.2 Pump dithering characterization in recirculation loop transmission with MZ-FOPA	106
5.3 Summary.....	108
6 CONCLUSION AND FUTURE WORK.....	110
6.1 Conclusion.....	110
6.2 Future work.....	111
REFERENCES.....	113

LIST OF ABBREVIATIONS

AM	amplitude modulation
AOM	acousto-optical modulator
ASE	amplified spontaneous emission
AWG	arbitrary waveform generator
B2B	back-to-back
BER	bit error rate
BPF	band pass filter
DSF	dispersion shifted fiber
DSP	digital signal processing
EDFA	Erbium-doped fiber amplifier
FBG	fiber Bragg grating
FOPA	fiber optical parametric amplifier
FWM	four wave mixing
GFF	gain flattening filter
GVD	group velocity dispersion
MZ	Mach-Zehnder
HNLF	highly nonlinear fiber
NF	noise figure
OOK	on-off keying
OPC	optical phase conjugation
OSA	optical spectrum analyzer
OSNR	optical signal-to-noise ratio
PBS	polarization beam splitter
PC	polarization controller
PDG	polarization-dependent gain
PDSK	phase-difference shift keying
PM	phase modulator
PMD	polarization mode dispersion
PSA	phase-sensitive amplifier
PRBS	pseudo-random bit sequence
QAM	quadrature amplitude modulation

QPSK	quadrature phase shift keying
RF	radio frequency
RIN	relative intensity noise
SBS	stimulated Brillouin scattering
SER	symbol error rate
SNR	signal-to-noise ratio
SRS	stimulated Raman scattering
SSMF	standard single mode fiber
TFBG	tilted fiber Bragg gratings
VOA	variable optical attenuator
WDM	wavelength division multiplexer
ZDW	zero dispersion wavelength

NOMENCLATURE

A	signal amplitude
A_{eff}	effective mode area of the fiber
A_m	phase modulation amplitude
B	signal bandwidth
c	speed of light
d_{min}	distance between any two adjacent points on the constellation
E	electric field
$f_{base\ tone}$	base tone frequency
f_m	phase modulation frequency
f_s	signal frequency
Δf_{total}	total pump bandwidth
g	parametric gain coefficient
g_B	Brillouin gain coefficient
G_s	signal power gain
G_B	Brillouin gain
h	plank constant
h_3	complex amplitude parametric gain
J_n	Bessel function of the first kind
k	total propagation constant or wavevector mismatch
\mathbf{k}_A	wave vector of the acoustic wave
\mathbf{k}_p	pump wave vector
\mathbf{k}_{st}	stokes wave vector
K	weighting factor, representing the fraction of signal power
L	fiber length
L_{eff}	effective fiber length.
n	refractive index
n_2	nonlinear refractive index
N_{FWM}	number of generated FWM products
N_s	number of signals
N_{Rx}	receiver noise

P_{p1}, P_{p2}	pump powers
P_{th}	Brillouin threshold
ΔP_{SBS}^{th}	SBS threshold increase
Pr	error probability
ΔQ	q penalty
t	time
Δt	half period delay
T_r	rise time
V_π	voltage required to modulate the phase by π
XT	ratio of the FWM crosstalk power to the signal output power
α	fiber loss
β	propagation constant or wavevector
β_2	group velocity dispersion
β_3	fiber dispersion slope
β_4	fourth-order propagation constant
$\Delta\beta$	propagation constant phase mismatch
$\Delta\beta_{NL}$	nonlinear wavevector mismatch
Γ_B	inverse phonon lifetime
γ	nonlinearity coefficient
γ_e	electrostrictive constant
λ	wavelength
μ	center of gaussian distribution
ν_B	Brillouin frequency shift
$\Delta\nu_B$	Brillouin linewidth
$\Delta\nu_P$	pump laser linewidth
ρ_0	material density
σ	standard deviation
v_A	velocity of acoustic waves
φ	phase
Φ	nonlinear phase shift
x_0	decision threshold
ω	angular frequency
$\Delta\omega$	frequency offset of signal from the pump

Ω acoustic frequency
 Ω_B Brillouin acoustic frequency

LIST OF FIGURES

Figure 1. Interaction among two pumps, signal, and idler (a) and.....	21
Figure 2. The evolution of the bitrate-distance product of state-of-the-art fiber communication links as function of time [12].....	23
Figure 3. Optical amplifiers for broadband low-noise amplification beyond the EDFA-enabled C&L bands [18].	23
Figure 4. The bitrate versus distance of reported records of transmission experiments [55][56].....	25
Figure 5. Gain Amplitude spectrum (left) and Gain Phase shift spectrum (right). FOPA parameters for pump wavelength of 1566.2 nm, ZDW of 1562.9 nm, fiber dispersion slope of $43 \text{ s} \cdot \text{m} - 3$, pump power of 4.3 W, HNLf length of 50 m, γ of $14 \text{ W} - 1 \text{ km} - 1$. No loss, no pump depletion case.	29
Figure 6. The maximum FOPA gain as a function of the nonlinear phase shift. Signal gain (blue) is calculated using an analytic solution (2.6). The large gain approximation (yellow) is calculated using an approximation from (2.7) and conversion efficiency (orange) derived in [19].....	30
Figure 7. Schematic of a loop diversity architecture for a PI-FOPA: ‘Gain-Loss’ (a), ‘Loss-Gain’(b) [57].	35
Figure 8. Schematic of a Mach-Zehnder architecture for a PI-FOPA [60].....	36
Figure 9. A range of unwanted FWM of 1st and 2nd-order products [62].	37
Figure 10. Schematic of a loop diversity architecture for a PI-FOPA with.....	38
Figure 11. Backscattered power versus pump power: the measured points(blue), the fitted curve (linear+exp) (red), SBS Threshold is defined as a pump power at the intersection of green and blue curves.	42
Figure 12. Bessel functions of first kind (a),.....	47
Figure 13. Simulated Power spectrum with $Am=1.435$ and $fm= 100 \text{ MHz}$	48
Figure 14. Examples of phase modulated pump spectra from literature (from left to right [93],[51],[6],[53], [94],[42]), modulation frequencies are listed in MHz, $Am=1.435$	49

Figure 15. The phase over time (a) and Spectra (b) with different modulation amplitudes of chirped phase modulation with a chirp rate of 534 THz/s and frequency varying from 50 MHz to 400MHz over 600 ns. The insert shows the magnified spectra..... 50

Figure 16. RF spectrum being low pass filtered at 1.3 GHz (a) and optical spectrum of phase modulated by white noise (b) [107]. 51

Figure 17. Phase modulated by PRBS over time with inserted rising edge by the eq. (2.27) (a) and its optical spectra (b)..... 52

Figure 18. Q penalty as a function of signal wavelength (left), FOPA gain spectrum for reference(right). 55

Figure 19. Normalized Brillouin gain spectra of silica fiber with FWHM linewidth of 28 MHz [72]. 59

Figure 20. (a) The relative Brillouin gain for set of Base tone frequencies of Sine tone phase modulation, (b) The SBS threshold improvement versus base tone frequency. Black line shows approximate Brillouin gain linewidth for Silica fiber. 60

Figure 21. Relative Brillouin gain of pump phase modulated by filtered white noise with different modulation amplitudes, insert shows the increase gain peak. 61

Figure 22. (a) Relative Brillouin gain and (b) power spectra for unmodulated pump (black), pump phase modulated with filtered white noise of 1 GHz (red), PRBS with data rate of 2.2 Gb/s (patter length 212 – 1) and rise time of 30 ps (blue), 4 sine tones of 20 MHz, 61MHz,186 MHz, 567 MHz (green). 61

Figure 23. (a) Instantaneous frequency over time for pump phase modulated by PRBS with data rate of 2.2 Gb/s (patter length 212 – 1) and rise time of 30 ps (blue), filtered white noise of 1 GHz (red), and 4 sine tones of 20 MHz, 61MHz,186 MHz, 567 MHz (green). (b) Distribution of instantaneous frequency over 1 us of white noise (red) and 4 sine tones (green). 63

Figure 24. Timeline of the pump frequency detuning from its central frequency due to phase dithering, $|h_3|$ and phase shift (h_3) at signal wavelength of 1531 nm; FOPA parameters for pump wavelength of 1566.2 nm, ZDW of 1562.9 nm, fiber dispersion slope of 43 s – 1m – 3, pump power of 4.3 W, HNLf length of 50 m, γ of 14 W – 1km – 1. No loss, no pump depletion case. Pump phase modulation base tones of 25 MHz (yellow), 40 MHz (blue) and 85 MHz (red) [105]..... 65

Figure 25. The 16QAM constellation diagram represents the input signal, assuming no input noise. 66

Figure 26. (a) constellation diagram of amplified a 16QAM signal by FOPA with Pump phase modulation base tones of 25 MHz (yellow), 40 MHz (blue) and 85 MHz (red). (b) Same diagram with a SNR of 25 dB. Signal wavelength 1531 nm [105]..... 68

Figure 27. BER versus SNR for different pump bandwidth for a..... 70

Figure 28.(a) modulus $|h_3|$ (blue) and phase shift of h_3 (red) calculated with parameters from Figure 5 and (b) rOSNR penalty vs wavelengths for 4 pump modulation waveforms employing 3 tones with f_{base} tone of 100 MHz and 150 MHz (crosses) and 4 tones with f_{base} tone of 25 MHz and 40 MHz (dots) [99]. 71

Figure 29. Scheme of Looped PI-FOPA with different fiber lengths between fiber coupler and EDFAs. PBS – polarization beam splitter, AWG – arbitrary waveform generator..... 72

Figure 30. Schemes for different signal polarisation splitting on PBS in Looped PI-FOPA with different fiber lengths between fiber coupler and EDFAs. 74

Figure 31. (a) Looped PI-FOPA gain modulus $|h_3|$ and (b) Phase shift (h_3) when pump modulation waveforms are counter-phase and tones are multiple for $h_3, X, h_3, Y, h_3, f_{base}$ tone = 25 MHz, $\Delta t = 20$ ns, 75

Figure 32. (a) Looped PI-FOPA gain modulus h_3 and (b) Phase shift (h_3) when pump modulation waveforms are counter-phase and tones are multiplied by $m = 3.05$ for $h_3, X, h_3, Y, h_3, f_{base}$ tone = 25 MHz, $\Delta t = 20$ ns, $K = 0.5$, signal wavelength 1531 nm..... 76

Figure 33. Looped PI-FOPA gain modulus $|h_3|$ when pump modulation waveforms are a) in-phase, b) counter-phase as well as Phase shift (h_3) c) in-phase, d) counter-phase for three different K factors of 1, 0.5 and randomly distributed in range [0,1]. $|h_3|$ and phase shift (h_3) are calculated using the parameters from Figure 5 with pump phase. 77

Figure 34. Probability density of Beta distribution on the interval (0, 1) with parameters $\alpha = 3/2$ and $\beta = 3/2$ 77

Figure 35. Distribution of $|h_3|$ and phase shift (h_3) when pump modulation waveforms are counter-phase for different K factors. Total number of samples is 1000 [105]. 78

Figure 36. rOSNR penalty versus signal wavelengths for three K factors of 1, 0.5, random. Pump optical paths are in counter-phase. Plots are simulated using the parameters from Figure 5 with pump phase modulation employing 4 tones, with $f_{base\ tone} = 25$ MHz and $m = 3.05$ [105]. 79

Figure 37. rOSNR penalty versus path difference between pumps for PDM signal polarization aligned with the PBS axes (blue), equally split (red) or randomly scrambled (yellow). Tones multiplier = 3.05. 80

Figure 38. rOSNR penalty calculated for combinations of pump path difference in meters and pump modulation base tone frequencies for PDM signal polarization (a) equally split or (b) randomly scrambled. 81

Figure 39. The experimental setup for measurements of the pump optical spectra, input, and backscattered pump power for a range of pump phase modulation waveforms employed by the Looped PI-FOPA for SBS mitigation. 84

Figure 40. Measured pump optical spectra for several modulation waveforms, where pump was modulated by tones with an integer multiplication factor between them $m=3$: (a) 4 sine tones, Base tone frequency 25 MHz, (b) 4 sine tones, Base tone frequency 50 MHz, (c) 3 sine tones, Base tone frequency 100 MHz, (d) 4 sine tones, Base tone frequency 200 MHz. Simulated spectra are shown for reference. 86

Figure 41. Measured pump optical spectra for modulation waveforms with an integer and non-integer multiplication between sine tones: (a) 4 tones, $f_{base\ tone} = 25$ MHz and (b) 3 tones, $f_{base\ tone} = 100$ MHz. 86

Figure 42. (a) Backscattered-to-input pump power ratio dependence on input Pump power, (b) the SBS threshold increase versus total pump bandwidth. 88

Figure 43. (a) Backscattered-to-input pump power ratio dependence on Pump power for modulation waveform with 4 tones with $f_{\text{base tone}} = 25$ MHz and an integer and non-integer multiplier between tones..... 89

Figure 44. Experimental setup: OSA – Optical spectrum analyser, ASE – amplified spontaneous emission, BPF – bandpass filter, AWG – arbitrary waveform generator, VOA – variable optical attenuator, PC – polarization controller. 90

Figure 45. Setup for characterization receiver penalty. AWG – arbitrary waveform PC – polarization controller, PM fiber – polarization maintaining fiber [105]. 91

Figure 46. Required received penalty versus sine tone frequency for phase modulation amplitudes ranging from 0.002 to 0.008 radians. 92

Figure 47. (a) required Rx power penalty vs phase modulation amplitude, (b) required Rx power penalty vs amplitude modulation depth. Modulation frequency is 100 MHz. Blue dashed line is linear fit after a 0.2 dB implementation penalty had been subtracted [105]..... 92

Figure 48. rOSNR penalty versus total pump bandwidth for 6 wavelengths across 3 dB FOPA gain bandwidth. Red dots – experiment data with 4 sine tones with $f_{\text{base tone}}$ in range between 25 MHz and 85 MHz, blue dots – experiment data with 3 sine tones with $f_{\text{base tone}}$ in range between 100 MHz and 225 MHz, red circles – simulation with 4 sine tones with $f_{\text{base tone}}$ in range between 25 MHz and 85 MHz, blue circles - simulation with 3 sine tones with $f_{\text{base tone}}$ in range between 100 MHz and 225 MHz. Tones were obtained by integer multiplier $m = 3$. FOPA parameters from Figure 5, and including performance of real receivers..... 94

Figure 49. Measured delay between pumps of 20.56 ± 0.02 ns by comparing PRBS patterns saved from the two FOPA arms..... 95

Figure 50. rOSNR penalty vs Pump base tone frequency for signal wavelength of (a) 1531 nm and (b) 1545 nm. Black – experimental data with error bars, Red –simulation using the FOPA parameters from Figure 5, $K = \text{random}$, and including performance of real receivers [105]..... 96

Figure 51. rOSNR penalty vs signal wavelength. Red - simulated real receiver, Yellow – simulated real receiver considering only induced phase modulation, Green – simulated real receiver with only induced amplitude modulation, Blue –simulation of ideal receiver, Black – experiments. Simulation using the FOPA parameters from Figure 5, K = random and including data scaling from Figure 47 [105].	97
Figure 52. Experimental setup for recirculating loop transmission to investigate WDM signal amplification using cascaded MZ-FOPA.....	99
Figure 53. The polarization-insensitive MZ-FOPA setup [62].	100
Figure 54. Optical power spectra at the input and output of the MZ-FOPA (left), MZ-FOPA gain spectra for two polarizations (labelled as X and Y) and PDG (right).....	101
Figure 55. Optical power spectra of WDM signal at the input of recirculation loop (black) and output after 1 to 10 recirculations.....	102
Figure 56. Optical power spectra at the output of MZ-FOPA (before GFF and supplementary EDFA) with 3 omitted channels for 1 to 10 recirculations. Pump wavelength 1553.43 nm [109]......	102
Figure 57. (a) BER versus number of recirculations, (b)BER versus launched power to transmission fiber per channel for 2 (red), 5 (green), 7 (blue) and 10 (purple) recirculations. The points are experimentally measured, and lines are fittings based on Eq.(5.1), (5.2) [105].	103
Figure 58. BER versus launched power to transmission fiber per channel for 1530, 1534, 1540 nm for (a) 2 recirculations and (b) 5 recirculations.	105
Figure 59. BER versus wavelength for number of recirculations.	105
Figure 60. Experimental setup of recirculating loop transmission arrangement to examine impact of pump dithering MZ-FOPA.	106
Figure 61. (a) BER as a function of signal power at the transmission fiber for different dithering parameters; (b) Backscattered power from HNLF versus base tone frequency.	107
Figure 62. (a) BER versus versus signal power launched into transmission fiber after 2 recirculations for a range of pump phase modulation frequencies (dots – experiment, lines – fitting with Eq.(5.1),(5.2)), (b) BER floor (left) and Backscattered power (right) versus base tone frequency.	108

LIST OF TABLES

Table 1. Comparison of SBS mitigation techniques for state-of-the-art FOPA.....	53
Table 2. Parameters of pump modulation waveforms	84
Table 3. Parameters of HNLFs used in Looped PI-FOPA.....	87

LIST OF PUBLICATIONS

Peer-reviewed

1. V. Gordienko, S. Boscolo, **M. Bastamova**, A. D. Ellis, and N. J. Doran, "Record bandwidth waveband-shift-free optical phase conjugation in nonlinear fiber optical loop mirror," *Opt. Express*, vol. 16, pp. 27894-27905, 2024.
2. **M. Bastamova**, V. Gordienko, N. J. Doran, and A. D. Ellis, "Impact of pump phase modulation on QAM signals in polarization-insensitive fiber optical parametric amplifiers," *Optical Fiber Technology*, vol. 84, pp. 103758, 2024.

Conference proceedings

1. **M. Bastamova**, V. Gordienko, S.s Sygletos, T. Mingming, A. Donodin, L. Nguyen, F. Bessin, S. Boscolo, N. J. Doran, and A. D. Ellis, "Performance evaluation of a polarisation insensitive Mach-Zehnder fiber parametric amplifier with 38 channel transmission," In European Conference and Exhibition on Optical Communication, pp. W2A.1, Optica Publishing Group, 2024.
2. V. Gordienko, F. Bessin, **M. Bastamova**, S. Boscolo, N. J. Doran, and A. D. Ellis, "Recent advances in fiber optical parametric amplifiers for optical communications," In 2024 IEEE Photonics Society Summer Topicals Meeting Series (SUM), pp. 1-2. IEEE, 2024.
3. V. Gordienko, S. Boscolo, **M. Bastamova**, N. J. Doran, and A. D. Ellis, "Waveband-shift-free optical phase conjugation in fiber loop mirror across 35-nm bandwidth," In 2024 Optical Fiber Communications Conference and Exhibition (OFC), pp. 1-3. IEEE, 2024.
4. **M. Bastamova**, V. Gordienko, N. J. Doran, and A. D. Ellis, "Employment of polarization diversity architecture to mitigate an impact of pump phase modulation in FOPA," In Optical Fiber Communication Conference, pp. M1B-2. Optica Publishing Group, 2024.
5. **M. Bastamova**, V. Gordienko, N. J. Doran, and A. D. Ellis, "Performance of Fibre Optical Parametric Amplifiers for QAM signals amplification," In British and Irish Conference on Optics and Photonics, pp. PS-8. Optica Publishing Group, 2023.

6. V. Gordienko, **M. Bastamova**, A. Ellis, and N. Doran, "Nonlinear optical loop mirror for waveband-shift free optical phase conjugation," In Optical Fiber Communication Conference, pp. Th2A-12. Optica Publishing Group, 2023.
7. **M. Bastamova**, V. Gordienko, and A. Ellis, "Impact of pump phase modulation on fibre optical parametric amplifier performance for 16-QAM signal amplification," In European Conference and Exhibition on Optical Communication, pp. Tu5-6. Optica Publishing Group, 2022.

1 INTRODUCTION

This thesis focuses on investigating techniques to address a major challenge in the development of fiber optical parametric amplifiers (FOPAs): mitigation of the stimulated Brillouin scattering (SBS). SBS limits the significant performance potential of FOPAs and prevents them from being competitive with other optical amplifiers.

1.1 Motivation

Optical parametric devices, such as optical parametric amplifiers (OPA), wavelength converters, optical phase conjugators (OPC), optical parametric oscillators (OPO), optical frequency combs generators (OFC) and others rely on optical nonlinear processes called parametric. This class of nonlinear phenomena has a feature that the interaction among several optical waves occurs through the medium's electronic response, in contrast to Brillouin or Raman scattering, where the nonlinear scattering depends on molecular vibrations or density variations of the optical medium. The parametric process is governed by the nonlinear response of bound electrons in a material to an electromagnetic field. This response is characterized by higher-order susceptibilities. The second-order susceptibility χ^2 exists in media without inversion symmetry, such as certain crystals, and is responsible for three-wave mixing (TWM) [1]. Four-wave mixing (FWM), on the other hand, arises from the third-order susceptibility χ^3 in isotropic media such as optical silica fibers[2]. FWM involves a nonlinear interaction among four optical waves called pumps, signal and idler (Figure 1), with the relationship between four frequencies shown in Eq. (1.1) or among three frequencies, if pump's frequencies $\omega_1 = \omega_2$ [3].

$$\omega_1 + \omega_2 = \omega_3 + \omega_4 \quad (1.1)$$

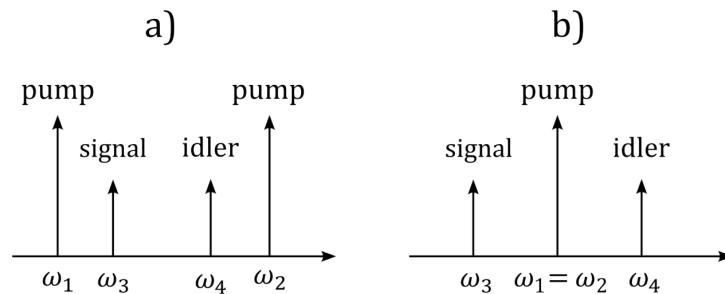


Figure 1. Interaction among two pumps, signal, and idler (a) and among three waves, where pump's frequencies $\omega_1 = \omega_2$ (b).

Due to TWM or FWM phenomena and its independence of fiber material, these devices can operate in a wide range of optical transmission windows covering near and mid infrared ranges. The bandwidth of operation of these devices depends on phase-matching conditions between waves, so in theory it can extend up to several hundreds of nanometers [5]. It is easy to obtain a high gain in FOPA [6] or fiber optical parametric oscillators (FOPO) [7], as their gain is proportional to pump power. Wavelength converters with high signal-to-idler conversion efficiency can be used for generation of new wavelengths [8] and OPC can be used for counteracting negative nonlinear effects that occurs during optical signal propagation through optical fibers [9]. OPO is used in mid-infra-red data transmission in a free-space optical communications [11].

Due to these advantageous properties, optical parametric devices hold significant potential for application in the field of optical communications. The ongoing digital revolution has led to an unprecedented demand for high-speed data transmission. The communication industry faces significant challenges due to the exponential growth in data traffic and the ensuing need for higher capacity and transmission rates [12]. Innovations such as cloud-to-edge computing, artificial intelligence, machine learning, augmented and virtual reality, digital twins, and the internet of things are increasingly interconnecting people, processes, data, and devices. As the number of internet users continues to rise globally, this growth fuels a surge in devices and connections [13] [14].

So far, capacity has been increased by improving modulation techniques with higher spectral efficiency (Figure 2), employing high-order modulation and constellation shaping, transmitting data in parallel using wavelength-division multiplexing (WDM) technologies, deploying multimode or multicore fibers (SDM), developing coherent receivers, and continuously enhancing digital signal processing (DSP) and forward error correction (FEC) [12]. However, there is still a need for innovative solutions to identify which are the most promising research directions in the coming years.

One solution is expanding the bandwidth used by fiber optical communications into new bands [15]. The five available bands (O, E, S, C, and L) have attenuation coefficients below 0.4 dB/km in standard silica fibers. A multiband approach allows transmission over the entire low-loss optical spectrum of single-mode fibers (SMF) from 1260 nm to 1625 nm. This solution is preferable as it maximizes the return on investment of already deployed optical infrastructure.

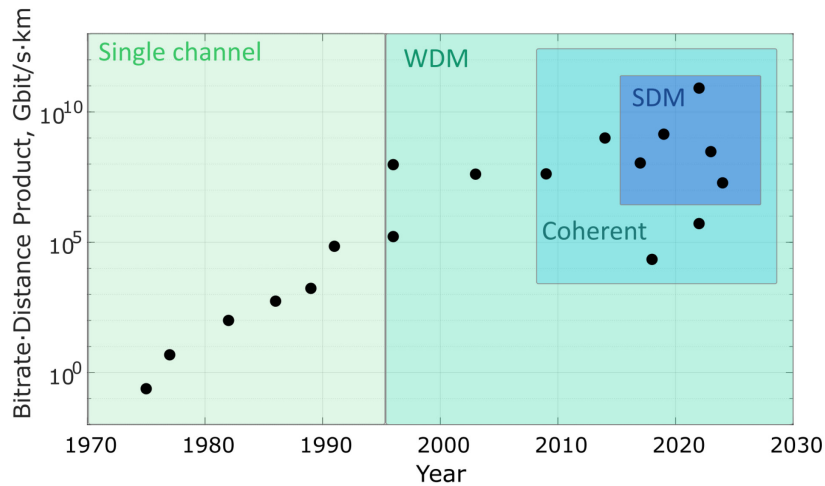


Figure 2. The evolution of the bitrate-distance product of state-of-the-art fiber communication links as function of time [12].

Fiber optical amplification is the enabling technology for this expansion in both long-haul systems and networks. Therefore, one of the major research topics today is the development of novel optical amplifiers that provide broadband low-noise amplification beyond the EDFA-enabled C&L bands [18] (Figure 3).

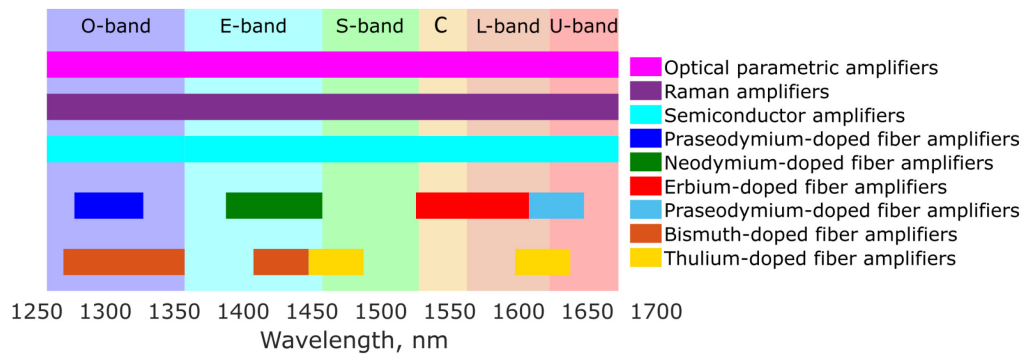


Figure 3. Optical amplifiers for broadband low-noise amplification beyond the EDFA-enabled C&L bands [18].

All rare-earth doped amplifiers, such as EDFA, BDFEA, and others, are limited by their gain bandwidth. Even Raman amplifiers are restricted by the stimulated Raman scattering (SRS) gain spectrum with a certain shape. The optical parametric amplifiers, in contrast, demonstrate potential to address bandwidth limit. FOPA [19] [20] and OPA based on periodically-poled-LiNbO₃ (PPLN) [21][22], integrated gallium phosphide (GaP)[23] and silicon nitride (Si₃N₄) nonlinear integrated waveguides [24] can be used in broadband transmission systems, for their potential to amplify across multiple bands with ultra-wide bandwidth.

Despite, fiber optical parametric amplifiers (and other devices) have a few advantages compared to their crystal-based counterparts, such as compatibility with all-fiber devices and less price, they suffer from another nonlinear process – SBS [25]. FOPA performance is particularly restricted by SBS, as it limits the maximum pump power necessary to achieve high parametric gain [26]. Once the pump power becomes high enough to invoke SBS, it backscatters an exponentially increasing fraction of pump power until the pump is depleted. Several SBS mitigation techniques have been proposed in the literature.

Passive techniques have been employed over the past twenty years to mitigate SBS in optical fibers: changing the core diameter along the length of a fiber [27], changing the dopant concentration in the fiber [28], introducing strain [29] and temperature [30] gradients along the fiber, designing acoustically guiding and anti-guiding refractive index profiles, using isolators [31], and employing tilted fiber Bragg gratings [32]. Generally, these passive methods provided a relatively small increase in the SBS threshold but induce dispersion variations in the fibers and incur additional insertion loss, which is undesirable in FOPA implementation as the longitudinal changes of the fiber dispersion prevent achieving a broadband FOPA gain spectrum [19].

The active SBS mitigation method, i.e. pump phase modulation, allows for the highest SBS suppression up to 20 dB [6]. Pump phase modulation has a negative impact on the idlers, generated by FWM, as idlers inherit twice pump phase shift during FWM. For a long time, the impact of pump phase modulation on signals amplified by FOPA received little attention, as it was assumed that the signal phase was independent of the pump phase. However, several studies have reported that pump phase modulation induces significant FOPA gain distortions, which in turn lead to signal degradation [33]-[36].

SBS mitigation is still the major source of signal degradation in state-of-the-art FOPAs [26]. So far, this effect has been studied in detail for directly detected on-off keying signals (OOK). These studies have not considered signal phase noise introduced by phase dithering and do not address penalties for quadrature modulated (QAM) signals. Moreover, coherent detection relies on signal amplitude rather than signal power, which has not been considered in previous studies, which examined directly detected signals. Overall, the results of existing studies on the impact of dithering in FOPA are not applicable to coherently detected QAM signals widely used in modern optical communications.

In this thesis, the impact of pump phase modulation on the performance of FOPAs when amplifying polarization-multiplexed QAM signals is revisited, with a focus on the characteristics of state-of-the-art polarization-insensitive FOPAs. The pump phase

modulation scheme has been optimized to minimize signal quality penalties. The findings of this research have enabled further increases in both the bitrate and transmission distance of fiber optic systems employing FOPAs as in-line amplifiers in comparison with previously reported records (Figure 4).

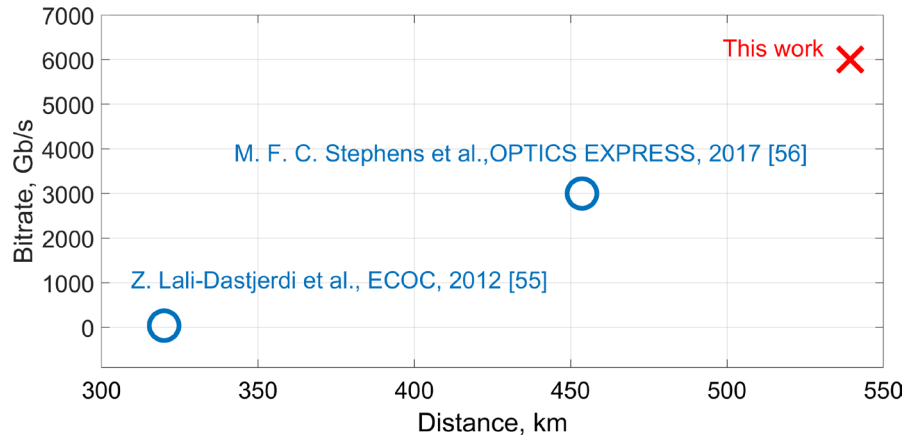


Figure 4. The bitrate versus distance of reported records of transmission experiments [55][56].

1.2 Thesis structure

Chapter 2 provides an overview of the FOPA background, including foundational theories and the latest FOPA advancements in the field of optical communications. It begins with the main theoretical concepts for FOPA design, followed by a discussion of FOPA development for modern optical communications, highlighting the challenges addressed to achieve competitive results with other optical amplifiers. Next, the chapter describes the phenomena of SBS and explains the concept of the SBS threshold, which is crucial for FOPA design. The major challenge of SBS mitigation is explored through both passive and active techniques, summarizing with a comparison of their effectiveness. Finally, the chapter details the impact of pump phase modulation, a key aspect of this thesis.

Chapter 3 assesses the impact of pump phase modulation on QAM signals amplified by FOPA by means of theoretical study and simulations. A theoretical model is formulated and derived to quantify signal degradation in terms of the required optical signal-to-noise ratio (rOSNR) penalty to achieve a specified the bit error rate (BER) reference level. The theoretical model is described, and the results are presented and interpreted. The chapter concludes by discussing the implications of QAM signal degradation on FOPA performance.

Then, the chapter examines the impact of pump phase modulation specifically within the context of polarization-insensitive FOPA design. It offers a more focused theoretical analysis tailored to the characteristics of PI-FOPA architecture.

Chapter 4 describes an experimental study, detailing the experimental setups, methodologies for measurements, and comparisons between simulation and experimental results.

First SBS suppression effectiveness and rOSNR were investigated for a range of phase modulation schemes. The impact of pump phase modulation was studied with different multi-sinusoidal waveforms on a coherently detected 16-QAM signal. The performance of commercial coherent receivers in handling induced signal modulations was additionally done through experimental measurements and estimations. Distribution of rOSNR across the wavelength range is presented and analyzed in detail.

Chapter 5 investigates the application of an optimized pump phase modulation scheme in a transmission experiment utilizing a recirculation loop setup with a PI-FOPA that amplifies 38x50-GHz spaced channels. The chapter assesses the performance enhancements achieved through the Mach-Zehnder architecture and the optimized pump phase modulation strategy. It details the experimental setup of the transmission experiment using a recirculation loop and analyses the BER as a function of launched power into the transmission fiber per channel across multiple measured recirculations. Then the transmission of a single channel in the recirculation loop setup was used to characterize the impact of pump dithering.

Chapter 6 provides a conclusion of the research outcomes and outlines future directions for further research in SBS mitigation techniques to enhance FOPA performance.

2 STATE-OF-THE-ART

Chapter 2 presents a comprehensive overview of FOPA, covering both foundational theories and the latest advancements in optical communications. It begins by introducing the key theoretical principles of FOPA design, followed by a discussion of FOPA's development for modern optical systems. The chapter then explores the phenomenon of SBS, explaining the SBS threshold, which plays a critical role in FOPA design. Various SBS mitigation strategies, both passive and active, are examined and compared for their effectiveness. Lastly, the chapter focuses on the effects of pump phase modulation, a central topic of this thesis.

2.1 Theoretical Foundations and Design Principles of FOPA

FOPAs have been a research topic for more than 40 years. The underlying physical phenomenon of FWM has been studied since the 1970s. The first demonstration of signal amplification using the parametric process in optical fibers was conducted in [2]. Since then, dozens of papers and several books have explained the physics of FWM in optical fibers in detail.

This thesis assumes that the reader is familiar with FWM and the basic theory of FOPAs from Marhic's book [4]. I would like to note that the same nomenclature, symbols, and equations were derived in the same style as in that book. The goal of this section is to provide a brief introduction to the key design principles of FOPAs, which are necessary for further discussion. This section covers the key relations between the main parameters that define FOPA gain and its shape, the emergence of gain due to third-order nonlinearity, and the key principles defining the FOPA gain spectrum. For simplification, all waves are considered co-polarized, allowing for important conclusions.

The signal FOPA gain spectrum depends on three quantities. First, $r = 2\gamma\sqrt{P_{p1}P_{p2}}$ is the amplitude of the FWM coupling coefficient between the four waves. The fiber nonlinearity coefficient γ can be introduced as [4]

$$\gamma = \frac{\omega n_2}{cA_{eff}}, \quad (2.1)$$

where A_{eff} is the effective area of the mode and n_2 is the nonlinear refractive index coefficient. As the nonlinear phase shift $\Phi = \gamma PL_{eff}$ is crucial for estimating the maximum

gain of FOPA, γ should be as large as possible for the given FOPA design. A large n_2 and a small A_{eff} are required. Highly nonlinear fibers (HNLF) are used in FOPA as a gain medium, they have a high fiber nonlinearity coefficient γ of $\sim 10\text{-}20 \text{ W}^{-1}\text{km}^{-1}$. Their effective length is denoted as L_{eff} . Long HNLF can contribute to Φ , providing high gain, although zero-dispersion wavelength (ZDW) variation along fiber length is more severe and effectively decrease FOPA bandwidth. FOPA pump powers, P_{p1}, P_{p2} (in case of one-pump FOPA ($P_{p1} = P_{p2} = P$)) should be high to provide high gain and broad bandwidth.

Second, the linear wavevector mismatch $\Delta\beta$, which refers to the difference between the propagation constants β of four interacting waves during FWM, is determined by the dispersion of the type of fiber used and plays a crucial role in determining the shape of the gain spectrum. When introducing $\Delta\beta$, only even the highest-order terms are in practical interest, as due to a symmetry of signal and idler frequencies around the pump all odd derivatives are being cancelled:

$$\Delta\beta(\Delta\omega) = \beta_2(\omega_p) \cdot \Delta\omega^2 + \frac{\beta_4(\omega_p) \cdot \Delta\omega^4}{12}, \quad (2.2)$$

where ω_p – pump frequency and $\Delta\omega$ the frequency offset of signal from the pump. Due to a symmetry of signal and idler frequencies around the pump, the FOPA signal gain is symmetric around the pump frequency ω_p and allows to find the propagation constant phase mismatch $\Delta\beta$ as a function of signal detuning from the pump. The group velocity dispersion at the pump frequency β_2 can be adjusted by altering the pump frequency ω_p . Conversely, the fourth-order propagation constant β_4 shows minimal frequency dependency within a practical pump frequency range. It is also challenging to measure or manufacture with high accuracy, so it is typically characterized by its sign and order of magnitude [4].

Finally, the nonlinear wavevector mismatch $\Delta\beta_{NL} = \gamma P$ (in case of one-pump FOPA $\Delta\beta_{NL} = 2\gamma P$) determines at which wavelengths the total propagation constant or wavevector mismatch $\kappa = \Delta\beta + \Delta\beta_{NL}$ vanishes, and where maximum gain can be achieved as phase-matched gain requires $\kappa=0$ to obtain phase-matching along all fiber length. $\Delta\beta_{NL}$ and r can be calculated without any knowledge of fiber dispersion since they depend only on the pump powers P_{p1}, P_{p2} and γ .

When talking about signal amplification, there is no idler at the input, so power gain is independent of the initial phases of the pumps and the signal. They are assumed to be zero. Complex amplitude gain h_3 in FOPA defined as the ratio between output A_{out} and input

signal amplitudes A_{in} to consider both power amplification and phase shifts introduced by FOPA:

$$h_3 = \frac{A_{out}}{A_{in}} = \left[\cosh(gL) + i \frac{k}{2g} \sinh(gL) \right] \times \exp \left[i \left(2\gamma P - \frac{k}{2} \right) L \right]. \quad (2.3)$$

Eq. (2.3) assumes no loss, no pump depletion case, where g is the parametric gain coefficient:

$$g = \sqrt{(\gamma P)^2 - k^2/4}. \quad (2.4)$$

Figure 5 shows spectra of the amplitude gain modulus $|h_3|$ and phase calculated for pump power of 4.3 W, pump wavelength of 1566.2 nm, ZDW of 1562.9 nm, and dispersion slope of $43 \text{ s} \cdot \text{m}^{-3}$.

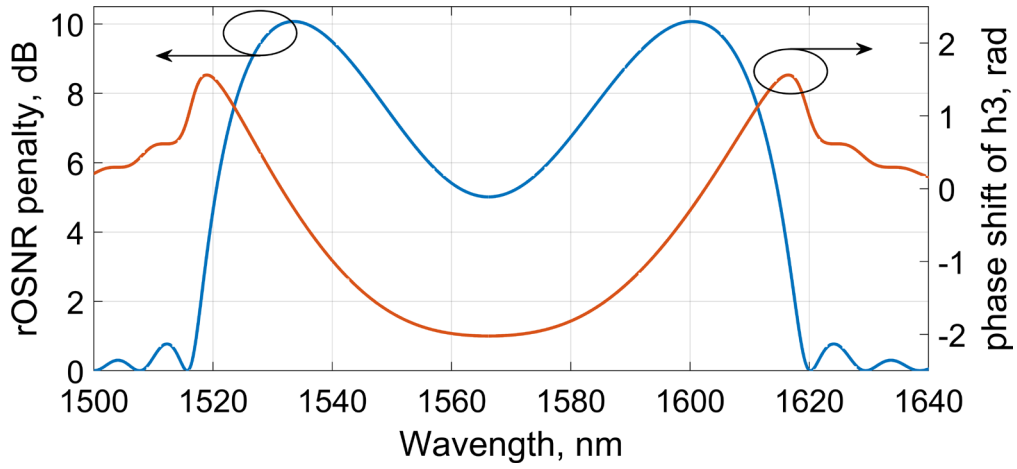


Figure 5. Gain Amplitude (left) and Gain Phase shift spectrum (right). FOPA parameters for pump wavelength of 1566.2 nm, ZDW of 1562.9 nm, fiber dispersion slope of $43 \text{ s} \cdot \text{m}^{-3}$, pump power of 4.3 W, HNLf length of 50 m, γ of $14 \text{ W}^{-1} \text{ km}^{-1}$. No loss, no pump depletion case.

The amplitude gain modulus is the square root of the power gain, so its peak of 10 dB corresponds to the power gain of 20 dB.

The signal power gain G_s :

$$G_s(L) = |h_3(L)|^2 = \left| \frac{r}{g} \sinh(gL) \right|^2 + 1. \quad (2.5)$$

The highest gain is therefore obtained when the gain coefficient is at its maximum

$$g_{max} = r = \gamma P:$$

$$G_{s,max}(L) = [\cosh(\gamma PL)]^2. \quad (2.6)$$

It was derived in [4] that for large gain, $G_{s,max}$ can be expressed in dB and simplified as

$$G_{s,max}^{dB}(L) \approx 8.69\Phi - 6 \text{ dB.} \quad (2.7)$$

The nonlinear phase shift $\Phi = \gamma PL_{eff}$ allows to estimate FOPA maximum gain. Figure 6 shows the large gain, $G_{s,max}$, signal gain, and signal-to-idler conversion efficiency as a function of nonlinear phase shift.

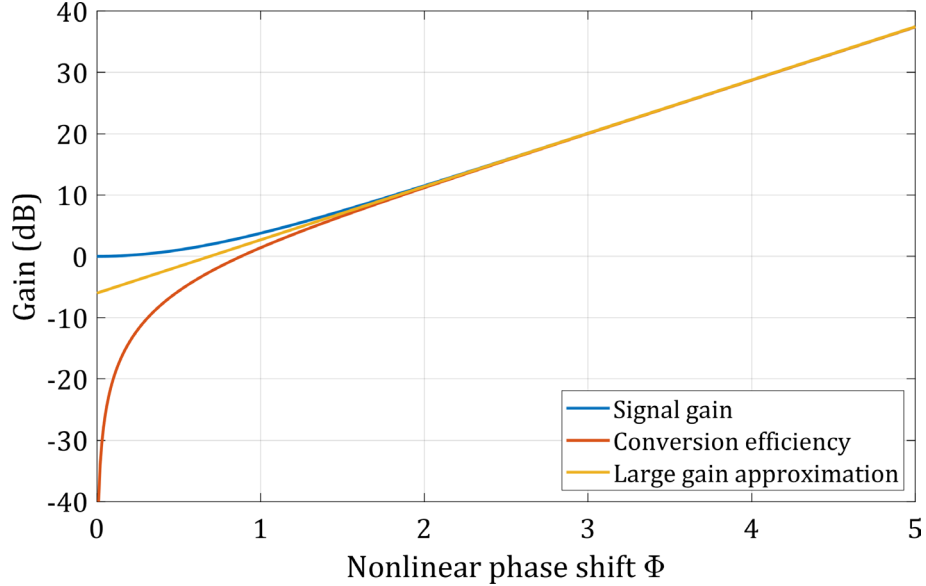


Figure 6. The maximum FOPA gain as a function of the nonlinear phase shift. Signal gain (blue) is calculated using an analytic solution (2.6). The large gain approximation (yellow) is calculated using an approximation from (2.7) and conversion efficiency (orange) derived in [19].

Knowledge about fiber nonlinearity γ , length L_{eff} , and pump power P allow to obtain a particular gain in FOPA. A nonlinear phase of shift of 2.99 is required to achieve a gain of 20 dB, [4][19].

2.2 FOPA in optical communications

This section provides a comprehensive literature review on the capabilities of FOPAs, highlighting their distinct advantages in the field of optical communications. Experimentally demonstrated achievements reported at conferences and published in journals are listed and discussed.

FOPAs has a range of unique features enabled by their underlying principle of FWM that could be leveraged to enhance the capabilities of optical communication systems beyond their current limits of operation. FOPA can amplify commonly used modulation formats such as binary modulation (OOK and binary PSK), high-order amplitude and phase

modulation formats, such as QAM, amplify WDM signals, and bursty traffic. However, several challenges arise when amplifying high-order PSK or QAM, as they are susceptible to phase noise introduced during the amplification process. Additionally, polarization-multiplexed modulation formats require specific engineering designs to address the inherent polarization sensitivity in FOPA.

Theoretically, a FOPA can provide very broad gain bandwidth, as its gain spectrum is determined by the fiber's nonlinearity, dispersion properties, and pump power. If the fiber dispersion is constant along the entire fiber length and satisfies the perfect linear phase matching condition across all frequencies, gain can be achieved at those frequencies [4]. In two-pump FOPA, the record bandwidth of 155 nm was reported [38]. Record bandwidths of 270 nm has been demonstrated in single-pump FOPA in a 114-m long step-index HNLF with fiber nonlinearity $15 \text{ W}^{-1}\text{km}^{-1}$, and the pump power 5 W [20], however only half of reported bandwidth occupied the one side of the central frequency. Reported gain shape in [20] exhibited significant gain variations (gain varies from 10dB to 25dB between 1475nm and 1550nm), which potentially bring additional noise from compensating for gain flattening filter loss. Further development was done in advanced dispersion management techniques such as use of dispersion-stabilized HNLFs. Improved dispersion parameters such as stability and, optimal pump wavelength allowed for a new record wide flat gain of 9.2 ± 0.7 dB in a range of 104 nm [19]. Finally, merging the parametric gain spectrum with a forward Raman gain spectrum provided by the same pump enhanced FOPA bandwidth up to 111 nm [39].

FOPA operation across the whole low-loss transmission window of silica fibers is possible. The parametric gain can theoretically be achieved around any pump wavelength as Kerr nonlinearity changes gradually with wavelength in low-loss transmission window. However, pump lasers must meet specific requirements, including high power output of approximately 10W and narrow linewidth of 100 kHz, low noise and high wavelength stability to amplify OOK. Even tighter specifications are needed for QAM amplification. The combination of these stringent requirements means that manufacturing these lasers outside the C-band are complex and costly. The state-of-the-art FOPAs employ an EDFA to produce a pump of sufficient power (≥ 10 W) and quality, having narrow linewidth and low noise. Nevertheless, a Raman generated pump was used as an example to demonstrate the possibility of parametric amplification with more than 10 dB gain within 35 nm bandwidth [41], which implies possibility to generate a pump for FOPA anywhere in O,E,S,C,L bands.

Experimental demonstrations of WDM amplification by both single-pump and two-pump FOPAs in the S, C, and L bands have been reported in several studies. The development of WDM amplification started in C-band with amplification of 7 OOK signals with a total data rate of 7x2.5 Gb/s using a single-pump FOPA in [42]. Subsequently, the amplification of 12x10 Gb/s channels using a two-pump FOPA showed a signal power penalty below 0.5 dB [43]. Further advancements included the amplification of 26x43.7 Gb/s RZ-DPSK channels [4]. This was followed by the successful amplification of a broadband WDM spectrum with a 1 Tb/s data rate, accompanied by a slightly increased power penalty of 0.7 dB [37]. Most recently, the amplification of 23x100 Gb/s PDM-QPSK signals, achieving a total of 2.3 Tb/s, was demonstrated using a polarization-insensitive single-pump FOPA [44].

The amplification of WDM signals in S-band by FOPA, covering wavelength between 1517 nm to 1528 nm, was studied in [45]. The performance of a FOPA assisted by a Raman pump was analyzed with a 16-channel WDM system operating in the optical S-band to prove the capability of FOPA operation in this band. At the same time, the operation of a polarization-insensitive FOPA in the S-band was studied experimentally. A system with 42 WDM channels with 100 GHz spacing, covering 22 nm in the S-band, exhibited a slightly increased power penalty of 1.4 dB compared to C-band [46].

Due to the symmetric shape of the FOPA gain spectrum, both sides of the gain spectrum can be utilized for signal amplification. Depending on where the pump wavelength is set within the FOPA spectrum, either the C-band or L-band can be used for WDM signal amplification. For instance, FOPA operation in the L-band was demonstrated in [47], where 8xPDM-16-QAM signals, with a total data rate of 2.048 Tbit/s, were amplified using a polarization-insensitive two-pump FOPA from 1575 nm to 1580 nm. Additionally, PI-FOPA simultaneously amplifying WDM signals in both the C and L bands was described in [48], where 10x 100G PDM-QPSK channels in the C-band (1528.8–1535.8 nm) and 10x bursty 10G OOK channels in the L-band (1588.7–1596.3 nm) were amplified.

FOPAs offer ultrafast amplification due to their $\chi^{(3)}$ nonlinearity in optical fibers, with a response time of less than 0.1 fs at frequencies below 600 THz [49]. This rapid response makes FOPA ideal for burst networks, significantly increasing the power budget of optical links carrying bursty traffic and enhancing the required dynamic range when the amplified signal experiences transient effects during amplification. Experimental results have demonstrated that EDFA and Raman amplifiers suffer from >5dB and >3 dB worse sensitivity than FOPA for a 75% traffic density [49].

FOPAs are capable of a very high gain. A huge FOPA gain up to 70 dB has been experimentally demonstrated in [6] which is very difficult to achieve in most other amplification technologies. The reason for this is that the unidirectional gain prevents backward-propagating ASE noise. It should be noted that achieving such high gain is possible only with efficient SBS suppression, not just on the pump to increase the SBS threshold but also on the amplified signal. The measurement range was limited at low input powers by low OSNR and at higher input powers by SBS on the amplified signal. Consequently, the output power was constrained by SBS on the amplified signal, as well as saturation effects from quantum ASE noise amplified in the FOPA, which saturated the gain. This makes SBS mitigation key to achieving high FOPA performance.

FOPA can function as phase-sensitive amplifier (PSA), which requires both the signal and idler to have equal amplitude at the input and precise phase matching between the signal, idler, and pump at the PSA gain medium input [50]. The signal and idler waves are mutually coherent and will thus combine coherently, while their noise components are uncorrelated and add only in terms of power like in coherent receivers. That is why, in theory, such devices can achieve a noise figure (NF) close to the quantum-limited 0 dB [51], meaning that the output signal has almost the same signal- SNR as the input signal. When used for periodic amplification in transmission links with lossy fibers, PSA can offer a 6 dB advantage in system noise figure over EDFA-based systems as it amplifies the in-phase component of the signal while suppressing the out-of-phase component [[52]. This significant improvement can be used to extend transmission range, support higher-order modulation formats, and more. Although implementing a PSA in a transmission link requires transmitting additional idlers, effectively halving the available bandwidth, it allows for an increase in overall link capacity when the signal SNR is below 3 dB [50],[53]. Consequently, PSAs for WDM signals require simultaneous phase-matching across a wide signal bandwidth. In [54], this challenge was addressed using a combination of inverse dispersion fiber and standard single mode fiber (SSMF) to accurately compensate for phase mismatch over a bandwidth of ~ 10 nm. A phase sensitive FOPA with a record continuous bandwidth of 8 nm, a noise figure below 3 dB, and a gain greater than 10 dB has been demonstrated to amplify 11 WDM channels simultaneously [54].

The performance of amplified signals by cascaded single-polarization FOPA in long-haul transmission experiment within a recirculation loop for the first time was demonstrated in [55] showing error-free performance for OOK and PDSK signals up to 320km. WDM transmission with cascaded polarization insensitive (PI)-FOPA within a recirculating loop

was reported in [56]. 30 PM QPSK channels with 50 GHz spacing were transmitted and amplified by PI-FOPA over 6 recirculations (453.6km) and detected with $BER < 1.5 \times 10^{-2}$. The performance shown of amplified by FOPA signals in those studies was limited by two major factors. First, increased FWM crosstalk between channels limits the number of channels [56]. The second and more significant limiting factor was induced phase noise from pump phase modulation necessary for SBS mitigation. The induced phase noise accumulates and transfers to amplitude modulation through dispersion in periodically amplified systems [57],[58].

Recently, significant progress has been done in other parametric devices based on the FWM phenomenon like wavelength converters [59],[60] and phase conjugation [9],[10],[61],[62]. Wavelength converters utilizing FWM in HNLFs have demonstrated impressive performance, achieving broad wavelength tunability and high conversion efficiencies. The use of these devices in modern optical communication systems allows for easy wavelength changes and efficient routing, which are important for creating flexible and expandable networks. Recent studies have also highlighted the enhanced capabilities of phase conjugation techniques leveraging FWM. These techniques effectively mitigate signal distortions caused by fiber nonlinearities and chromatic dispersion, thereby improving signal integrity over long-haul transmissions. The application of phase conjugation in systems using QAM formats has shown a marked reduction in bit error rates and an overall enhancement in system performance [10].

These devices are not only sensitive to SBS as well, but require more stringent SBS mitigation techniques, as idlers inherit double phase shift during FWM process. The methods described in chapter 3 of this thesis can be applied to Wavelength converters and OPCs as well.

2.3 Polarization-insensitive FOPA

Fundamentally, polarization-sensitive FOPAs have limited interest for optical communication systems since optical signals are typically arbitrary polarised and polarization-multiplexed. Several techniques have been proposed to make FOPAs polarization insensitive. For two-pump FOPA, the solution was using orthogonally polarized pumps [47], [64]. The drawback of this technique was maximum gain achievable, as gain coefficient is reduced by a factor of 2 ... 3 as compared to a co-polarized case [5]. For single pump FOPA, polarization-diversity scheme was suggested [65],[66]. The idea

was to split an input signal with arbitrary polarization into two orthogonal linear polarization components using a polarization beam splitter (PBS) and to amplify each of them independently by a corresponding co-polarised pump. Polarization-diversity schemes were investigated in [67] demonstrated the practical potential of technology and applicability for variety of applications (Figure 7).

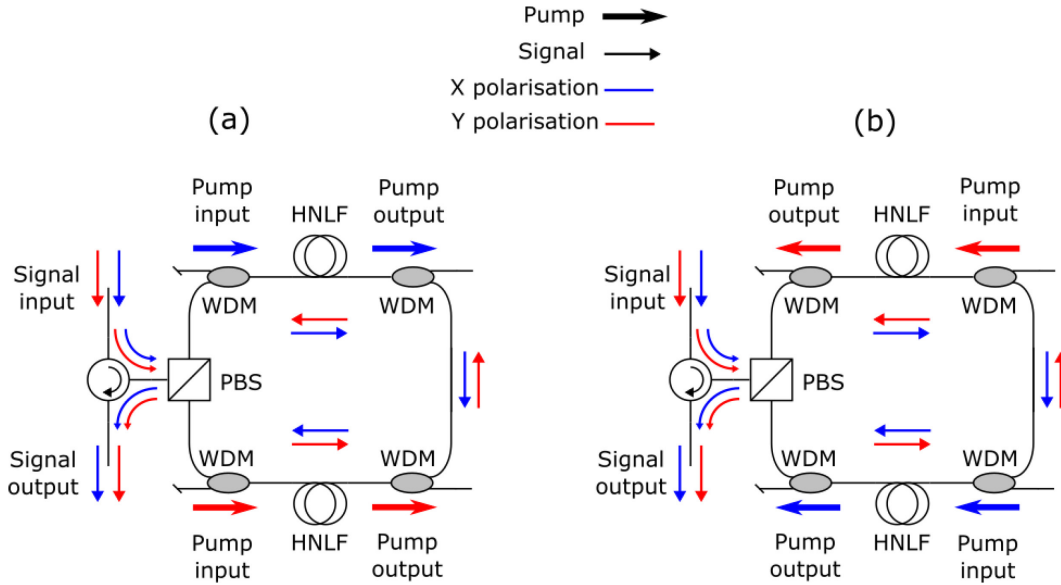


Figure 7. Schematic of a loop diversity architecture for a PI-FOPA: ‘Gain-Loss’ (a), ‘Loss-Gain’(b) [67].

In all configurations under study a signal was split into two orthogonally polarized components using a PBS. Signal components counter-propagate in a Sangac loop and independently but equally amplified within the loop before being recombined. The loop employed two nominally identical HNLF lengths each pumped unidirectionally and therefore amplifying only the signal component co-propagating with a pump. A looped architecture is employed to ensure a stable path matching the two signal components. Nonlinear interaction between counter-propagating dithered pumps was prevented by providing unidirectional gain sections[66] . Signal components first either amplified in first HNLF and then passively propagated through the second HNLF (Figure 7 (a)) or vice versa (Figure 7 (b)). The first approach allowed for minimizing noise figure, while the second mitigated nonlinear impairments in FOPA.

The further development of polarization-diversity loop was design of Mach-Zehnder (MZ) FOPA architecture [68]. In MZ configuration (Figure 8) an input signal component first split into two single-polarization components in first PBS, each component propagating in one of the two arms of the MZ (each containing an independent gain

section), and finally recombined. There is no loop, so the signal components do not propagate through passive sections responsible for losses and nonlinear crosstalk. MZ-FOPA has demonstrated robust amplification of PDM-QPSK 100G WDM signals with signal quality factor Q^2 up to ~ 11 dB or BER of $2 \cdot 10^{-4}$ matching a commercial EDFA performance [69].

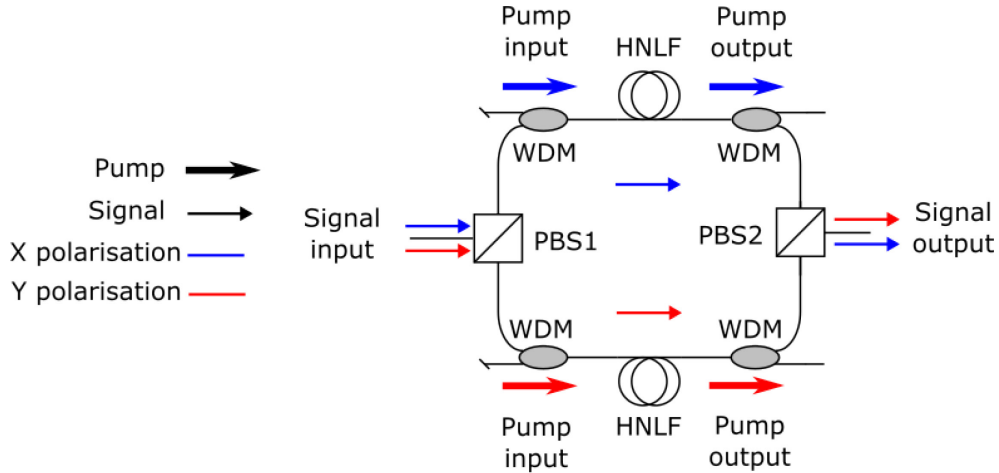


Figure 8. Schematic of a Mach-Zehnder architecture for a PI-FOPA [68].

2.4 Nonlinear crosstalk in FOPA

For WDM signal amplification, where channels are spaced 50-100 GHz apart, the generation of unwanted FWM between signals and/or idlers results in a large number of unwanted FWM products. The nonlinear crosstalk limits the maximum number of channels with a particular FOPA gain. Broadband FOPA operates in the vicinity of the ZDW, where chromatic dispersion is small, allowing signal–signal FWM between closely spaced signals to be very well phase-matched. The idlers also generate unwanted FWM products by interactions among themselves, with the pumps, and with the signals. The overlap between these products and signals causes a nonlinear crosstalk degrading signal SNR. Further discussion will focus on a single-pump FOPA.

The FWM products involving pump are called the 1st order. Nomenclature is taken from [63]. They are generated symmetrically around the pump, occupying the entire WDM bandwidth on both sides of the pump. Products of the 1st-order FWM overlap with signals and idlers only if the guard band is less than the signal band. The FWM products involving only signals and idlers are called 2nd order. They are generated symmetrically around the centre of the signal band, occupying the band three times wider than the signal band. Therefore, signal, and idler bands always overlap with the inner 2nd-order FWM [70]. The

1st-order products have the pump involvement, consequently they have higher power than the 2nd-order products. Figure 9 shows a range of unwanted FWM of 1st and 2nd-order products.

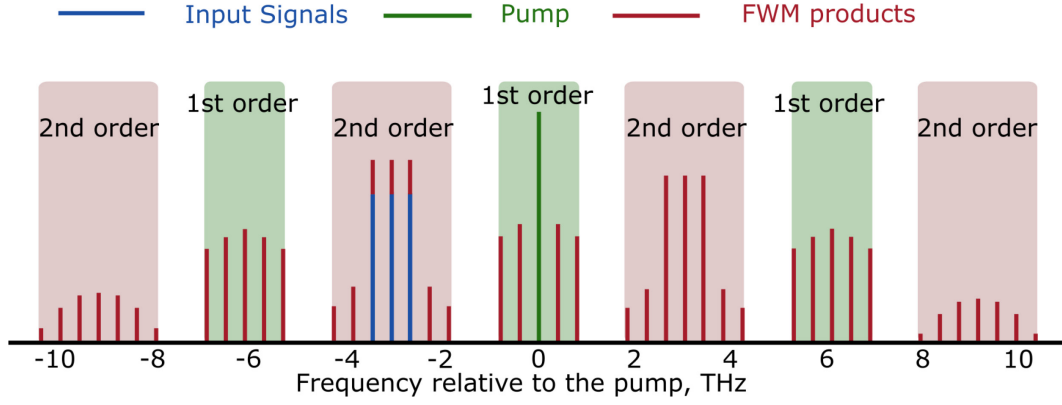


Figure 9. A range of unwanted FWM of 1st and 2nd-order products [70].

The equation (2.8) estimates the number of generated FWM products N_{FWM} for the 2nd-order FWM [63]:

$$N_{FWM} \approx \frac{3}{2} \cdot \frac{N_s}{2} \cdot \left(\frac{N_s}{2} - 1 \right) + 1. \quad (2.8)$$

The power of 1st- and 2nd-order products was derived in [70]:

$$P_{1,FWM} \sim \frac{P_{signal\ out}^2}{P_{Pump}}, \quad (2.9)$$

$$P_{2,FWM} \sim \frac{P_{signal\ out}^3}{P_{Pump}^2}. \quad (2.10)$$

The approximate ratio of the FWM crosstalk power to the signal output power is shown in equations, illustrating how it scales with the number of signals N_s [70]:

$$XT^1 \sim \frac{P_{1,FWM} \cdot N_s}{P_{signal\ out}} \sim \frac{P_{signal\ out} \cdot N_s}{P_{Pump}} \quad (2.11)$$

$$XT^2 \sim \frac{P_{2,FWM} \cdot N_s^2}{P_{signal\ out}} \sim \left(\frac{P_{signal\ out} \cdot N_s}{P_{Pump}} \right)^2. \quad (2.12)$$

The number of 1st- and 2nd-order FWM products overlapping with every signal channel has been shown to scale as N_s^2 and N_s respectively. The impact of unwanted FWM is

independent of gain or signal input power and is defined by the total output signal powers and the pump power.

In real world transmission systems, the WDM channels are weakly phase matched. However, state-of-the-art FOPAs are limited with maximum total output signal power to $\sim 10\text{dBm}$ to keep NF below 6 dB [69].

There were several solutions proposed to mitigate nonlinear crosstalk in FOPA. The polarization-diversity loop design (LG configuration), where low power signal first propagates through the unamplified section and then being amplified in the next section, has been demonstrated to reduce nonlinear crosstalk up to 11.5dB for amplification of 22x100GHz-spaced channels, but causes a significant noise figure penalty (the minimal noise figure measured in this case was 12 dB) [71]. Alternatively, a filter removing idlers can be inserted between two fiber sections to eliminate inter-channel nonlinear crosstalk involving idlers (Figure 10). Nonlinear crosstalk was decreased by 4.5dB in [73] employing this approach without incurring a noise figure penalty.

Raman-assisted FOPA [74],[75] and uneven channels spacing [63] were also suggested to reduce unwanted FWM.

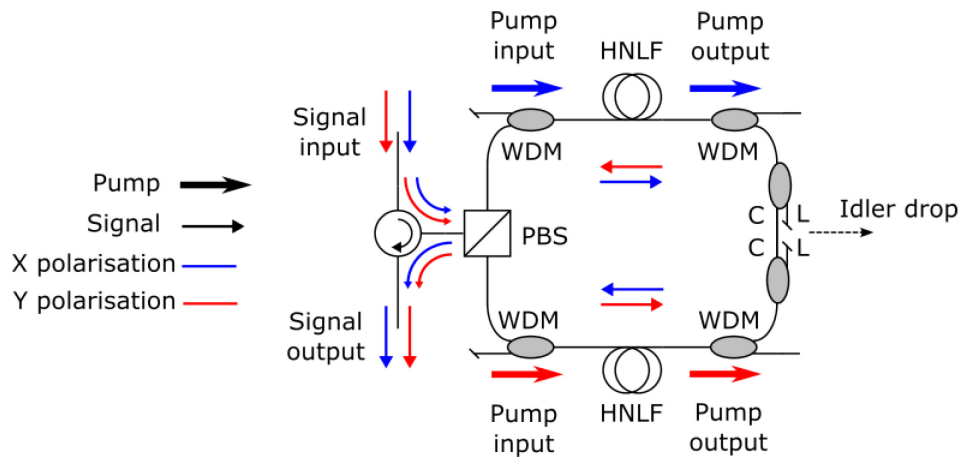


Figure 10. Schematic of a loop diversity architecture for a PI-FOPA with mid-stage Idler removal [73].

The employment of high pump power was proposed to reduce signal–signal FWM and short HNLF to achieve a required gain with additional benefits, such as ZDW fluctuations and random birefringence reduction [71]. However, high pump power cannot be employed until SBS is successfully mitigated, highlighting once again that SBS mitigation is a critical challenge.

2.5 Stimulated Brillouin scattering in FOPA

SBS has a particular importance to optical fiber communication systems and FOPAs, since it severely limits the pump power that can be pumped into a fiber [77]-[79].

2.5.1 SBS phenomenon in optical fibers

SBS manifests through the generation of a Stokes wave that is downshifted in frequency from the pump wave by an amount determined by the nonlinear medium. In the case of FOPAs, this medium is silica HNLF with χ^3 nonlinearity. In single-mode optical fibers, due to their geometry, the generated Stokes wave propagates in the backward direction. When the pump power reaches a certain level, the process becomes stimulated and highly dependent on the pump power. This critical power level, at which the Stokes wave power increases rapidly reaching some limit, is called the SBS threshold. The SBS threshold depends on the optical fiber parameters and pump linewidth, and it plays a major role in FOPA design. This section covers the basic concepts of SBS, including the Brillouin spectrum and Brillouin threshold power.

The process of SBS can be described classically as a nonlinear interaction between the pump and Stokes fields and a thermally excited acoustic wave through the process of electrostriction [25]. The backscattered Stokes light interferes with the input pump light and generates an acoustic wave through the effect of electrostriction [76]. The acoustic wave produces density modulations that in turn modulate the refractive index of the medium. This pump-induced index grating scatters the pump light through Bragg diffraction. The forward propagating acoustic wave acts as a Bragg grating, which scatters even more light in the backward direction. Scattered light is downshifted in frequency because of the Doppler shift associated with a grating moving at the acoustic velocity. The same scattering process can be viewed quantum mechanically as if annihilation of a pump photon creates a Stokes photon and an acoustic phonon simultaneously. As both the energy and the momentum must be conserved during each scattering event, the frequencies, and the wave vectors of the three waves are related by [25]

$$\Omega_B = \omega_p - \omega_{St}, \mathbf{k}_A = \mathbf{k}_p - \mathbf{k}_{st}, \quad (2.13)$$

where Ω_B is the angular frequency shift of the Stokes wave and \mathbf{k}_A is the wave vector of the acoustic wave, ω_p is pump frequency and ω_{St} is Stokes frequency, and \mathbf{k}_p is pump wave vector and \mathbf{k}_{st} is Stokes wave vector.

The Brillouin frequency shift is derived from Ω_B as:

$$v_B = \frac{\Omega_B}{2\pi} = \frac{2n_p v_A}{\lambda_p}. \quad (2.14)$$

For silica fibers $v_B \approx 10.5 - 11.1$ GHz, where $n_p = 1.45$ is the effective mode index at the common pump wavelength $\lambda_p = 1550$ nm and $v_A = 5.96$ km/s is typical for silica fibers the velocity of acoustic waves [25].

The growth of the Stokes wave is characterized by the Brillouin gain spectrum. This spectrum has a relatively small spectral width, approximately between 20 MHz and 50 MHz. The width is defined by the lifetime of the acoustic phonons in optical fibers, which is typically $\Gamma_B^{-1} < 10$ ns [80]. For the continuous wave case the Brillouin gain coefficient has a Lorentzian spectrum as in [25]:

$$g_B(\Omega) = \frac{g_p(\Gamma_B/2)^2}{(\Omega - \Omega_B)^2 + (\Gamma_B/2)^2}, \quad (2.15)$$

with peak value at the Brillouin frequency shift of Ω_B :

$$g_p = g_B(\Omega_B) = \frac{4\pi^2 \gamma_e^2 f_A}{n_p c \lambda_p^2 \rho_0 v_A \Gamma_B}. \quad (2.16)$$

Parameters in the equation are the material density $\rho_0 = 2210$ kg/m³, the electrostrictive constant of silica $\gamma_e \approx 0.902$ and the fraction f_A , by which the SBS gain is reduced if the acoustic and optical modes do not fully overlap inside the fiber [25].

The Brillouin gain is:

$$G_B = \frac{g_B P L_{eff}}{A_{eff}}, \quad (2.17)$$

where $L_{eff} = [1 - \exp(-\alpha L)]/\alpha$ is the effective fiber length.

2.5.2 Concept of the SBS threshold

SBS occurs at some critical pump power launched into optical fiber. The backreflected Stokes power has an exponential dependence on the input pump power. Once SBS occurs, and the pump is reflected to the input end of the fiber, so the forward traveling pump is attenuated and the pump intensity noise is increased [81],[82].

A weak Stokes wave grows from noise, provided by spontaneous Brillouin scattering occurring throughout the fiber, and experiences amplification through SBS process by virtue of the gain g_B .

In literature the Brillouin threshold is defined at a critical pump power P_{th} [26],[25],[78],[79]

$$P_{th} = \frac{21K A_{eff} \Delta\nu_P \otimes \Delta\nu_B}{g_B L_{eff} \Delta\nu_B}. \quad (2.18)$$

For the case where $\Delta\nu_B \ll \Delta\nu_P$, $\Delta\nu_B$ is the Brillouin linewidth, $\Delta\nu_P$ pump laser linewidth, K is the pump polarization factor. In case when pump laser linewidth as well as Brillouin linewidth has a Lorentzian profile, $\frac{\Delta\nu_B}{\Delta\nu_P}$ can be substitute with $\frac{\Delta\nu_B}{\Delta\nu_P + \Delta\nu_B}$ [77].

The number 21 was derived in [83] as a natural logarithm of the SBS gain required to amplify the spontaneous emission to the level of input pump power. That means that once the pump power reaches the defined Brillouin threshold, it is completely depleted, and backward propagating Stokes wave carries most of the input pump power. However, for FOPA, the SBS threshold should be defined to prevent notable pump degradation. The practical approach, where the pump power should be kept below a fraction of the maximum pump power launched into the optical fiber. This fraction can be chosen as 1% or 0.1% of maximum pump power depending on FOPA design requirements. For example, Figure 11 shows measured backscattered pump power versus pump power in blue and the fitted curve in red. The dotted curve was measured with $L = \sim 55 \text{ m}$, $\Delta\nu_B = 28 \text{ MHz}$ (for silica fiber [80]), $\Delta\nu_P = 1600 \text{ MHz}$.

The eq.(2.18) can be rewritten considering practical definition of the SBS threshold by reducing coefficient 21 on $\ln(100)$ to be 16 [26]:

$$P'_{th} = \frac{16 K A_{eff} \Delta\nu_P \otimes \Delta\nu_B}{g_B L_{eff} \Delta\nu_B}. \quad (2.19)$$

The equation above shows that SBS threshold depends on peak value of Brillouin linewidth g_B , effective mode area A_{eff} and effective fiber length L_{eff} and relation between pump laser linewidth $\Delta\nu_P$ and Brillouin linewidth $\Delta\nu_B$. SBS gain coefficient g_B is also affected by fiber parameters: material density ρ_0 , the electrostrictive constant of silica γ_e , the fraction of overlapping acoustic and optical modes, acoustic velocity v_A , and silica refractive-index n . It also depends on the longitudinal fiber uniformity.

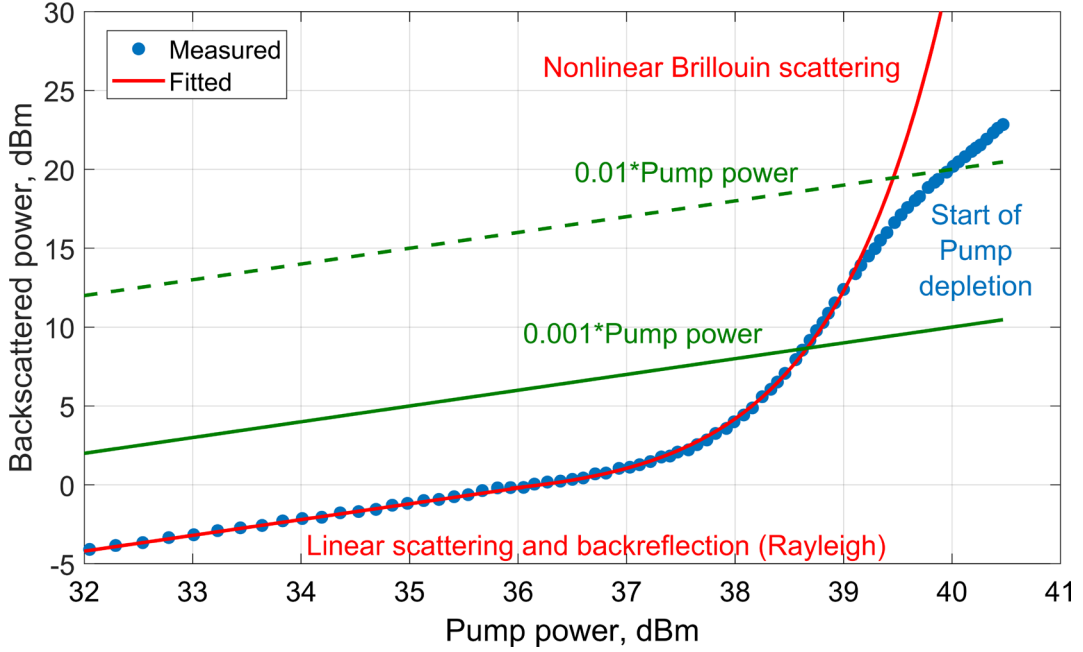


Figure 11. Backscattered power versus pump power: the measured points(blue), the fitted curve (linear+exp) (red), SBS Threshold is defined as a pump power at the intersection of green and blue curves.

For a long span of a standard single-mode fiber ($L_{eff}=20$ km) and a narrow linewidth ($\Delta\nu_P \ll \Delta\nu_B$) pump, the P_{th} was estimated to be only a few mW [84]. This level of power is not enough to invoke significant SRS or the third-order nonlinear effects. Therefore, SBS appears to be the predominant nonlinear phenomenon for narrow linewidth pumps propagating through long fibers.

To estimate the SBS threshold for FOPA design more precisely, several additional factors should be considered. Significant pump instabilities may rise at a threshold level significantly lower than typically needed for SBS with a stronger pump. This occurs because counterpropagating waves within a Brillouin-active medium become temporally unstable above a certain threshold intensity [85].

With such a low SBS threshold, the nonlinear phase shift is expected to be within $\Phi_{th,1\%} = 0.2 - 0.3$ rad for a range of HNLF [5], [19], [26] limiting the maximum phase-insensitive FOPA gain to be $G_{max.th}=0.4$ dB, and phase sensitive $G_{max.th}=2.6$ dB, while the nonlinear phase shift of 3 is required to reach a peak FOPA gain of 20 dB. Thus, the SBS threshold must be increased by a factor of at least 10 to allow for a single stage FOPA with gain up to 20 dB [66]. In practice the SBS threshold increase by a factor of >20 is required [66]. Since both SBS and FWM are nonlinear phenomena based on third-order

nonlinearity, the maximum nonlinear phase shift depends on γ , P (P'_{th}) and L_{eff} for both. Therefore, it is important to increase P'_{th} without compromising γ and L_{eff} .

2.5.3 SBS mitigation principles

The SBS mitigation techniques can be divided into two categories: passive and active. Passive methods rely on the dependence of the SBS gain and threshold on the properties of the optical fiber. The main idea of these methods is broadening the effective Brillouin gain bandwidth $\Delta\nu_B$ thus reducing the Brillouin peak gain g_B by applying a nonuniform Brillouin frequency shift distribution to an optical fiber.

The most known passive techniques for the past twenty years are changing the core diameter along the length of a fiber, changing the dopant concentration in the fiber, introducing temperature gradients along the fiber, designing acoustically guiding and antiguiding refractive index profile, introducing longitudinal strains, using isolators, and Fiber Bragg Gratings. Variations in fiber parameters along the fiber length are helpful in controlling the SBS threshold as the inhomogeneous Brillouin shift along the fiber length shifts by more than the SBS gain bandwidth, the Stokes will cease to grow after the shift because of a substantial reduction in the Brillouin gain. Brillouin gain bandwidth ν_B depends on both the acoustic velocity v_A and the mode index n_p at the pump wavelength, and it can be shifted if one of these parameters changes along the fiber length.

Active SBS mitigation is achieved by broadening the linewidth of the pump laser $\Delta\nu_p$ by phase or frequency modulation. This technique allows to increase SBS threshold more than 15 dB and was employed in high power laser system with pump power of several Watts.

2.5.4 Fibers with a nonuniform core diameter and co-doping in the fiber core

Backscattered light appears from interaction between acoustic modes and the optical modes. The reduction of Brillouin gain by 3.6 dB (SBS threshold increase of 3.6 dB) was done by nonuniform frequency shift of 49 MHz over the entire fiber [27].

In optical fibers the core is usually doped to change its refractive index. Nonuniform doping of the fiber core along the fiber length with Germanium and fluorine shifts Brillouin gain peak along the fiber length decreasing Brillouin Gain. SBS threshold increases with increase of the change in the relative index of doped-core fibers. For example, the change in the relative index of 0.7% results in SBS threshold increase more than 15 dB being provided by the dopant change ratio of 0.0032%/km [87]. However, to achieve such a large SBS threshold increase, several km of fiber is required. The losses would increase as 0.03

and 0.02 dB/km/% for GeO₂ and F dopants, respectively, as excess Rayleigh scattering loss was induced due to the addition of dopants throughout the fiber cross section. The dispersion of the fiber would decrease by -2.4 ps/km/nm/%, which is unacceptable for FOPA operation. Despite the study about increasing SBS threshold by varying both fiber core radius and dopant concentration along fiber length to keep uniform chromatic dispersion with dispersion slope of 0.058 ps/km/nm [86]. The resulting SBS threshold increase was only 4 dB of a 10.0-km long conventional dispersion-shifted fiber (DSF), which is not acceptable for FOPA as well.

Variations in the doping along the radial direction of a fiber core led to changes in the acoustic velocity in that direction, resulting in the Brillouin gain changes. Doping fiber with Aluminum and Germanium demonstrated 6 dB improvement in SBS threshold by increasing the acoustic loss, or by decreasing the overlap integral between the optical and acoustic fields [28]. The overlap integral can be controlled by fiber refractive index profile design and acoustic velocity profile design. The acoustic loss can be controlled by glass composition design. The overlap integral between the optical and acoustic fields is proportional to $\frac{\Delta v_B}{\Delta v_P + \Delta v_B}$ in eq. The acoustic modes that contribute to the Brillouin scattering propagate with a unique phase velocity, and therefore, a unique Brillouin shift. If there are many of these acoustic modes, then the Brillouin spectrum is spread over all these acoustic modes. This leads to broadening of the Brillouin spectrum, and thus an effective decrease in g_B , therefore leading to an increased Brillouin threshold [28]. Doping fibers with the Al reduce the SBS gain coefficient g_B on 7 dB relative to the Ge doped fiber, so a corresponding 7 dB increase in the SBS threshold power. Which makes use of Al-doped fibers preferable. This technique was applied to HNLF with 6 dB decrease in SBS gain compared to Ge-doped HNLF. However, the decrease in nonlinear refractive index by 1.2 dB reduces the improvement in the SBS threshold increase to 4.8 dB [88]. Al-doped fibers with alumina content approximately 54 mole % potentially suppress Brillouin gain by 15 dB compared to conventional SMF as predicted in [89]. Nevertheless, one must be aware of historically high loss of Al-doped fibers, which was significantly decreased from 15 to 0.78 dB/km [90]. The typical effective mode area A_{eff} is 11.2-13.5 μm^2 and nonlinear parameter γ is approximately 0.0065-0.0074 $\text{W}^{-1}\cdot\text{m}^{-1}$, which is lower than state-of-the-art 0.008- 0.0014 $\text{W}^{-1}\cdot\text{m}^{-1}$ [19]. Trade-off between the core diameter, nonlinear refractive index n^2 and the Brillouin gain coefficient must be considered when fabricating Al-doped fiber for FOPA.

Overall, the maximum γPL achieved with Al-doped fibers is ~ 1.2 rad – 4-6 times increase of the SBS threshold, which is insufficient for amplification just by itself. Further SBS suppression is possible if Al-doped fiber will be accompanied by strain distribution along the fiber length [88], [91].

2.5.5 Fibers with a nonuniform strain and temperature distribution

When axial strain is applied to the fiber uniformly along its length, SBS frequency shifts and Brillouin gain bandwidth expands. When the fiber strain is not uniform and varies along the fiber length, the SBS shift is distributed, so Brillouin gain is decreased. SBS threshold increase of ~ 7 dB was reported by applying this technique [92]. The SBS threshold will increase depending on strain coefficient as relation of the elongation to the initial length in percentage [92],[93]. The strain can be applied with coefficient up to 3% resulted in SBS threshold increase by 15 - 17 dB, by broadening Brillouin gain bandwidth up to 1400 MHz [93]. In general, such fiber strain changes ZDW dramatically, reaching 11-13.8 nm. This is not acceptable when using HNLF for FOPA, as parametric gain bandwidth is limited to maximum 5 nm [96]. To address this issue, the strain control techniques have been proposed to mitigate or cancel the induced dispersion change [29], [94]. Both ZDW shift and SBS suppression by strained fiber can be combined to optimize gain and bandwidth of FOPAs and other parametric devices [94], [95]. For example, designed dispersion decreasing HNLF with dispersion shift from 0.6 to 0.02 ps/nm/km along the fiber length performed the uniform dispersion after applying the strain distribution [29]. The SBS threshold increase was 7.2 dB. Even though this approach allows for broadening the FOPA bandwidth up to 40 nm, as demonstrated in [95], it should be noted that pump dithering was necessary in that work to further increase the SBS threshold. Overall, simply fabricating HNLF and applying strain is not sufficient for high-gain FOPA.

The similar SBS mitigation method is to apply different temperature distributions along the fiber as the Brillouin frequency shifts with temperature gradient applied. The SBS threshold increase was estimated to be 4.8 dB with a temperature difference of 140°C and can be increased up to 8 dB with a temperature difference of 350°C [30]. The ZDW shifts with 0.062 nm/°C, it will be shifted on 8.68 nm in 100-meter long HNLF. Despite this shift less than in strained fiber, it will decrease FOPA gain bandwidth as well. The ZDW shift in HNLF can be compensated if HNLF will be segmented of dispersion-decreasing HNLF and dispersion-flattened HNLF spliced together. Both HNLF have different SBS shift frequencies, their distribution will increase the SBS threshold by 2.1-dB compared to each HNLF separately [97].

2.5.6 Fibers divided by optical isolators

The SBS can be mitigated more by using optical isolators which suppresses the backscattering power of the SBS. This technique can be combined with other techniques based on the narrow linewidth of the Brillouin gain. Isolators cut off the backscattered light in every fiber segment, so the SBS is mitigated. When the $(N + 1)$ fiber sections are connected by N isolators, the interaction between fiber sections is absent and the SBS threshold power is increased by a factor $(N + 1)$ [31].

FOPA net gain of 10 dB within 3 nm 3-dB bandwidth has been achieved employing this method [31]. SBS threshold increase was 11 dB by combining four pieces of standard HNLf spliced together with isolators separating them. It must be noted that all pieces were strained gradually to have improved SBS threshold by 6 dB and SBS threshold increase from isolator was 5 dB [31]. Further this technique had been improved to allow for 16 dB FOPA net gain [100].

The added loss must be considered when adding isolators and additional splices. Moreover, the isolator's pigtails have dispersion different from HNLf.

2.5.7 Fibers with fiber Bragg gratings

One more scheme for SBS suppressing in optical fibers is employing tilted fiber Bragg gratings (TFBGs). A specially designed TFBG operates as ultra-narrow spectral filter, providing high loss at the Brillouin frequency shift, suppressing backscattered SBS more than 10 dB [32]. However, the reported pump laser power was increased by about 33% or 1.2 dB [32]. The TFBG disadvantage is the transmission spectrum drifting due to the temperature change.

2.5.8 Pump phase modulation with sine tones

Pump phase modulation or pump dithering, using a combination of radio-frequency (RF) tones at different frequencies, effectively mitigates SBS by broadening the pump linewidth $\Delta\nu_P$ beyond the Brillouin gain bandwidth $\Delta\nu_B$. As the power of a pump phase modulated with sine tones remains constant, but its power is uniformly distributed between equally spaced discrete lines in the frequency domain.

The simple sine wave driven phase modulator is described as

$$E = |A| \cos\left(\omega_c t + \varphi_c + \frac{\pi}{V_\pi} \{A_m \cdot \sin(2\pi f_m t + \varphi_m)\}\right). \quad (2.20)$$

Where ω_c is the input optical carrier frequency, φ_c - its phase. V_π is the voltage required to modulate the phase by π . A_m is the phase modulation amplitude of an applied sinusoidal signal, $2\pi f_m$ its frequency and φ_m its phase.

As this is a periodic signal, the corresponding optical spectrum is composed of uniformly separated spaced Dirac peaks [101]:

$$E = |A| \sum_{n=-\infty}^{\infty} J_n \left(\frac{\pi}{V\pi} m \right) \cos(\omega_c t + \varphi_c + n2\pi f_m t + n\varphi_m), \quad (2.21)$$

$J_n \left(\frac{\pi}{V\pi} m \right)$ is the Bessel Function of the first kind with order n [101]. The spectrum of the electric field E is Fourier Transform of eq.(2.21).

The resulting Amplitude spectrum is uniformly separated frequencies. The order of Bessel function connected with the number of tones and the argument of Bessel function defines the modulation amplitude of tone. The 5 first Bessel functions and the power spectrum of electric field $P(v) = |A|^2$ are shown on the Figure 12.

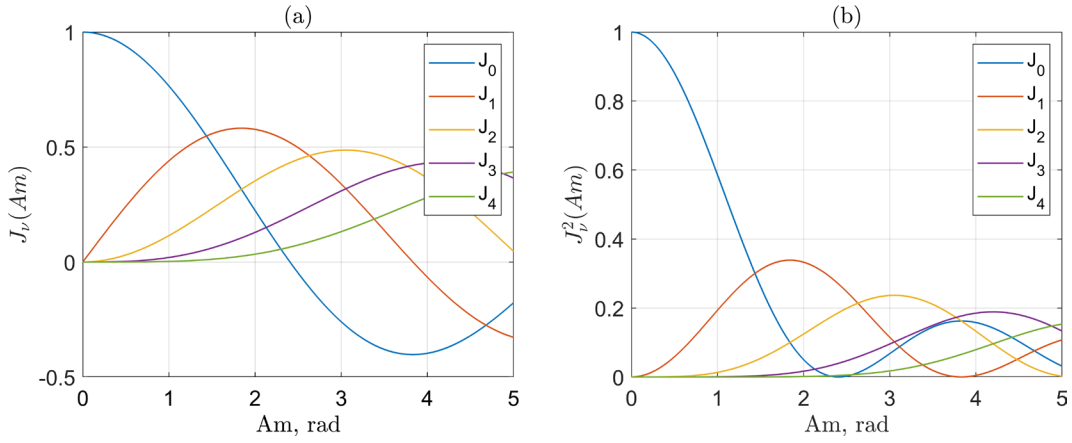


Figure 12. Bessel functions of first kind (a), Spectral Power of harmonics (b).

Pump phase modulation with an amplitude Am of ~ 1.43 rad splits the pump into 3 equal power lines of zero and first orders spaced with the modulation frequency as such modulation amplitude is the cross point of the Bessel functions J_0 and J_1 leading to equal power of the carrier and the side lobes (Figure 13).

Pump phase φ_p modulated with N sinusoidal tones is shown by equation (2.22), where the $f m_n$ is the modulation frequency of the n -th tone:

$$\varphi_p(t) = Am \cdot \sum_{n=1}^N \sin(2\pi \cdot f m_n \cdot t). \quad (2.22)$$

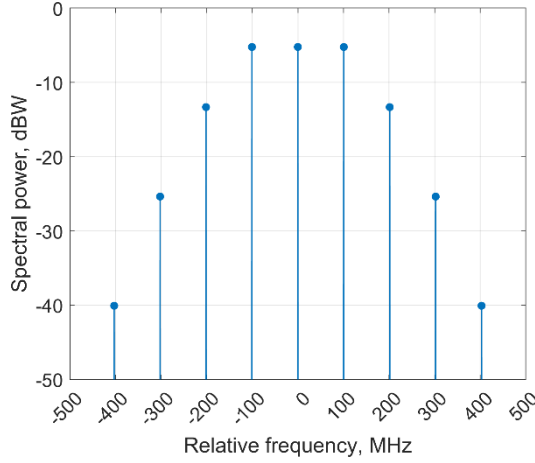


Figure 13. Simulated Power spectrum with $Am=1.43$ and $fm= 100$ MHz.

Pump phase modulation with sinusoidal tones can be very effective because it provides control over the pump bandwidth and uniformity of the spectrum by applying a voltage equal to amplitude Am of $1.43V_{\pi}$ for each individual tone [102]. Therefore, pump phase modulation with N sine tones in the electrical frequency spectrum splits the pump into 3^N first order lines in optical spectrum. High order harmonics are much weaker and usually are not taken into account. If the frequency of the n -th tone is three times the frequency of the $(n-1)$ -th tone, then all first order lines are equally spaced with the frequency of the lowest tone, which called the base tone. If the base tone frequency is larger than the Brillouin gain bandwidth $\Delta\nu_B$, then the pump power is split between $3N$ tones which do not interact via Brillouin, and consequently the SBS threshold increases by a factor of 3^N . The most common number of tones employed by FOPAs is three or four. Three tones allow to increase the SBS threshold by a factor up to 27, more than a factor of ~ 20 required for high gain FOPA applications [66]. Four tones allow even more spectral power distribution within same total pump bandwidth and thus more efficient SBS mitigation by a factor up to 81 in theory. The total pump bandwidth is defined as the bandwidth occupied by the first order lines. It is equal to twice the sum of all modulation frequencies fm_n

$$\Delta f_{total} = 2 \cdot \sum_{n=1}^N fm_n. \quad (2.23)$$

Tones with a non-integer multiplication factor between them prevent the Bessel function harmonics from overlapping, resulting in flatter pump spectrum. Figure 14 shows pump spectra simulated with different modulation frequencies reported from literature assuming that the modulation amplitude is $Am=1.435$ [102], [55], [6], [57], [103],[44].

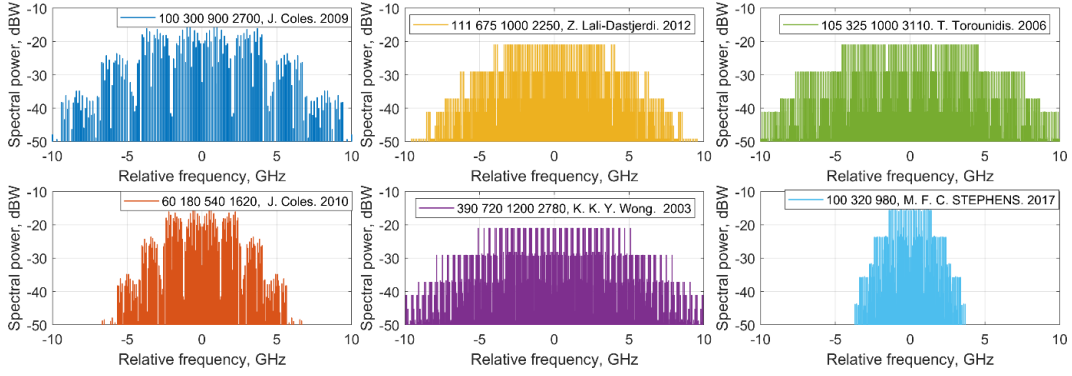


Figure 14. Examples of phase modulated pump spectra from literature (from left to right [102],[55],[6],[57], [103],[44]), modulation frequencies are listed in MHz, $A_m=1.435$.

The multiplication factor should be close to 3 to allow for almost equal spacing between the first-order harmonics and their combinations and thus to achieve the highest bandwidth efficiency. In other words, the resulting pump bandwidth must have the highest spectral filling ratio, while being just broad enough to achieve the required SBS threshold increase in FOPA.

2.5.9 Alternative phase modulation

Continuous pump spectrum can be achieved by means of the deterministic linear sinusoidal chirp waveform [57], phase modulation with white or thermal noise [104],[104] or pseudo-random bit sequence (PRBS) phase modulation [104].

Phase modulation with linear sinusoidal chirp is derived as

$$\varphi_p(t) = A_m \cdot \sin(2\pi \cdot (f_m + C \cdot t) \cdot t), \quad (2.24)$$

where C is the chirp rate, the rate at which the frequency increases or decreases. The frequencies must be consecutive and separated by more than Brillouin gain bandwidth, for the same reason as first order lines in subsection 2.5.8. The switching time between the consecutive modulation frequencies should be shorter than 10 ns (the phonon lifetime τ_p in the HNLF) to provide efficient SBS mitigation [57]. However, the flat pump spectrum with optical power uniformly distributed can be achieved by increasing modulation amplitude of the driving electrical waveform to be many times greater than the $V\pi$ voltage of the phase modulator. For example, for a FOPA employing an HNLF with Brillouin linewidth of ~ 25 MHz, the chirp rate must be 25 MHz/10 ns or 2500 THz/s to obtain a pump bandwidth of several GHz, which is practically complicated. Figure 15(a) shows the phase over time for a phase modulated by a chirp with a chirp rate of 534 THz/s, varying the modulation frequency from 50 MHz to 400 MHz over 600 ns. The phase distribution is

illustrated with a modulation amplitude of $A_m=1.435$ and an overdriven modulation amplitude $A_{m_{\text{overdriven}}} = 6 \times A_m$.

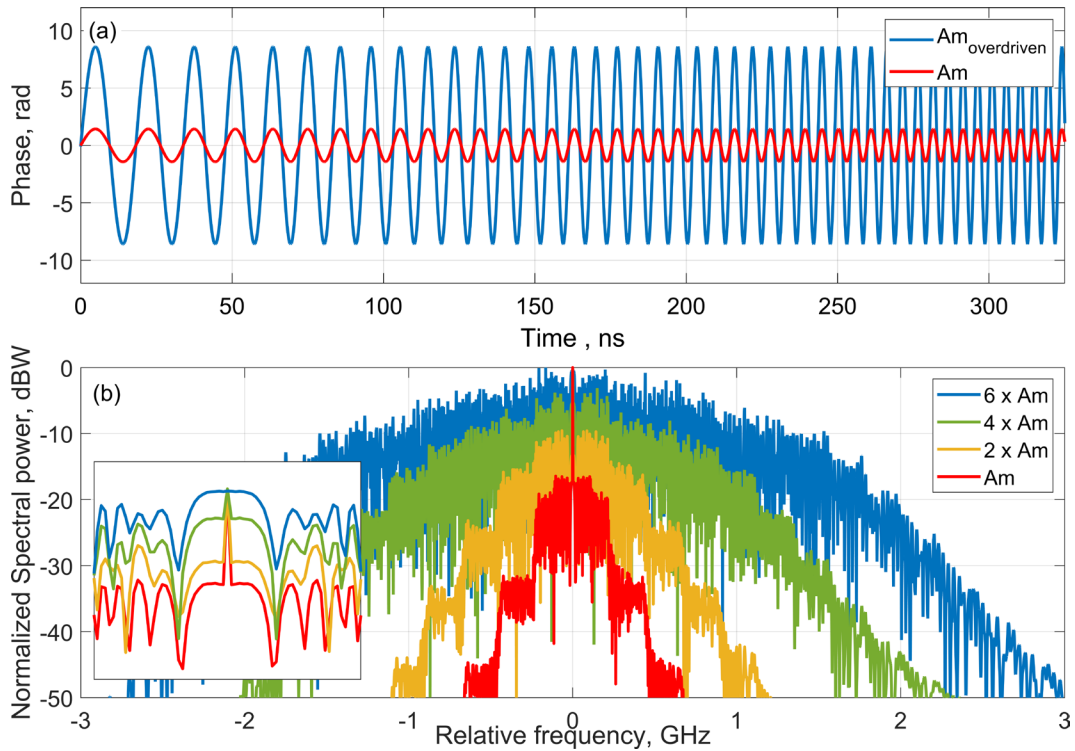


Figure 15. The phase over time (a) and Spectra (b) with different modulation amplitudes of chirped phase modulation with a chirp rate of 534 THz/s and frequency varying from 50 MHz to 400MHz over 600 ns. The insert shows the magnified spectra.

Figure 15(b) shows the spectra plotted with different modulation amplitudes, indicating that it is necessary to operate in the overdriven mode to achieve carrier suppression [57].

Phase modulation with white noise provides a bandwidth efficient electrical and optical pump spectrum, densely occupying the whole spectral shape [57]. The shape and bandwidth of continuum optical spectrum depends on the combination of RF low pass filter, modulation amplitude and RF amplification [104]. A white-noise source is sent through a RF low pass filter with a pass band control mechanism, and then through an RF amplifier. In case of true white noise source, the noise is generated randomly, the spectral modes do not have defined spacing, resulting in an almost continuous spectrum. Figure 16(a) shows electrical low pass filtered at 1.3 GHz spectrum of white noise and. Figure 16(b) shows optical spectrum with spectral width at the -10 dB of 2.6 GHz.

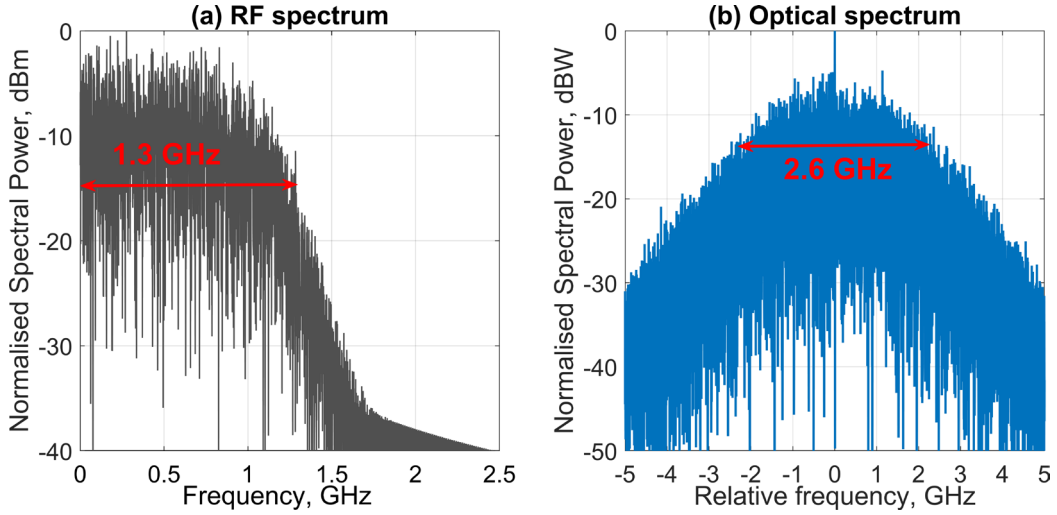


Figure 16. RF spectrum being low pass filtered at 1.3 GHz (a) and optical spectrum of phase modulated by white noise (b) [105].

The maximum SBS threshold increase in dB in this case can be approximately estimates via ratio between pump bandwidth $\Delta\nu_p$ and Brillouin gain bandwidth $\Delta\nu_B$, defined at the same level of spectral power as

$$\Delta P_{SBS}^{th} = \left(1 + \frac{\Delta\nu_p}{\Delta\nu_B}\right). \quad (2.25)$$

In [105] pump was phase modulated with a power spectral density in the 10 MHz to 18 GHz range and filtered to have an optical pump bandwidth of 2.6 GHz. The SBS threshold was reported to be 29 dBm, and the FOPA on/off gain was 16 dB.

When the pump phase is modulated with is pi-binary phase-shift-keying PRBS, optical spectrum shape and width is a function of the modulation frequency and the PRBS pattern length. The PRBS pattern length is $2^n - 1$, where n-an integer. So, the $2^n - 1$ patterns contain every possible combination of n number of bits 0 and 1. The bits 0 and 1 represent modulation amplitude of 0 and π , and temporal spacing between each bit is determined by the modulation frequency f_m of the PRBS generator [104]. The bit rates of PRBS generator are in the range 3–10 Gb/s. The pump spectral peaks are separated by $\Delta\nu = f_m / (2^n - 1)$. The rise time T_r is time during which pump phases change from 10% to 90% and the falling time is vice versa. It must be below 100 ps to provide a carrier suppression. Which means that frequency at the trailing edges reaches up to 40 GHz. The phase is changing as raised cosine at the trailing edges shown by

$$\varphi_p(t) = \frac{\pi}{2} \left(1 - \cos \left(\frac{\pi \cdot t}{T_r} \right) \right). \quad (2.26)$$

Figure 17 shows an example of PRBS modulated phase with data rate of 3GHz/s and time with rise time of 30ns (a) and its spectrum (b).

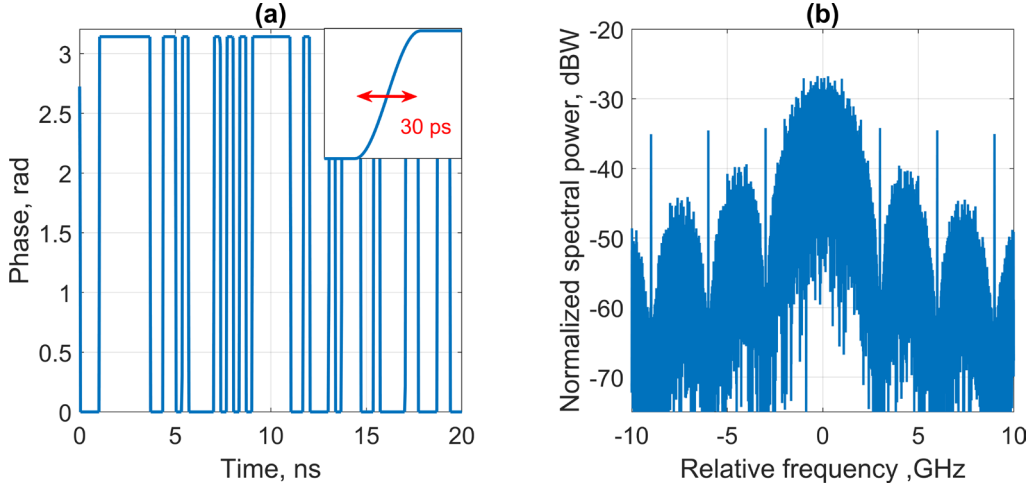


Figure 17. Phase modulated by PRBS over time with inserted rising edge by the eq. (2.27) (a) and its optical spectra (b).

2.5.10 Summary on SBS mitigation principles for state-of-the-art FOPA design

Passive SBS suppression methods alone allow for SBS threshold increase from 2 to 11 dB could be not enough to reach high FOPA gain of 20 dB and above. High FOPA gain has been reported when passive methods were combined with pump phase modulation. For example, combining nonuniform strain with phase modulation allowed to achieve 20 dB FOPA gain in [95], while combining temperature distribution in HNLF with phase modulation resulted in 35 dB gain in [106]. Additionally, inserting an isolator between two segments of HNLF, along with pump phase modulation, enabled a FOPA gain of 60 dB in [103]. However, if the SBS threshold increase is accompanied by the chromatic dispersion nonuniform distribution along the fiber length, this prevents from satisfying phase-matching condition and dramatically limits FOPA gain bandwidth. Overall, proposed passive techniques for the SBS threshold increase require additional compensation of dispersion nonuniform distribution along the fiber, reduction of nonlinear coefficient or increased fiber losses. Despite simple implementation into FOPA design due to the lack of necessary additional components, the FOPA performance limitation makes them less preferable. Described techniques are well suited for other low-gain parametric devices as wavelength converters [95],[96], [97] or OPC [91].

The Table 1 below summarizes the passive and active technique’s impact on FOPA performance.

Table 1. Comparison of SBS mitigation techniques for state-of-the-art FOPA

	Incurs dispersion variation	Incurs additional insertion loss	Max demonstrated SBS threshold increase	Demonstrated with high gain FOPA
Nonuniform core diameter	yes	no	3.6 dB [27]	no
Nonuniform dopants	yes	no	6 dB [28]	no
Doping with Aluminum	possibly	slightly/ significantly	4.8 dB [88], 15 dB [89]	no
Nonuniform strain	yes	no	7.2 dB [29]	yes, 16 dB gain in combination with isolators [100]
Nonuniform temperature	yes	no	4.8 dB [30], 6dB [98]	no
Optical isolators	slightly	significantly	5 dB [31]	yes, 16 dB in combination with strain [100]
Tilted fiber Bragg gratings	no	slightly	1.2 dB [32]	no
Pump phase modulation	indirectly	no	20 dB [6]	Yes, 70 dB gain [6]

Based on the table, pump phase modulation offers a significant SBS threshold increase of up to 20 dB without additional insertion loss. The phase modulation system is a separate module, which can be considered a black box for FOPA design, with just input and output for the pump. Therefore, I consider pump phase modulation as the optimal technique to overcome SBS and design high-gain and broadband FOPAs. However, OSNR penalty have been observed during signal amplification by FOPA with phase modulated pump. This highlights the need for a deeper investigation into what causes these penalties and their impact on FOPA performance.

2.5.11 Impact of pump phase modulation on FOPA performance

Several theoretical and experimental papers have shown that pump phase modulation causes temporal variations in FOPA gain. These gain variations occur due to instantaneous pump frequency modulation, which is the first derivative of the pump phase $d\phi_p(t)/dt$. The parametric gain becomes time-dependent as the phase-matching condition fluctuates,

and small variations in pump power are transferred to the signal and idler through changes in FWM.

The parametric gain coefficient from eq.(2.4) can be rewritten as

$$g(t)^2 = -\Delta\beta \left(\gamma P + \frac{\Delta\beta}{4} \right). \quad (2.28)$$

It becomes time-dependent due to the instantaneous phase mismatch $\delta\beta(t)$ induced by the phase modulation of the pump as suggested in [33]:

$$g(t)^2 = -(\Delta\beta + \delta\beta(t)) \left(\gamma P + \frac{\Delta\beta + \delta\beta(t)}{4} \right). \quad (2.29)$$

The instantaneous phase mismatch $\delta\beta(t)$ depends on the derivative of the pump phase $\frac{d\varphi_p(t)}{dt}$ and the fiber dispersion slope β_3 [33]:

$$\delta\beta(t) = \beta_2 \frac{d\varphi_p(t)}{dt} - \beta_3 \left(\frac{d\varphi_p(t)}{dt} \Delta\omega^2 + \frac{1}{3} \left(\frac{d\varphi_p(t)}{dt} \right)^3 \right) + \frac{\beta_4}{12} \left(\frac{d\varphi_p(t)}{dt} \right)^4 + 6 \left(\frac{d\varphi_p(t)}{dt} \right)^4 \Delta\omega^2. \quad (2.30)$$

It can be observed that when the first derivative of the pump phase $d\varphi_p(t)/dt = 0$, the parametric gain coefficient for a monochromatic pump wave remains constant and all time-dependent components disappear for $\beta_3 = 0$.

The level of parametric gain variations increases with the signal frequency offset from the pump. The maximum signal degradation occurs at the outer slopes of the gain curve, where the gain slope with respect to the signal wavelength is the steepest. Conversely, the minimum signal degradation is observed near the pump wavelength, where the gain is parabolic and less sensitive to the phase-matching variations induced by the pump frequency dithering [35].

If the Pump is located with the distance from the ZDW of the fiber, it experiences a dispersion inside the fiber during propagation, as a result pump phase modulation is converted into amplitude modulation (PM-to-AM conversion) through the group-velocity dispersion. The similar process occurs when the filtering is applied to the phase modulated pump [36]. This PM-to-AM conversion process makes pump powers vary with time and transfer this fluctuation to the signal and idler through the FWM process. However, for single broadband FOPA, the offset between pump wavelength and ZDW is designed to be very small < 1 nm and HNLF length is ~ 100 m, so the PM-to-AM conversion is negligible. On the other hand, as the pump wavelength approach ZDW, the gain variations increase as small variations of ZDW produce larger variations of the shape of the gain spectrum.

Overall, there is a trade-off between the gain bandwidth and the signal degradation in FOPA with a phase-modulated pump.

The signal degradation caused by pump phase modulation can be expressed through Q penalty in dB as shown in [35]:

$$\Delta Q = 10 \log \left(\sqrt{1 + Q_i^2 \frac{\sigma_G}{\langle G \rangle}} \right), \quad (2.31)$$

where Q_i (dB) is reference level of Q factor, σ_G is the standard deviation and $\langle G \rangle$ is the mean of the parametric gain variations. Figure 18 shows the Q penalty distribution across FOPA gain spectrum analytically calculated with state-of-the-art HNLF parameters and FOPA gain spectrum for reference.

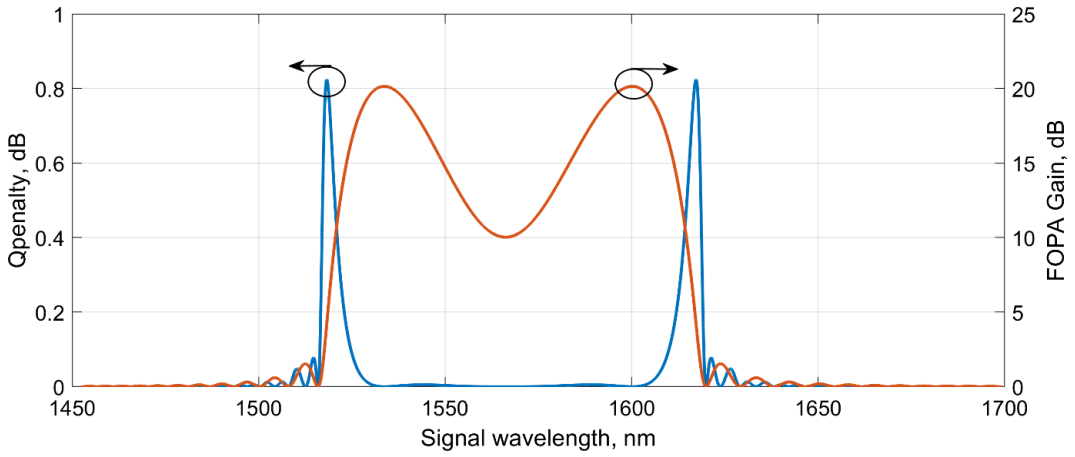


Figure 18. Q penalty as a function of signal wavelength (left), FOPA gain spectrum for reference(right). FOPA parameters are taken from Figure 5.

The Q penalties are zero only for signal wavelengths located around the pump at 1566.2 nm or around the gain peaks, as predicted in [34]. Previously reported in [35] large Q penalties reached up to 10 dB for the chosen FOPA parameters of HNLF length and dispersion parameters of β_3 and β_4 . However, this was reported about 20 years ago when gain fibers were several kilometers long. With the development of dispersion-stabilized and shorter HNLFs (less than 100 meters), Q penalties have decreased to 0.8 dB. These highest penalties are located at the outer slopes of the gain spectrum, where the gain spectrum varies more rapidly with signal wavelength offset from the pump wavelength. The minimum penalties occur for signal wavelengths located around the extremes (maxima or minima) of the gain spectrum.

The impact of pump relative intensity noise (RIN) on signal quality was studied in [35]. Although a larger pump RIN resulted in a greater Q penalty, it was much smaller compared to the Q penalty from pump phase modulation (<0.65 dB vs. 10.5 dB). Overall, it is recommended to use a pump laser with RIN lower than -145 dB/Hz to keep the Q penalty below 0.2 dB.

Across all pump phase modulation techniques, such as sine tones, white noise or PRBS patterns. The most pronounced parametric gain variations are raised from PRBS pump phase modulation. The PRBS modulation causes parametric gain distortions that significantly exceed those caused by noise modulation. In the case of PRBS modulation, the parametric gain experienced a huge variation during both the leading and falling edges of the pump phase. The pump frequency variations increase significantly with the steepness of the PRBS phase jumps. The significant gain modulation interferes with the data modulation format, particularly in the context of OOK signal modulation. The experiments conducted while amplifying OOK data at 10 Gbit/s demonstrated that during each phase jump, the detected signal exhibited abrupt power spikes or dips, with peak amplitudes exceeding 50% of the average power [34]. The penalty in OSNR for a BER of 10^{-9} ranged from 1 dB to 3.7 dB. The least penalty occurred close to the pump wavelength, while the highest penalty occurred at the gain curve's inflection point, where the gain slope is most pronounced [34].

However, it must be reminded that pump phase modulation bandwidth is limited by instantaneous pump frequency. This suggests that with PRBS modulation the instantaneous pump frequency can reach tens of GHz. Therefore, pump phase modulation using sine tones is expected to incur a smaller penalty compared to PRBS modulation. This is because the fluctuation in instantaneous pump frequency is significantly lower with sine modulation, due to its less steep phase changes. Experimental investigation of pump dithering schemes in FOPA amplifying 59 Gb/s QPSK signals showed that a scheme using pump phase modulation with 3 tones and a total bandwidth of 2.8 GHz resulted in fewer penalties compared to PRBS phase modulation, even when the PRBS signal ($2^7 - 1$ PRBS pattern) was low-pass filtered with 1.2 GHz [36].

To compare with white noise modulation, which was stated as the most bandwidth efficient technique, the maximum signal power penalty of 2 dB was reported, where pump bandwidth was broadened to 2.6 GHz by thermal noise in [105]. There is not sufficient evidence if pump phase modulation with white or thermal noise brings less penalty than modulation with sine tones, as the comparison must be made between same pump

bandwidths of two. The measurement of OSNR penalties in [57] showed that modulation with sine tones and total bandwidth of 4.8 GHz resulted in 0.7 dB bigger penalty than modulation with white noise of 3 GHz total bandwidth for the case with propagation of 10 Gb/s OOK signal in 10 km of SMF. At the same time, the tones showed better performance (0.3 dB less penalty) in back-to-back configuration. So, more investigation is needed to say, what penalty could be expected if the tones would be optimized to provide the same bandwidth as in case of white noise modulation. Moreover, studies on the instantaneous pump frequency of white or thermal noise phase modulation have not been explicitly reported in the literature.

Two techniques have been proposed to mitigate the negative impact of dithering, to the best of my knowledge. Counter-phase modulation in a two-pump FOPA, where the pump phases are modulated synchronously but in opposite directions. Initially, this technique was proposed to mitigate a detrimental effect on the idler's inherited twice spectral broadening of the phase-modulated pump. In FOPA systems, counter-phase modulation almost eliminates induced gain variations. The first derivative of pump modulation in this scenario can be expressed as:

$$\frac{d\varphi_p(t)}{dt} = \frac{d\varphi_{p1}(t)}{dt} - \frac{d\varphi_{p2}(t)}{dt}, \quad (2.32)$$

where P1 and P2 stand for the FOPA pumps. When they compensate each other, $d\varphi_p(t)/dt = 0$, and the parametric gain coefficient $g(t)$ is no longer time-dependent [107]. This can also be explained by the fact that, while both pumps are dithered around their frequencies, the central frequency remains unchanged with respect to the ZDW, preventing fluctuations in the phase-matching condition. However, since the pumps are offset from the ZDW by approximately 50 nm in a two-pump FOPA, the PM to AM conversion would be more pronounced compared to the single-pump case, although several kilometers of fiber are required to make this effect noticeable. For instance, numerical simulations in [107] showed that the PM-to-AM conversion caused pump power fluctuations of less than 0.5% of the total continuous pump power in a 300 m HNLFF with a pump offset from the ZDW of 43 nm.

The second approach to mitigate the negative impact of pump phase modulation is to apply a specific digital signal processing (DSP) algorithm for correcting the phase and amplitude distortions caused by the pump phase modulation [58].

Considering this, I regard pump phase modulation by sine tones, as the optimal technique, as its bandwidth can be designed efficiently and its deterministic impact on the

signal amplified by FOPA can be compensated by counter-phase modulation in a two-pump FOPA and by a DSP algorithm in a single-pump FOPA. Conversely, phase modulation by white noise cannot be compensated, as it is not deterministic.

Overall, the impact of pump phase modulation on signals amplified by FOPA has been studied extensively, but these studies have primarily focused on directly detected on-off keying signals over 15 years ago. Prior to the commencement of this thesis, the signal phase noise introduced by phase dithering was not considered. It is reasonable to suspect that the results and conclusions could differ significantly if signal phase noise from phase dithering were included in the study, potentially revealing additional factors affecting system performance. Furthermore, coherently detected quadrature-amplitude modulation (QAM) has since become the dominant signal modulation in optical communication systems. Coherent detection relies on signal amplitude rather than signal power, which previous studies have not addressed. Therefore, the results of existing dithering impact studies in FOPA are not applicable to the coherently detected QAM signals widely used in modern optical communications.

3 IMPACT OF PUMP PHASE MODULATION ON QAM SIGNALS AMPLIFICATION BY FOPA

3.1 Comparative analysis of pump phase modulation techniques

A fair comparison of different pump phase modulation methods requires that they achieve the same level of SBS threshold increase.

From eq.(2.18) it can be seen, that for different modulation techniques, all terms are the same as they depend on HNLF properties except convolution between Brillouin gain spectrum shape $\Delta\nu_B$ (Figure 19), and pump spectrum shape $\Delta\nu_P$, which varies for different modulation. This convolution can be seen as a relative Brillouin gain with total gain coefficient normalized to 1 for pump spectral shape and total pump power normalized to 1 W. The normalized Brillouin gain spectrum is shown at Figure 19.

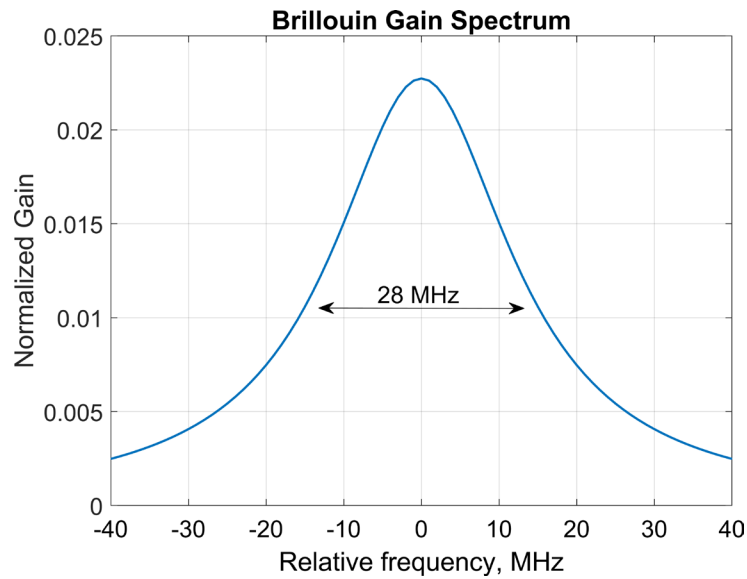


Figure 19. Normalized Brillouin gain spectra of silica fiber with FWHM linewidth of 28 MHz [80].

The sine tones were simulated to provide the most bandwidth efficient pump phase modulation (Figure 20). The base tone was chosen to be 20 MHz, and other tones were calculated as base tone frequency multiplied by $[3.05, 3.05^2, 3.05^3]$ to provide a flat spectrum and avoid high order harmonic overlapping. The red curve on the Figure 20 represents the relative Brillouin gain decrease of 17 dB obtained with the base tone

frequency of 20 MHz and the total pump bandwidth of 1550 MHz. The relatively high SBS suppression level of 17 dB was arbitrarily chosen as a reference for fair comparison in high-gain FOPA applications, enabling FOPA gains of over 20 dB. Figure 20 shows the relative Brillouin gain for a set of sine tones to demonstrate the relation between pump bandwidth and Brillouin gain decrease due to spectrum broadening. Despite the broad bandwidth beyond 50 MHz, the improvement in SBS suppression is low and not required for most applications. The optimal base tone frequency is typically near Brillouin gain linewidth.

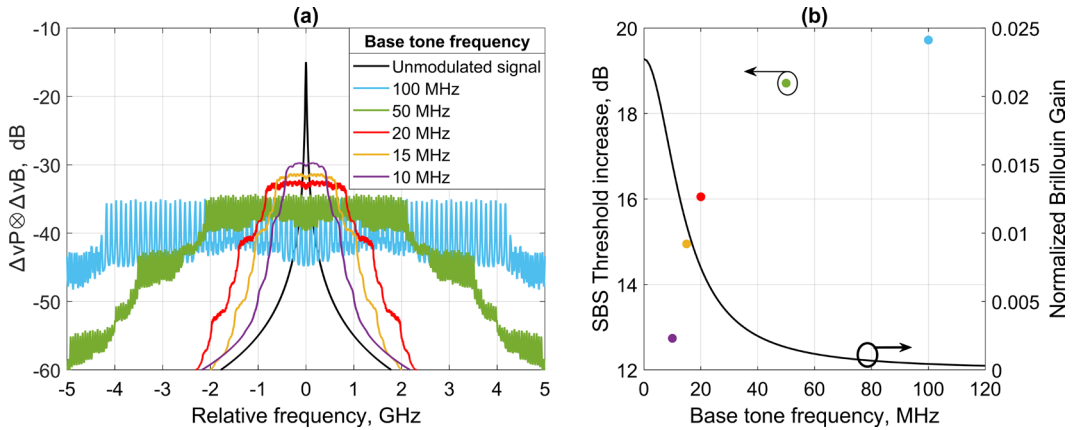


Figure 20. (a) The relative Brillouin gain for set of Base tone frequencies of Sine tone phase modulation, (b) The SBS threshold improvement versus base tone frequency. Black line shows approximate Brillouin gain linewidth for Silica fiber.

The White noise phase modulation was simulated as normally distributed random numbers in electrical domain. Then a Fourier transform was applied to electrical signal to convert it in frequency domain. In Frequency domain RF low-pass rect-shape filter of 0.5 GHz was multiplied with electrical noise. Then the filtered noise signal was converted back in time-domain to serve an array of phases for the electrical field. In optical domain the filtered white noise was of 1 GHz bandwidth. The filter width was chosen to satisfy Brillouin gain decrease of 17 dB, the same level as sine tones. The higher modulation amplitudes were examined at Figure 21, suggesting that optimal modulation amplitude should be between 2 and 2.5 rad to suppress the carrier frequency and to avoid a further pump broadening.

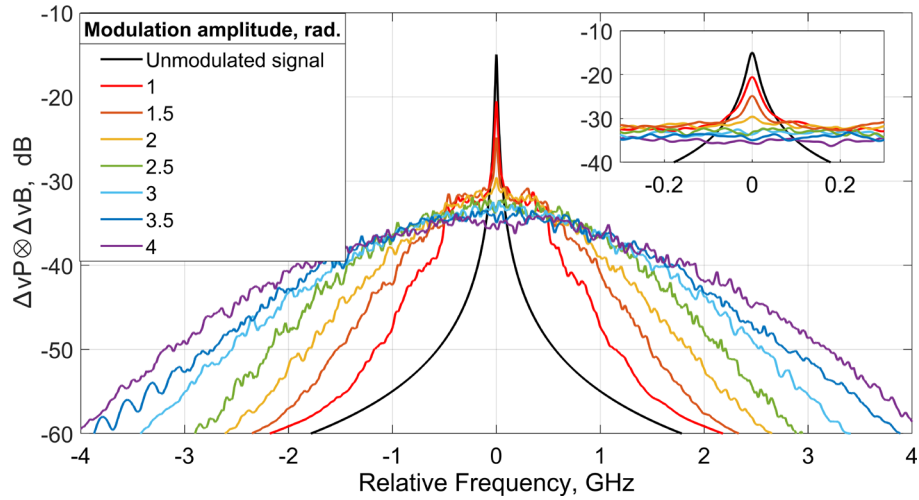


Figure 21. Relative Brillouin gain of pump phase modulated by filtered white noise with different modulation gain amplitudes, insert shows the increase gain peak.

The comparison of relative Brillouin gain for different modulation techniques is presented at Figure 22. The Figure 22 (a) shows the Brillouin gain for unmodulated pump, pump phase modulated with filtered white noise of 1 GHz (modulation amplitude 2.5 rad), PRBS with data rate of 2.2 Gb/s, pattern length $2^{12}-1$, modulation amplitude of π and rise time of 30 ps, and four sine tones of 20 MHz, 61MHz,186 MHz, 567 MHz (modulation amplitude of each tone is 1.43 rad).

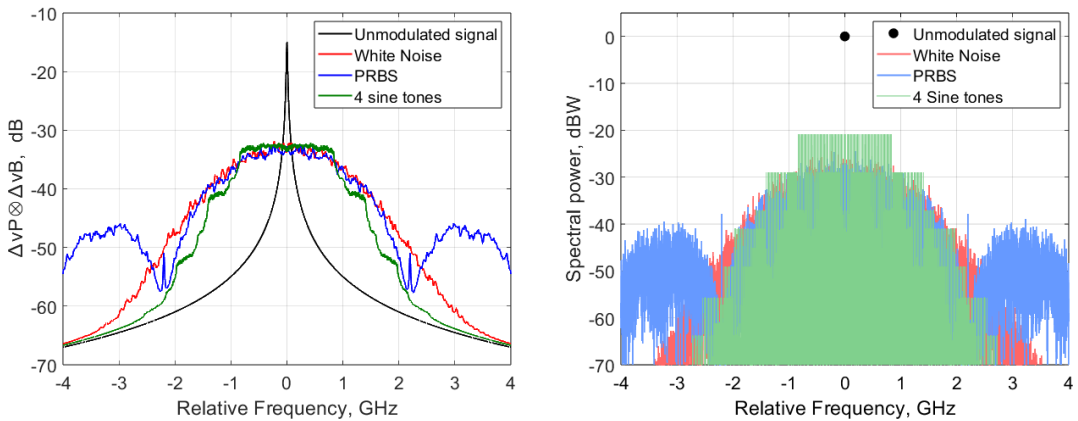


Figure 22. (a) Relative Brillouin gain and (b) power spectra for unmodulated pump (black), pump phase modulated with filtered white noise of 1 GHz (red), PRBS with data rate of 2.2 Gb/s (patter length $2^{12}-1$) and rise time of 30 ps (blue), 4 sine tones of 20 MHz, 61MHz,186 MHz, 567 MHz (green).

Relative Brillouin gain for unmodulated pump (black) is shown as reference level of unsuppressed Brillouin gain. The other three curves were calculated to show the same

Brillouin gain decrease of 17 dB compared to unmodulated pump. The Figure 22(b) shows the optical power spectra of phase modulated pump for all scenarios. There are big sidelobes of the blue curve indicating a massive phase noise at the 3 GHz from carrier frequency broadening pump spectrum far beyond 2.3 GHz. The pump spectrum with white noise modulation begins to broaden compared to that of sine wave modulation at 40 dBm of spectral power.

The pump phase modulation can be viewed as instantaneous pump frequency modulation. For phase modulated by sine tones, shown by Eq. (2.22), the instantaneous pump frequency modulation is derived in eq. (3.1), where f_p is the central pump frequency and $Am \cdot \sum_{n=1}^N fm_n \cdot \sin(2\pi \cdot fm_n \cdot t)$ is the first derivative of the pump phase $d\phi_p(t)/dt$ divided over 2π to convert from angular to ordinary frequency

$$f(t) = f_p + Am \cdot \sum_{n=1}^N fm_n \cdot \sin(2\pi \cdot fm_n \cdot t). \quad (3.1)$$

For PRBS phase modulation the maximum instantaneous pump frequency modulation is defined at trailing edges (eq.(2.26)) and derived as

$$f(t) = f_p - \frac{\pi^2}{2T_r} \sin\left(\frac{\pi \cdot t}{T_r}\right). \quad (3.2)$$

For white noise, the first derivative was calculated numerically without considering the possibility of performing it analytically at that stage. The instantaneous pump frequency modulation can be calculated only numerically.

The range of instantaneous frequency fluctuations defines the impact of pump phase modulation of signals amplified by FOPA. Figure 23 (a) shows the instantaneous frequency modulation of three modulation techniques, which spectra illustrated on Figure 22 (b). Note, Figure 23 (a) shows only a small part of the simulated time window (20ns out of 1 us) to make the fluctuations observable.

During phase modulation by PRBS, the instantaneous frequency of phase at the trailing edges reaches up to 27 GHz causing strong modulation in the parametric gain. That is why PRBS modulation is considered to be the worst pump phase modulation technique among others. The distribution of simulated instantaneous frequency over 1 us was plotted on Figure 23(b) to compare the range of instantaneous frequency variation of PRBS, white noise modulation and sine tones. The PRBS instantaneous frequency distribution consists of discrete peaks, with the spacing between peaks corresponding to the sampling frequency.

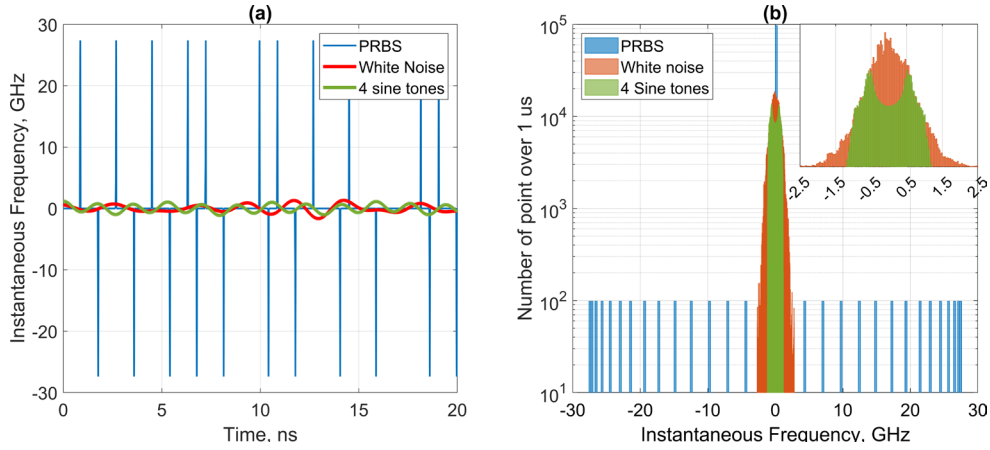


Figure 23. (a) Instantaneous frequency over time for pump phase modulated by PRBS with data rate of 2.2 Gb/s (patter length 2^{12-1}) and rise time of 30 ps (blue), filtered white noise of 1 GHz (red), and 4 sine tones of 20 MHz, 61MHz,186 MHz,567 MHz (green). (b) Distribution of instantaneous frequency over 1 us of white noise (red) and 4 sine tones (green).

The most distant peaks are associated with rise/fall phase jumps, causing the instantaneous frequency to increase up to 50 GHz, making this type of phase modulation detrimental to the phase-matching condition. The distribution of sine tones instantaneous frequency is strictly limited to 1.4 GHz, while the slopes of white noise distributed up to 5 GHz. This can indicate that during the long time of FOPA operation the impact of pump dithering with white noise can be more pronounced than pump dithering with sine tones. However, although white noise leads to larger maximum deviations of the instantaneous frequency than the sine tones, small instantaneous frequency deviations are more common in the white noise case. Therefore, it is uncertain which technique has less impact on the signal. However, modulation with sine tones is strictly controlled and deterministic and as such allows for their impact mitigation on both hardware (as will be further discussed) and software (DSP) levels. For this reason, this research is focused on the impact of pump phase modulation by sine tones in this thesis.

3.2 Impact of pump phase modulation on QAM signals in FOPA

3.2.1 Instantaneous pump frequency modulation and FOPA gain modulation

The impact of pump phase modulation on directly detected OOK signal amplification was discussed in 2.5.11, where eq. (2.31) was used to estimate signal Q penalty from parametric gain fluctuation caused by phase dithering [35]. In case of directly detected on-off keying signals the major source of signal degradation is power gain modulation due to

instantaneous pump frequency modulation. Other sources of signal degradation such as RIN and PM-to-AM conversion were shown in 2.5.11 to have a negligible effect compared to power gain fluctuations.

The coherently detected signals rely on electric field amplitude being square root of power, so the impact of power gain fluctuations on the signal quality is mitigated. On the other hand, quadrature-modulated signals are susceptible to induced signal phase modulation.

The impact of pump phase modulation on QAM signal performance arises from not just temporal variation of FOPA gain but phase shift and thus causes amplitude and phase noise for an amplified signal.

Therefore, FOPA gain should be derived in the complex domain as a function of pump frequency. The eq.(2.3) shows complex amplitude of gain h_3 , which combines the FOPA impact on both signal amplitude $|h_3|$ and phase shift (h_3): its modulus defines a signal amplification, and its argument defines an induced phase shift. Both values must be taken into account when calculating the impact of pump phase modulation on phase and amplitude modulated signals, e.g. M-QAM. The total propagation constant mismatch k in eq.(2.3) is the key parameter defining the impact of the pump phase modulation on signal because it depends on the group velocity dispersion β_2 at the pump frequency and the frequency detuning $\Delta\omega$ between a signal and the pump. Both β_2 and $\Delta\omega$ vary in time due to instantaneous pump frequency modulation. Therefore, the total propagation constant mismatch k and consequently the gain coefficient g are time dependent. Figure 24 shows traces of the pump frequency detuning from the unmodulated pump frequency and the corresponding $|h_3|$ and phase shift (h_3) calculated across 1000 uniformly spaced points within a 100ns time frame. The complex amplitude of gain h_3 is calculated with pump wavelength of 1566.2 nm, ZDW of 1562.9 nm, fiber dispersion slope of $43 \text{ s}^{-1}\text{m}^{-3}$, pump power of 4.3 W, HNLf length of 50 m, γ of $14 \text{ W}^{-1}\text{km}^{-1}$.

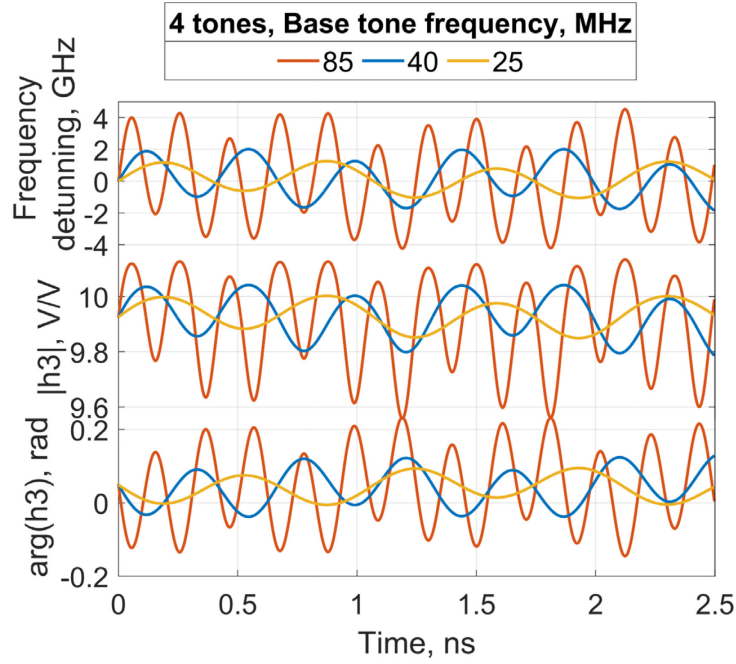


Figure 24. Timeline of the pump frequency detuning from its central frequency due to phase dithering, $|h_3|$ and phase shift (h_3) at signal wavelength of 1531 nm; FOPA parameters for pump wavelength of 1566.2 nm, ZDW of 1562.9 nm, fiber dispersion slope of $43 \text{ s}^{-1}\text{m}^{-3}$, pump power of 4.3 W, HNLF length of 50 m, γ of $14 \text{ W}^{-1}\text{km}^{-1}$. No loss, no pump depletion case. Pump phase modulation base tones of 25 MHz (yellow), 40 MHz (blue) and 85 MHz (red) [108].

The instantaneous pump frequency modulation was calculated by eq. (3.1). Each waveform was a combination of 4 sine tones, whereas the base tone was one of 25 MHz, 40 MHz or 85 MHz in the electrical frequency spectrum and higher frequencies were obtained via its multiplication by $[3.05, 3.05^2, 3.05^3]$. The modulation amplitude was 1.4 rad per tone in all simulations. The corresponding total pump bandwidths were calculated as twice sum of sine tone frequencies: 2086 MHz, 3338 MHz, 7094 MHz. The pump frequency modulation transfers to h_3 : its modulus $|h_3|$ varies inphase with pump frequency with peak-to-peak amplitude of 0.11 dB for $f_{\text{base tone}}$ of 25 MHz and of 0.57 dB for $f_{\text{base tone}}$ of 85 MHz. Phase shift of h_3 varies in counter-phase with peak-to-peak amplitudes of 0.075 rad and 0.37 rad responsibly. Higher frequencies lead to larger peak-to-peak fluctuations in FOPA gain amplitude as well as greater FOPA phase shift. The increased peak-to-peak phase shift of h_3 is expected to induce signal phase noise during FOPA amplification.

3.2.2 Induced phase noise in QAM signals due to pump phase modulation

The constellation diagram of 16-QAM signal amplified by FOPA was simulated to demonstrate an induced phase noise caused by induced phase shift. Input signals represented as array of 16 signal complex amplitudes corresponding to the 16-QAM constellation points. The Figure 25 illustrates the 16-QAM constellation diagram of input signal, no noise is assumed at the input to FOPA. The distance between any two adjacent points on the 16-QAM constellation is d_{min} :

$$d_{min} = 2 \sqrt{\frac{Ps}{10}} \quad (3.3)$$

where Ps signal power. Normalization factor of $1/\sqrt{10}$ is applied to ensure that the average power over all the constellation points is normalized to Ps . This is achieved by summing the power of each point and dividing by the total number of symbols (16). Electrical electric field of $\frac{1}{4}$ of constellation (as the constellation is symmetrical around 0) is

$$Es = \frac{d_{min}}{2} \begin{pmatrix} 1 + 1i \\ 1 + 3i \\ 3 + 3i \\ 3 + 1i \end{pmatrix}. \quad (3.4)$$

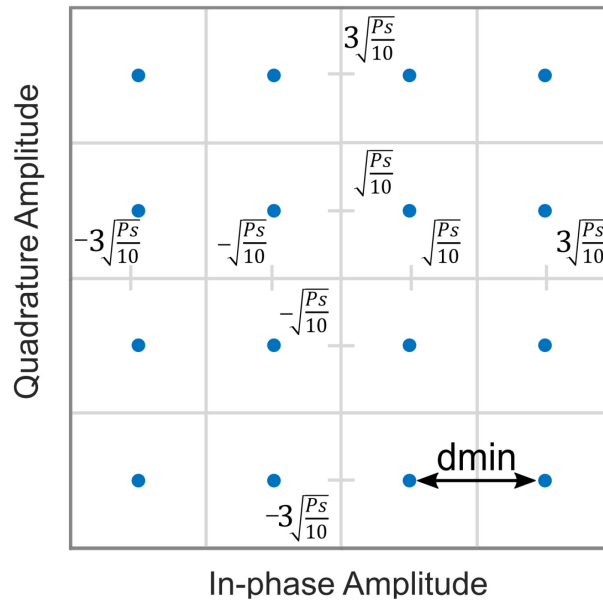


Figure 25. The 16-QAM constellation diagram represents the input signal, assuming no input noise.

Then, the calculated values of h_3 by eq.(2.3) were used to derive a set of output signal complex amplitudes corresponding to different instantaneous pump frequencies for each point of the 16-QAM constellation diagram.

Vector of n complex gains h_3 was calculated the same way as for Figure 24 in 3.2.1. The vector of h_3 was multiplied with a vector of 16 signal complex amplitudes corresponding to the 16-QAM constellation points (input signals) to obtain a matrix of output signal complex amplitudes for each constellation point:

$$ES_{out} = \begin{pmatrix} h_{3,t1} \\ h_{3,t2} \\ \vdots \\ h_{3,fn-1} \\ h_{3,fn} \end{pmatrix} \times ES_{in}. \quad (3.5)$$

Then, the matrix of output complex amplitudes ES_{out} was normalized by dividing it over average squared amplitude $\langle |h_3|^2 \rangle$ which is equivalent to signal attenuation by the average gain value, and dividing over the average FOPA induced phase shift $\exp(i \cdot \langle \arg(h_3) \rangle)$ which is equivalent to the signal derotation. This is shown by Eq.(3.6):

$$ES'_{out} = \frac{ES_{out}}{\langle |h_3|^2 \rangle \cdot \exp(i \cdot \langle \arg(h_3) \rangle)}. \quad (3.6)$$

The resulting signal amplitudes are shown at Figure 26(a). It demonstrates that the induced phase modulation is dominant over the induced amplitude modulation, and it scales dramatically with increase of pump bandwidth.

Finally, to simulate a matrix of SNR values, an amplified spontaneous emission (ASE) has been added via simulated 50% coupler to the matrix of signal complex amplitudes. Amplified quantum noise during amplification by FOPA with $NF = 4$ (6dB), B is the signal bandwidth of 34 GHz and gain $G = \langle |h_3|^2 \rangle$, so the noise power N_{out} within the signal band is:

$$N_{out} = \left(NF - \frac{1}{G} \right) \cdot h \cdot fs \cdot B \cdot G. \quad (3.7)$$

And subsequent attenuation by the average gain value:

$$N'_{out} = \frac{N_{out}}{G} + h \cdot fs \cdot B \cdot \left(1 - \frac{1}{G} \right), \quad (3.8)$$

where fs is the signal frequency of 195.8 THz, and $h = 6.6261 \cdot 10^{-34}$ is the Plank constant.

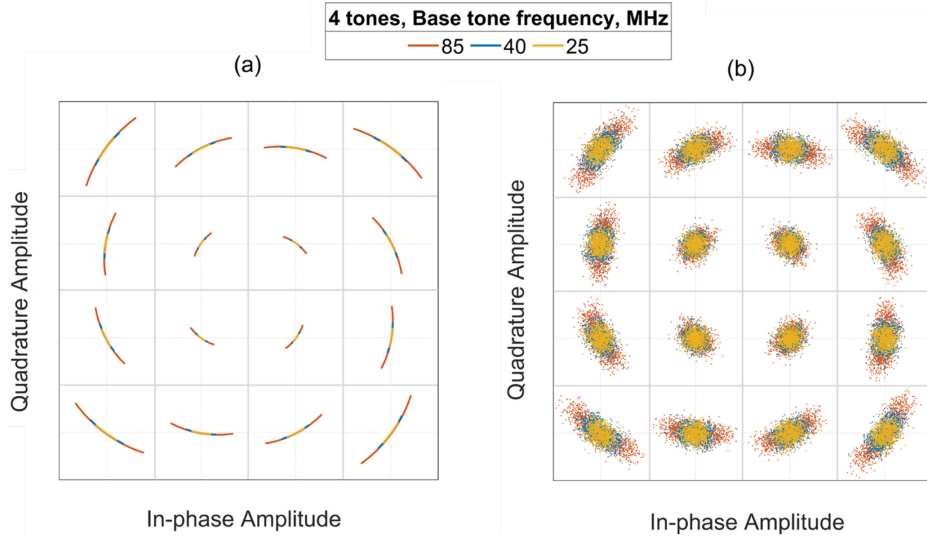


Figure 26. (a) constellation diagram of amplified a 16QAM signal by FOPA with Pump phase modulation base tones of 25 MHz (yellow), 40 MHz (blue) and 85 MHz (red). (b) Same diagram with a SNR of 25 dB. Signal wavelength 1531 nm [108].

The average signal power then was calculated as follows, where $4n$ is the number of elements of the matrix ES'_{out} according to Eq.(3.4) and Eq.(3.5):

$$S = \frac{\sum |ES'_{out}|^2}{4 \cdot n}, \quad (3.9)$$

The SNR was calculated as the average signal power over N'_{out} :

$$SNR = \frac{S}{N'_{out}}. \quad (3.10)$$

Figure 26(b) shows the same constellation diagram with added white noise to the matrix ES'_{out} to provide the SNR of 25 dB. It confirms that the induced phase noise is the major source of 16-QAM signal degradation due to pump phase modulation in FOPA.

3.2.3 Calculation of BER for QAM signals with induced phase noise

Further characterization of the impact of pump phase modulation was done through the required optical signal-to-noise ratio (rOSNR) penalty, defined as the OSNR difference between the simulated BER curve with FOPA and the theoretical (back-to-back) curve at a BER level of 0.01 (close to the forward error correction limit of modern transponders).

The simulated BER with FOPA was calculated using an error probability function to quantify the likelihood of detection errors for each vector of constellation point complex signal amplitudes ES'_{out} across a range of SNR values. Gaussian noise distribution was assumed for each case, because although temporal fluctuations of h_3 affect overall distribution of the output signal, at every instant moment of time the output signal has the

same noise distribution as the input signal which was assumed Gaussian. Hence, error probability for each point was found as a sum of error functions shown by Eq. (3.11),

$$Pr = \frac{1}{2} \operatorname{erfc} \left(\frac{x_0 - \mu}{\sigma\sqrt{2}} \right). \quad (3.11)$$

where μ is the center of Gaussian distribution for each constellation point, defined by each output signal's complex amplitude in the matrix Es'_{out} . While analyzing a quarter of the constellation diagram, the hard decision threshold is shown as $x_0 = 2 \left\lfloor \frac{|Es'_{out}|}{\sqrt{2}} \right\rfloor$ or 0. It is scaled for all points by the same h_3 corresponding to the central of the simulated pump frequencies. The standard deviation $\sigma = \sqrt{(N'_{out} + N_{Rx})/2}$ is defined by N'_{out} for corresponding SNR plus added receiver noise N_{Rx} [109]. Equations (3.12) show the calculation of error probability for each of point of $\frac{1}{4}$ 16-QAM constellation diagram:

$$\begin{aligned} Pr_{Es,1+1i} &= \frac{1}{4} \left(\operatorname{erfc} \left(\frac{x_0 - \operatorname{real}(Es'_{out})}{\sigma\sqrt{2}} \right) + \operatorname{erfc} \left(\frac{x_0 - \operatorname{imag}(Es'_{out})}{\sigma\sqrt{2}} \right) \right. \\ &\quad \left. + \operatorname{erfc} \left(\frac{0 - \operatorname{real}(Es'_{out})}{\sigma\sqrt{2}} \right) + \operatorname{erfc} \left(\frac{0 - \operatorname{imag}(Es'_{out})}{\sigma\sqrt{2}} \right) \right) \\ Pr_{Es,1+3i} &= \frac{1}{4} \left(\operatorname{erfc} \left(\frac{x_0 - \operatorname{real}(Es'_{out})}{\sigma\sqrt{2}} \right) + \operatorname{erfc} \left(\frac{x_0 - \operatorname{imag}(Es'_{out})}{\sigma\sqrt{2}} \right) \right. \\ &\quad \left. + \operatorname{erfc} \left(\frac{0 - \operatorname{real}(Es'_{out})}{\sigma\sqrt{2}} \right) \right) \\ Pr_{Es,3+1i} &= \frac{1}{4} \left(\operatorname{erfc} \left(\frac{x_0 - \operatorname{real}(Es'_{out})}{\sigma\sqrt{2}} \right) + \operatorname{erfc} \left(\frac{x_0 - \operatorname{imag}(Es'_{out})}{\sigma\sqrt{2}} \right) \right. \\ &\quad \left. + \operatorname{erfc} \left(\frac{0 - \operatorname{imag}(Es'_{out})}{\sigma\sqrt{2}} \right) \right) \\ Pr_{Es,3+3i} &= \frac{1}{4} \left(\operatorname{erfc} \left(\frac{x_0 - \operatorname{real}(Es'_{out})}{\sigma\sqrt{2}} \right) + \operatorname{erfc} \left(\frac{x_0 - \operatorname{imag}(Es'_{out})}{\sigma\sqrt{2}} \right) \right) \end{aligned} \quad (3.12)$$

The symbol error rate (SER) is found as the total probability of symbol error assuming all constellation points and instantaneous pump frequencies to be equally probable [111]:

$$SER = \frac{1}{2} (Pr_{Es,1+1i} + Pr_{Es,3+1i} + Pr_{Es,1+3i} + Pr_{Es,3+3i}). \quad (3.13)$$

The BER is found as a $\frac{1}{4}$ of the symbol error rate due to Gray coding used for 16-QAM signals [111]

$$BER = \frac{1}{4} SER. \quad (3.14)$$

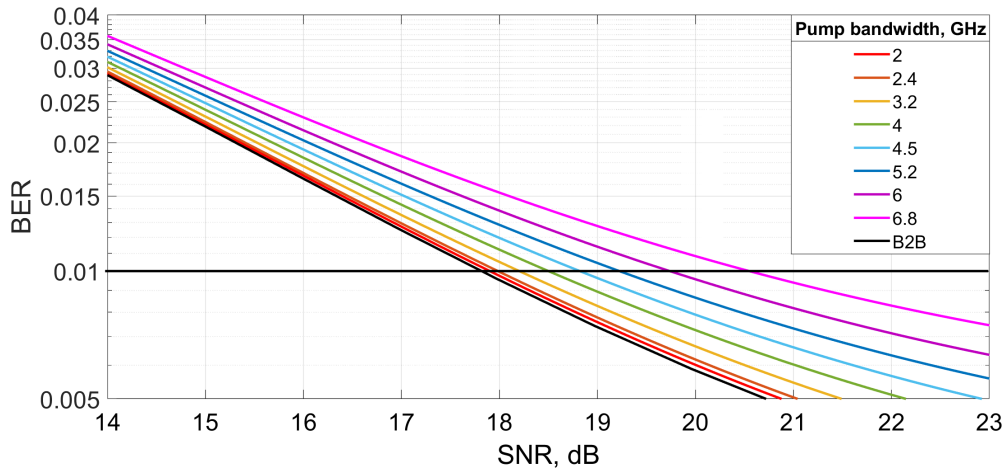


Figure 27. BER versus SNR for different pump bandwidth for a 16-QAM signal amplified at the FOPA gain peak wavelength 1534 nm.

Figure 27 shows simulated BER of a 16-QAM signal at the FOPA gain peak wavelength versus the signal OSNR for a set pump bandwidth. Figure 27 additionally shows a theoretical curve (black) for Gaussian-noise limited 16-QAM signals obtained with Eq. (3.14). A match observed between the theoretical curve and our simulated curves for pump bandwidth ≤ 2 GHz implies almost no performance penalties at a BER of 0.01 for such pump bandwidth. The required OSNR penalty for the 6.8 GHz pump linewidth is 2.8 dB.

The impact of pump phase modulation of higher pump bandwidth was characterized for a range of signal wavelengths across the FOPA gain spectrum. Figure 28(a) demonstrates spectra of the modulus and the argument of h_3 calculated with parameters from Figure 5, whereas Figure 28(b) shows rOSNR penalty simulated for a range of signal wavelengths across the FOPA gain bandwidth and for waveforms employing 3 and 4 tones with frequency ratios of $[1, 3.05, 3.05^2, 3.05^3]$. The rOSNR penalties appear to increase with the total pump bandwidth regardless of base tone frequencies and number of employed tones. Observed 16-QAM signal penalty distribution across the FOPA gain bandwidth is different to previous OOK results, where Q^2 penalties were minimal at the gain peak and have two maxima at the FOPA gain slopes [35]. The simulated penalties demonstrate minimum at the vicinity of pump wavelength (1566.2 nm) and increase significantly with signal detuning from the pump.

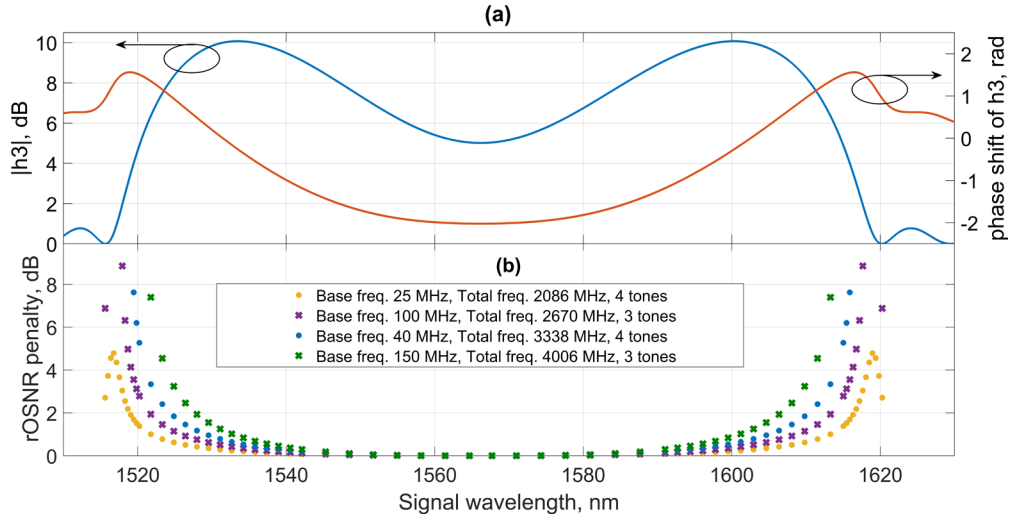


Figure 28.(a) modulus $|h_3|$ (blue) and phase shift of h_3 (red) calculated with parameters from Figure 5 and (b) rOSNR penalty vs wavelengths for 4 pump modulation waveforms employing 3 tones with $f_{\text{base tone}}$ of 100 MHz and 150 MHz (crosses) and 4 tones with $f_{\text{base tone}}$ of 25 MHz and 40 MHz (dots) [108].

The wavelength range of the largest rOSNR penalty is observed where $|h_3|$ has the largest slope and phase shift (h_3) reaches the maximum. The rOSNR curve does not have a minimum at gain peaks as in previous studies focused on OOK modulation formats [35], because quadrature-modulated signals, such as QPSK and higher-order formats, are susceptible to induced signal phase modulation, while coherently detected signals are more robust to power fluctuations than directly detected signals because they refer to signal amplitude rather than power. The correlation between curves for the rOSNR penalty and the phase shift implies that the induced phase noise is the major source of 16-QAM signal degradation due to pump phase modulation in FOPA. This explains not just quantitative but also qualitative difference between the OSNR penalties of directly detected on-off keying signals and coherently detected QAM signals.

3.3 Impact of pump phase modulation in polarization-insensitive FOPA

For this section I extended the model of required-OSNR penalties for 16-QAM signals induced by the pump dithering in FOPAs considering features of polarization-insensitive Looped FOPA architecture. The polarization-insensitive looped FOPA first was presented in [66] and referred to hereafter as the Looped PI-FOPA. A signal in single-pump Looped

PI-FOPA is split by a polarization beam splitter (PBS) into orthogonal linearly polarized components counter-propagating in a loop, and both components are independently but equally amplified within the loop before being recombined by the same PBS. The loop employs two nominally identical gain fiber lengths each pumped unidirectionally from one phase modulated pump laser.

Figure 29 shows that once the pump is split by a 50/50 coupler, the two patchcord lengths of fibers that deliver pump power to HNLF might have different length. That means the pump phase modulation waveforms and consequently distortions induced on the signal components might not be synchronized in the gain fibers, and moreover the delay between them is prone to drifting over time. Therefore, the signal components are split between two spatial parts and receive a different phase and amplitude shift depending on the instantaneous pump frequency shift in each arm at every moment. Hence, upon recombination of the amplified signal components, the signal distortion caused by pump phase modulation in looped PI-FOPAs is a linear combination of the signal distortions in each arm of the PI-FOPA yet with a delay between them. The linear combination of the signal distortions caused by the modulated complex gain h_3 can be expressed with a weighting factors K and $1 - K$ representing the fraction of each polarization multiplexed signal component power in the two FOPA arms ‘X’ and ‘Y’:

$$h_3 = h_{3,X} \cdot K + h_{3,Y} \cdot (1 - K). \quad (3.15)$$

This is more complicated than in previously studied single-polarization FOPAs and opens ways for compensation of the signal distortion caused by the pump phase modulation in PI-FOPAs.

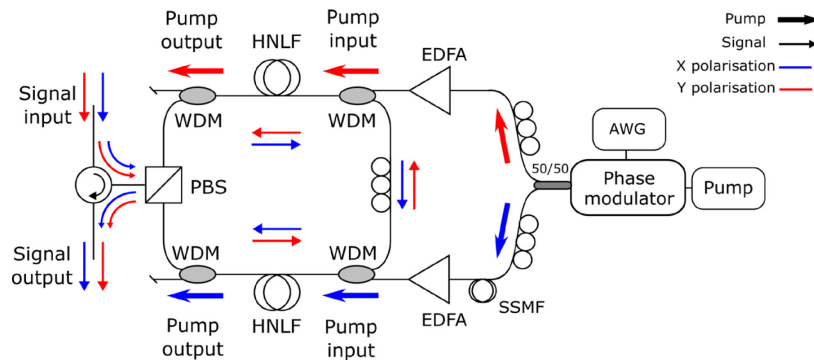


Figure 29. Scheme of Looped PI-FOPA with different fiber lengths between fiber coupler and EDFAs. PBS – polarization beam splitter, AWG – arbitrary waveform generator.

The impact of asynchronization between the pumps on the overall system performance depends on how a signal is split by the PBS. Assume a polarization division multiplexed signal, its components can be split equally ($K = 0.5$), asymmetrically ($[0 < K < 1]$) or aligned to PBS axes ($K = 0$ or 1). If a signal consists of a single component, that component can also be either divided or directed into one of two distinct spatial paths. However, in practice, PDM signal components split with a random factor between two paths in PBS ($K = \text{random}$).

If the pumps' modulations are in phase (i.e. pump optical paths are matched) both signal components experience the same distortion, and this is largely the same as in single-polarization FOPAs (Figure 30). If the polarization multiplexed signal components are aligned to the PBS axes, then pump synchronization has no impact on constellations of the signal components as each is amplified by a separate pump. However, in most cases two parts of the signal will inherit different modulations in each spatial path and the result will be averaged upon recombination in the PBS. If pumps' modulations are in counter phase and the signal components are split equally between the spatial paths (Figure 30), the inherited modulation in theory can be almost cancelled out due to coherent superposition of two signal components after recombination on a PBS. Therefore, there are two steps towards cancelling the inherited modulation: to control splitting of PDM signals in PBS and to adjust delay between pump optical paths.

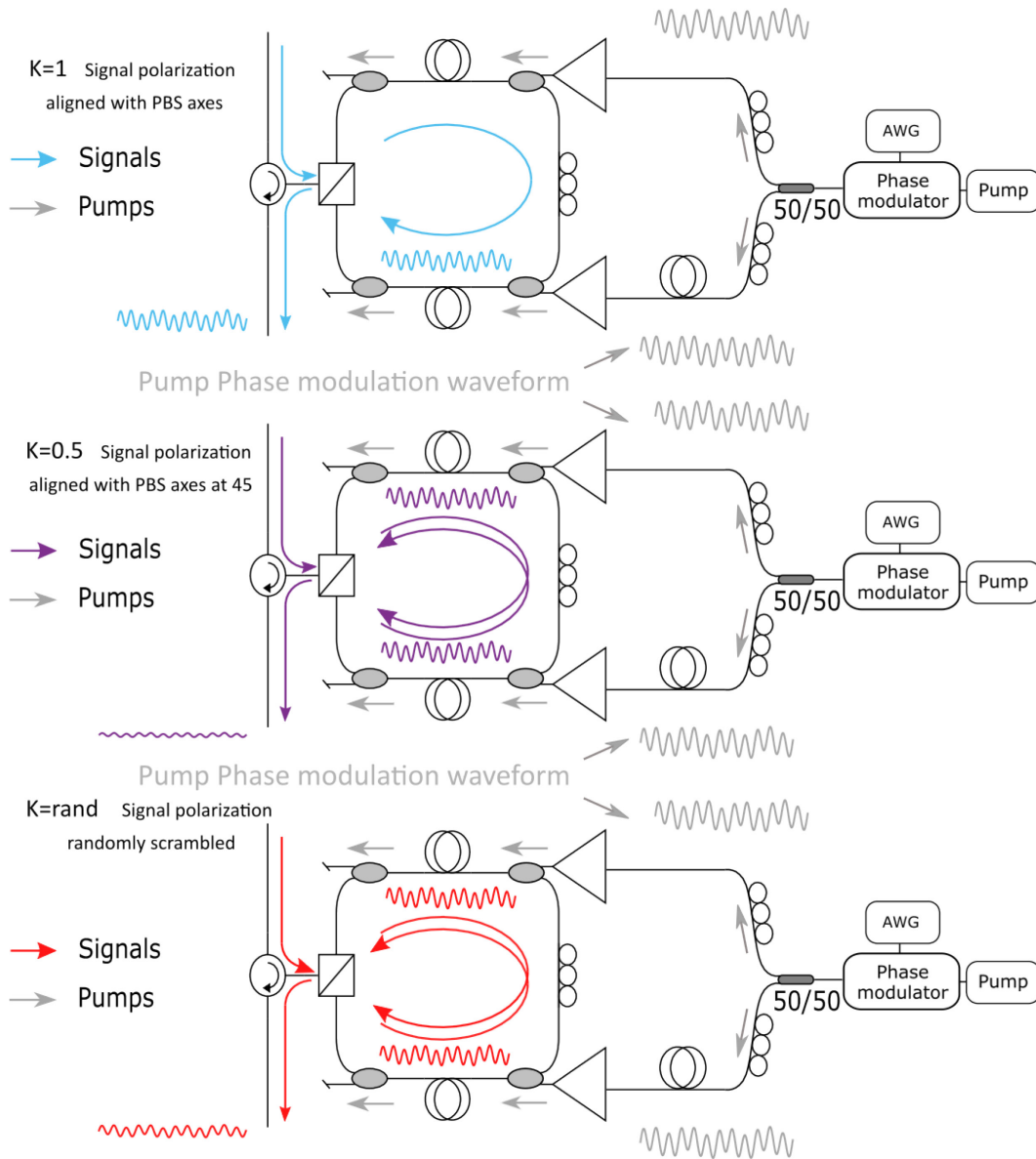


Figure 30. Schemes for different signal polarization splitting on PBS in Looped PI-FOPA with different fiber lengths between fiber coupler and EDFAs.

3.4 Employment of polarization diversity architecture to mitigate an impact of pump phase modulation in FOPA

The impact of dithering can be cancelled in a single-pump looped PI FOPA by ensuring that the impact of dithering on signal phase and amplitude is opposite in the PI-FOPA arms and the polarization components of the signal are split equally between arms. The opposite impact of dithering can be achieved thanks to the periodic nature of tones used for pump

phase modulation by introducing a half period delay $\Delta t = 1/(2f_{base\ tone})$ between pumps in the gain fibers, so the instantaneous pump frequency modulation for the pump delayed by Δt will be modified as

$$f(t) = f_p + Am \cdot \sum_{n=1}^N fm_n \cdot \sin(2\pi \cdot fm_n \cdot t + \Delta t). \quad (3.16)$$

Where the half period Δt delay between pumps can be expressed in fiber length:

$$\Delta L = \frac{c}{n} \cdot \Delta t = \frac{c}{n} \cdot \frac{1}{2 \cdot f_{base\ tone}}. \quad (3.17)$$

Half period delay is 20 ns or 4 m of fiber length for tones with multiplication factor of 3 and $f_{base\ tone}$ of 25 MHz. Figure 31 shows, how fluctuations of both modulus and angle of $h_{3,X}$ and $h_{3,Y}$ mitigate each other if they are shifted on a half period, assuming that signal polarizations are split equally between arms ($K = 0.5$) and multiplication factor = 3. The small ripples in $|h_3|$ on the Figure 31(a) are unavoidable, since the h_3 is a nonlinear function of pump frequency modulation through wavevector mismatch in Eq.(2.2).

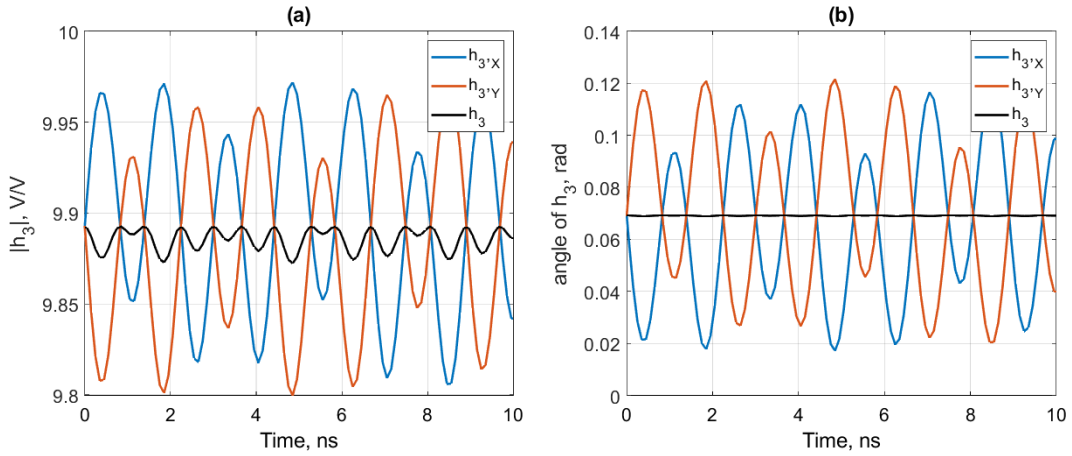


Figure 31. (a) Looped PI-FOPA gain modulus $|h_3|$ and (b) Phase shift (h_3) when pump modulation waveforms are counter-phase and tones are multiple for $h_{3,X}$, $h_{3,Y}$, h_3 , $f_{base\ tone} = 25\text{ MHz}$, $\Delta t = 20\text{ ns}$, $K = 0.5$, signal wavelength 1531 nm.

In case if multiplication factor is not integer and Δt is set to 20 ns, distortions of modulus $|h_3|$ and phase shift (h_3) are more pronounced, as shown on Figure 32.

One requires a hundred kilometers to create half period delay between pumps for the selected multiplier between tones of 3.05, which is practically inconvenient.

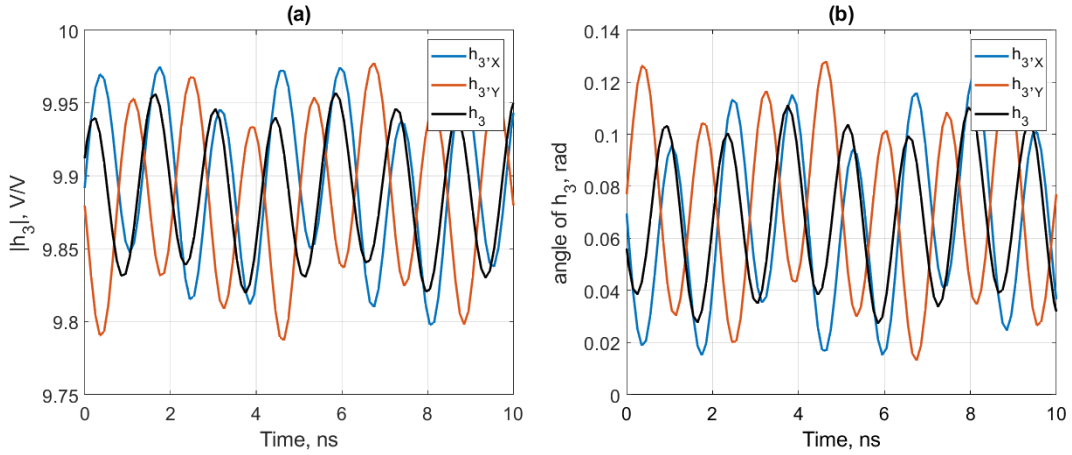


Figure 32. (a) Looped PI-FOPA gain modulus $|h_3|$ and (b) Phase shift (h_3) when pump modulation waveforms are counter-phase and tones are multiplied by $m = 3.05$ for $h_{3,X}$, $h_{3,Y}$, h_3 , $f_{base\ tone} = 25$ MHz, $\Delta t = 20$ ns, $K = 0.5$, signal wavelength 1531 nm.

Nevertheless, it is still possible to significantly mitigate the impact of dithering as the required delay to get minimum penalty can be adjusted to the provided optical path mismatch by adjusting tones' frequencies, as shown in eq. (3.17).

Given that the required delay between the pumps is achieved in the gain fibers, mitigation of the impact of dithering requires thorough splitting signal polarization equally between the PI-FOPA arms, as illustrated on Figure 30. This issue can be solved by adding a polarization tracker to set and maintain the target polarization at the FOPA input [110]. Alternatively, signal polarization can be randomized with a polarization scrambler to provide some mitigation of the dithering impact as compared to the 'single polarization' case. It must be noted that the optimum scrambler frequency lies between the frame rate and the symbol rate. If it is too slow, the worst-case scenario persists for a longer duration, causing outages. If it is too fast, unpredictable distortions in the signal's amplitude and phase may be caused, which may not be fully compensated by the DSP. Figure 33 shows a Looped PI-FOPA $|h_3|$ and phase shift (h_3) calculated over time for the above-mentioned scenarios.

Two cases are described: when the pumps in the gain fibers are either in phase or in counter-phase. For each case the signal polarization is either aligned to one of PBS axes ($K = 1$) or aligned with an angle of 45 degrees to the PBS axes and therefore signal power split equally between FOPA arms ($K = 0.5$) or varies randomly as beta distribution defined on the interval (0, 1) with parameters $\alpha = 3/2$ and $\beta = 3/2$ imitating distribution of polarization states over Poincare sphere and calculated for $N = 1000$ points.

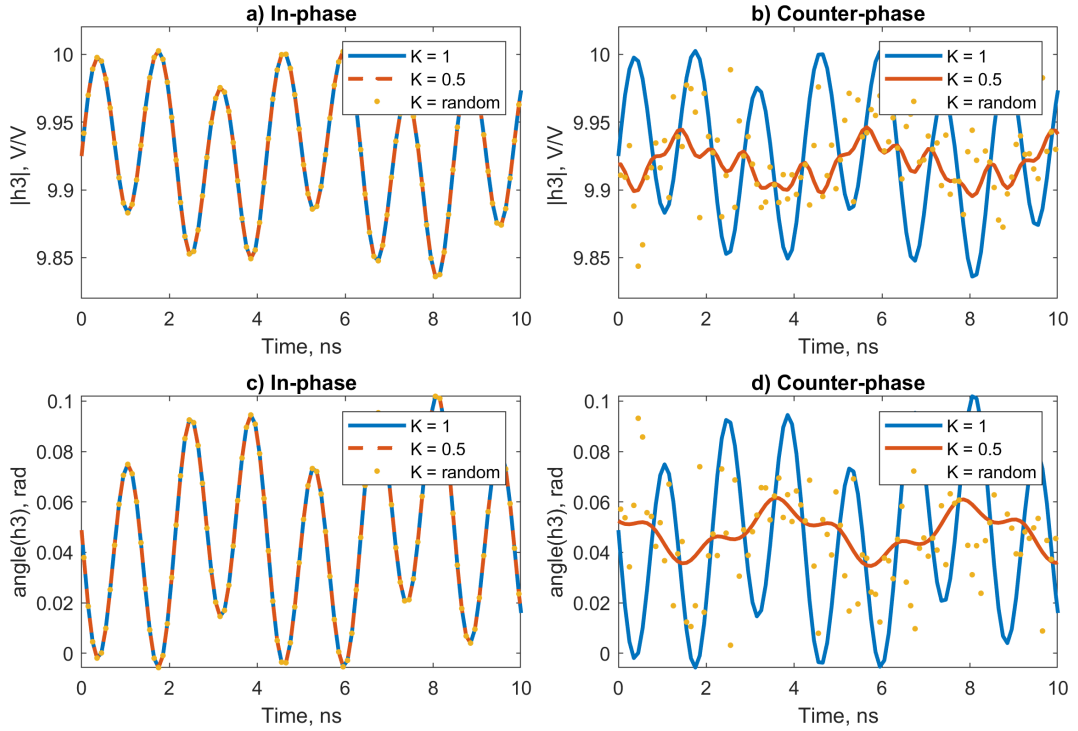


Figure 33. Looped PI-FOPA gain modulus $|h_3|$ when pump modulation waveforms are a) in-phase, b) counter-phase as well as Phase shift (h_3) c) in-phase, d) counter-phase for three different K factors of 1, 0.5 and randomly distributed in range $[0,1]$. $|h_3|$ and phase shift (h_3) are calculated using the parameters from Figure 5 with pump phase modulation employing 4 tones, with a $f_{\text{base tone}} = 25$ MHz and $m = 3.05$. Signal wavelength 1531 nm [108].

Figure 34 shows the probability density of Beta distribution on the interval $(0, 1)$ with parameters $\alpha = 3/2$ and $\beta = 3/2$.

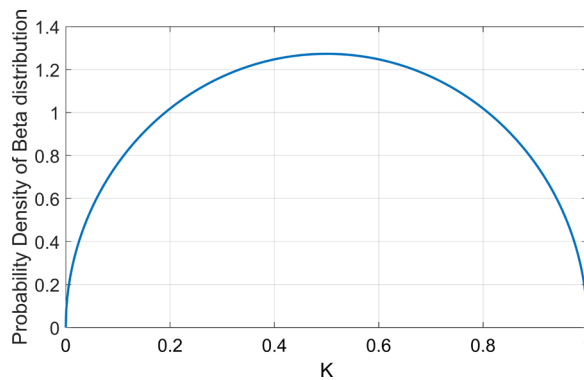


Figure 34. Probability density of Beta distribution on the interval $(0, 1)$ with parameters $\alpha = 3/2$ and $\beta = 3/2$.

The number of polarization states N was chosen to match the number of uniformly spaced frequency offsets from the pump (Figure 24), assuming that a new random polarization is generated for each symbol. Polarization changes occur more slowly compared to the symbol rate of 200 Gb/s 16-QAM signal used in the experimental study described in chapter 4. However, they are fast enough to allow for averaging BER within an error counting window of 1 second.

When the pumps are in-phase (Figure 33 (a)), the fluctuations of the PI-FOPA gain modulus and phase shift are independent of how signal components are split by the PBS, and they are the same in a single-polarization FOPA. However, when the pumps are in counter-phase (Figure 33 (b)), fluctuations of the PI-FOPA gain are reduced in some cases. The alignment of signal component's polarization with PBS axes ($K = 1$) causes the same fluctuation of FOPA gain even if pumps are in counter-phase. When signal component's polarization is equally split between PBS axes ($K = 0.5$), fluctuation of FOPA gain is noticeably suppressed: peak-to-peak amplitude of $|h_3|$ decreased from 0.16 dB to 0.04 dB and peak-to-peak amplitude of phase shift (h_3) decreased from 0.1 rad to 0.025 rad (Figure 33 (d)). If the polarizations of PDM signals are not controlled, they can undergo random fluctuations over time, enabling averaging between the two previous scenarios and partially mitigating the impact of dithering. Figure 35 shows that in case of the random signal polarization $K = \text{Random}$, (yellow) the distributions of both gain modulus $|h_3|$ and phase shift (h_3) are narrower than in case of the signal co-polarized with one of PBS axes ($K = 1$, blue).

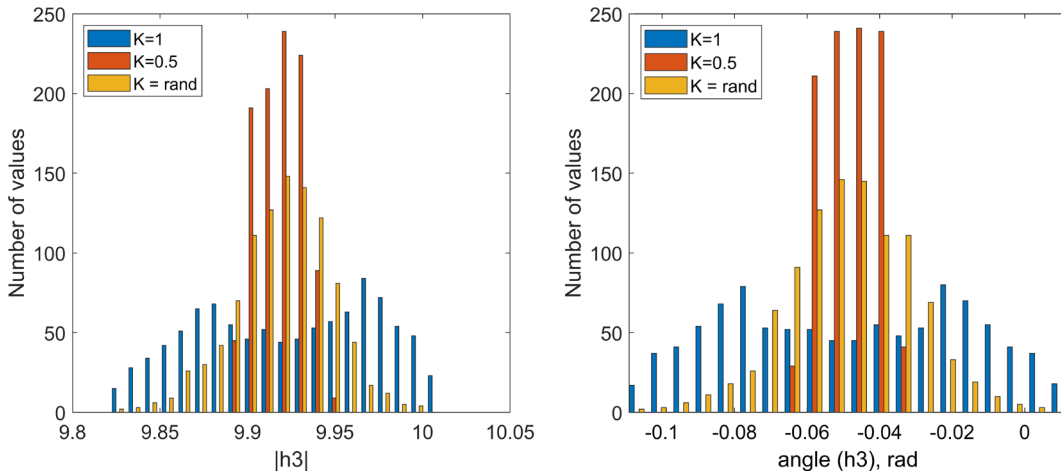


Figure 35. Distribution of $|h_3|$ and phase shift (h_3) when pump modulation waveforms are counter-phase for different K factors. The total number of samples is 1000 [108].

Therefore, the general case of randomly varying input signal polarization in a PI-FOPA provides less scattering of an amplified signal complex amplitude than the worst-case scenario equivalent to a single-polarization FOPA. Figure 36 shows rOSNR penalty as a function of signal wavelength for three scenarios: $K = 1$ (blue), $K = 0.5$ (red) and $K = \text{random}$ (yellow), calculated for FOPA and phase modulation parameters from Figure 5.

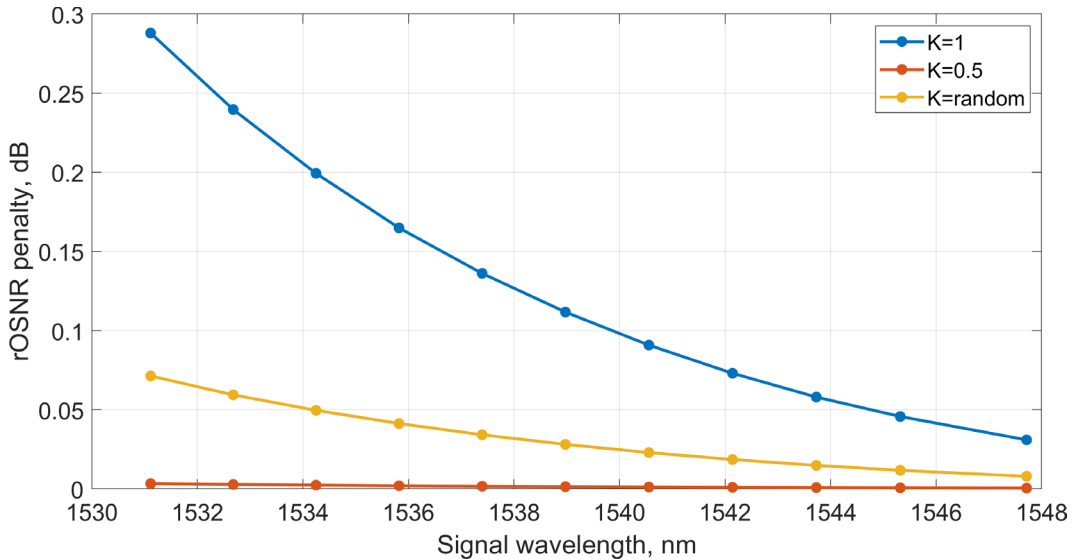


Figure 36. rOSNR penalty versus signal wavelengths for three K factors of 1, 0.5, random. Pump optical paths are in counter-phase. Plots are simulated using the parameters from Figure 5 with pump phase modulation employing 4 tones, with $f_{base\ tone} = 25$ MHz and $m = 3.05$ [108].

The rOSNR penalty calculated for $K = 1$ demonstrates the highest level of penalty the same as single-polarization FOPA on Figure 28. All other scenarios are better. Splitting PDM signals equally in PBS allows to decrease penalty below 0.005 dB across all examined wavelengths. Randomly scrambling polarization of PDM signal components minimizes rOSNR. Given beta distribution allows more likely to approach $K = 0.5$ than $K = 0$ or 1 since there are only two points on the Poincare's sphere where polarization aligns with the PBS axes.

To summarize, both approaches: splitting PDM signals equally in PBS or randomly scrambling and providing the required optical pump path difference are necessary to satisfy to minimize rOSNR penalties caused by pump phase modulation. Figure 37 summarizes the rOSNR penalty as a function of the optical pump path difference three scenarios described above.

When signal polarization is aligned with the PBS axes the rOSNR penalty is 0.28 dB regardless of the pump path difference (blue line). When signal polarization is equally split

between the Looped PI-FOPA arms, the rOSNR penalty strongly depends on the pumps' optical path difference.

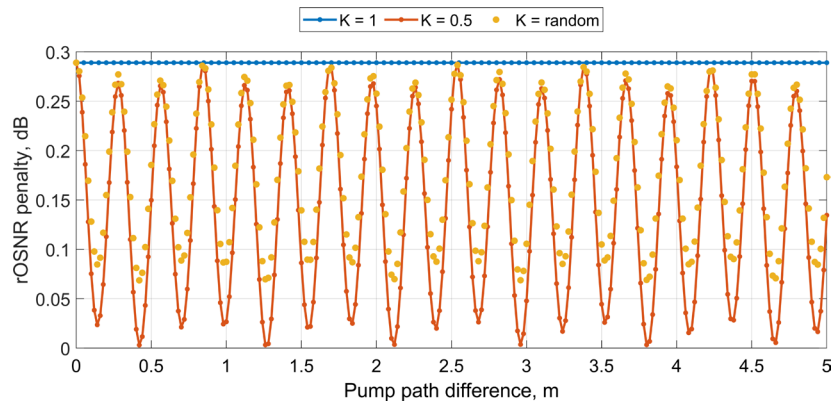


Figure 37. rOSNR penalty versus path difference between pumps for PDM signal polarization aligned with the PBS axes (blue), equally split (red) or randomly scrambled (yellow). Tones multiplier = 3.05. Signal wavelength 1531 nm.

Thus, there are two series of minimum with periods of $\sim 28\text{cm}$ and $\sim 84\text{cm}$. These minima correspond to the cancellation of distortion caused by the highest (709MHz) and second highest (233MHz) pump phase modulation tones respectively. These tones provide the most significant impact on amplified signals among the four tones, so their mitigation almost eliminates the rOSNR penalty, reducing it below 0.05dB. In case of random signal polarization (yellow), the result is averaged across all polarizations, so the achievable average rOSNR penalty is ~ 0.07 dB if an optimal pump paths difference (or equivalently, base frequency) is chosen.

It might not be practical to carefully measure and adjust the optical path difference to achieve the best performance, instead, the pump phase modulation frequencies can be adjusted to optimize performance with the existing optical path difference between pumps. Figure 38(a) shows that adjustment of both the pump path difference and the pump phase modulation base tone frequency allows the reduction of the rOSNR penalty by an order of magnitude when compared to the worst-case (i.e. 0.03dB vs 0.3dB) if the signal polarization is equally split between in the PBS. The penalty level can be maintained below 0.1 dB within an optical path difference margin of ~ 14 cm and base tone frequency margin of 0.8 MHz Figure 38(b) shows that if the signal polarization is random (each point is calculated as an average of many polarizations taken from the same set), adjustments of the

optical path difference and/or modulation frequencies can still reduce the rOSNR penalty by 30%.

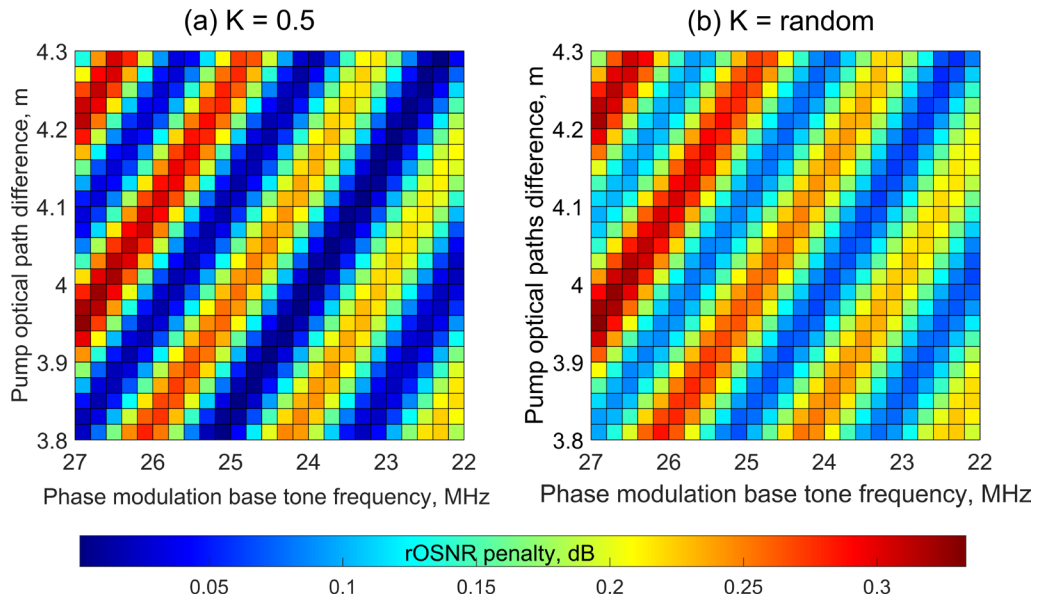


Figure 38. rOSNR penalty calculated for combinations of pump path difference in meters and pump modulation base tone frequencies for PDM signal polarization (a) equally split or (b) randomly scrambled. Signal wavelength 1531 nm.

This finding may have implications for other SBS-limited parametric devices, such as wavelength converters and optical phase conjugators, by enabling pump dithering compensation while employing a single pump.

3.5 Summary

This chapter presented a theoretical analysis of the impact of pump phase modulation on QAM signals amplified by PI-FOPA. It demonstrated that pump phase modulation using sine tones is the optimal approach, providing bandwidth efficiency and effective SBS mitigation compared to PRBS and white noise modulation.

The impact of pump phase modulation on QAM signals was assessed through the rOSNR penalty to achieve a target BER level of 0.01 for 16-QAM. A simulation model was developed to estimate the BER for QAM signals affected by phase noise induced by pump phase modulation in FOPA. The model showed that the rOSNR penalty increases with total pump bandwidth, irrespective of the base tone frequencies and the number of employed tones. The penalty reaches a minimum near the pump wavelength and increases

significantly with signal detuning from the pump. This behavior differs from previous studies focused on OOK modulation formats, as QAM signals are more susceptible to induced signal phase modulation while being more resilient to power fluctuations than directly detected signals.

The state-of-the-art polarization-diverse PI-FOPAs, such as Looped PI-FOPA and MZ-FOPA, minimize rOSNR penalties caused by pump phase modulation due to their design. By adjusting the pump path difference and the base tone frequency of the pump phase modulation waveform, while ensuring the signal polarization is equally split at the PBS, the rOSNR penalty can be reduced to below 0.1 dB.

4 EXPERIMENTAL STUDY OF PUMP PHASE MODULATION IN LOOPED PI-FOPA

This section performs experimental validation of simulations, described in chapter 3. First, I have examined the SBS suppression effectiveness of pump phase modulation with different multi-sinusoidal waveforms in 4.1. The required signal OSNR measurements were explained in 4.2 for a range of phase modulation schemes including the impact of an induced signal phase and amplitude modulation on a commercial receiver BER and validating the employment of polarization diversity architecture to mitigate an impact of pump phase modulation in FOPA.

4.1 SBS suppression effectiveness of pump phase modulation with different multi-sinusoidal waveforms

4.1.1 Experimental setup

The experimental setup to measure the pump optical spectrum, input, and backscattered pump power in looped PI-FOPA (LG configuration) is shown on the Figure 39. The PI-FOPA architecture was as explained in section 3.3.

The PI-FOPA pump was sourced from a 100 kHz linewidth CW tunable external cavity laser (IDPhotonics) at the wavelength 1566.2 nm (central frequency 191.414 THz). Its datasheet RIN is -145 dB/Hz [113]. The pump was then phase modulated with a range of multi tone waveforms to examine their SBS mitigation capability. The multi-tone waveforms were generated as described by eq.(2.22) in arbitrary waveform generator (AWG) and amplified with an RF amplifier (Figure 39, purple box). Each generated waveform consisted of three or four tones, whereas the base tone had frequency between 25 MHz and 225 MHz, and the rest of tones were obtained by subsequent multiplication by 3 or 3.05.

The Table 2 provides list of tones, base tone frequencies, and their corresponding total pump bandwidth further used for several scenarios. It must be noted that not all listed parameters were used for all experiments. The amplitudes of the tones produced by the AWG were adjusted so that all the first-order harmonics have equal power within a 1 dB variation, and this corresponds to the phase modulation amplitude of ~ 1.434 rad per tone.

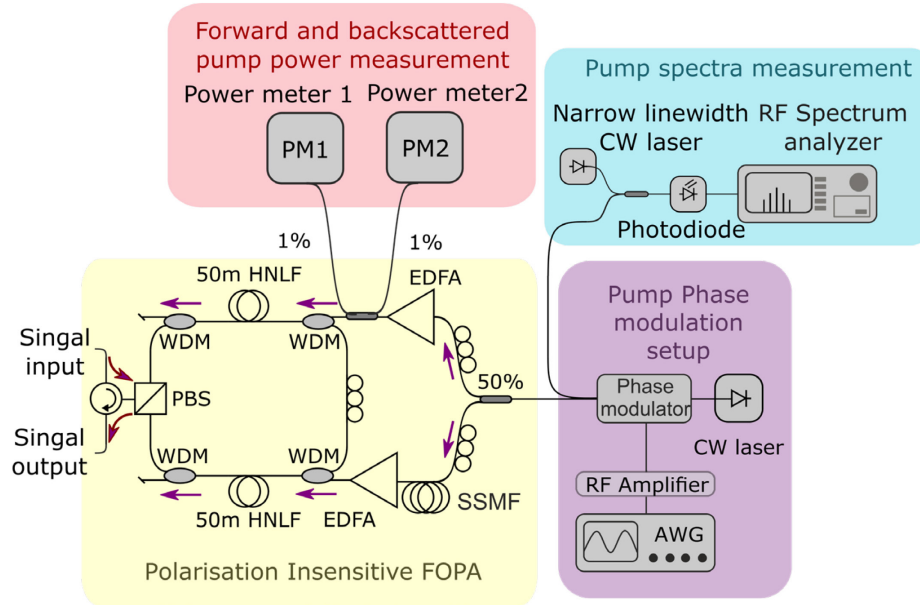


Figure 39. The experimental setup for measurements of the pump optical spectra, input, and backscattered pump power for a range of pump phase modulation waveforms employed by the looped PI-FOPA.

Table 2. Parameters of pump modulation waveforms

Number of sine tones in waveform	Base tone frequency, MHz	Total pump bandwidth when the tone multiplier is $m=3$, MHz	Total pump bandwidth when the tone multiplier is $m = 3.05$, MHz
4	20	1600	1669
4	25	2000	2086
4	30	2400	2504
4	35	2800	2921
4	40	3200	3338
4	45	3600	3755
3/4	50	1300/4000	1335/4173
4	65	5200	5424
3/4	75	1950/6000	2003/6259
3/4	85	2210/6800	2270/7093
3/4	100	2600/8000	2671/8345
3	125	3250	3338
3	150	3900	4006
3	175	4550	4673
3	200	5200	5341
3	225	5850	6009

The tone frequency spacing between them and power distribution of the first-order harmonics were observed at the 26.5 GHz RF spectrum analyzer by using a heterodyne detection with phase modulated pump laser output of phase modulator and a local oscillator which frequency was shifted by 8.9 GHz from the pump (Figure 39, blue box). The residual amplitude modulation of a phase-modulated pump was experimentally measured to be -60 dB per tone. This confirms that the quality of the phase-modulated pump was not compromised by residual amplitude modulation.

4.1.2 Measurement of phase modulated pump spectra

For spectra measurement the phase modulated pump was 50/50 coupled with narrow linewidth CW laser used as a local oscillator, then connected to the photodiode and to the RF spectrum analyzer. Figure 40 shows the measured and simulated spectra for four different waveforms, where sine tones multiplied by integer multiplier $m=3$.

The shown spectra match well with simulation. The measured total pump bandwidth validates the calculation of pump bandwidth from eq. (2.22). The peaks and dips are caused by first order harmonics overlapping, as pump was modulated by tones with an integer multiplication factor between them. For example, the 3rd harmonic of f_1 overlaps with the 1st harmonic of f_2 .

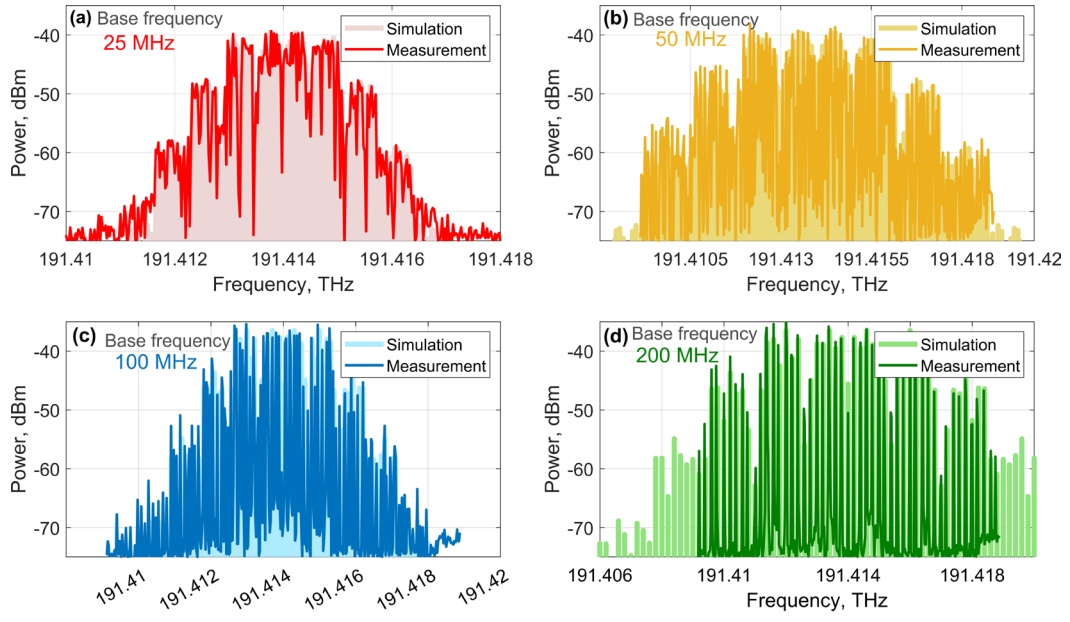


Figure 40. Measured pump optical spectra for several modulation waveforms, where pump was modulated by tones with an integer multiplication factor between them $m=3$: (a) 4 sine tones, Base tone frequency 25 MHz, (b) 4 sine tones, Base tone frequency 50 MHz, (c) 3 sine tones, Base tone frequency 100 MHz, (d) 4 sine tones, Base tone frequency 200 MHz. Simulated spectra are shown for reference.

Flatter pump spectra shown on Figure 41, confirm that phase modulation by tones with a non-integer multiplication factor prevent the Bessel function harmonics from overlapping. As a result, the highest spectral peak power decreased on 5 dB for pump waveform with base tone frequency of 25 MHz (a) and on 3 dB for pump waveform with base tone frequency of 100 MHz (b) (Figure 41).

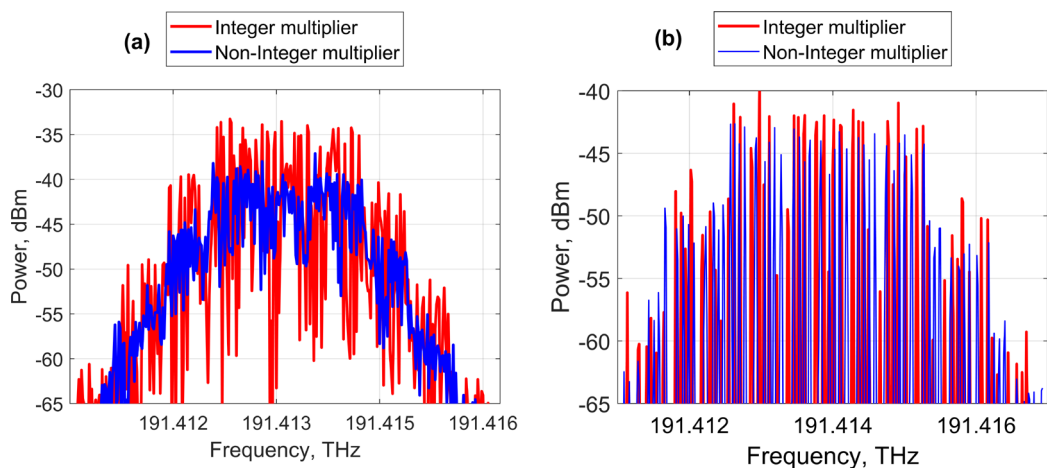


Figure 41. Measured pump optical spectra for modulation waveforms with an integer and non-integer multiplication between sine tones: (a) 4 tones, $f_{\text{base tone}} = 25$ MHz and (b) 3 tones, $f_{\text{base tone}} = 100$ MHz.

The multiplication factor should be close to 3 to allow for nearly equal spacing between the first-order harmonics and their combinations, thereby achieving the highest bandwidth efficiency.

4.1.3 Measurement of SBS threshold increase

The phase-modulated pump was split into two arms using a 50/50 beam splitter and amplified by high-power EDFAs in each arm. Pump powers launched into the 50 m long HNLFs were measured using a 1% calibrated tap coupler (e.g., at PM1). The parameters of HNLFs used in Looped PI-FOPA are listed in the Table 3.

The monitored pump powers were varied between 35 and 41 dBm. Then the backscattered pump power was measured at PM2 (Figure 39, red box) to study the effectiveness of SBS suppression. No signal was launched in FOPA at this stage. Then, the backscattered-to-input pump power ratio was derived and used to find the SBS threshold at the ratio of 35.5 dB as a point, where nonlinear behavior of backscattering started to appear. Figure 42(a) shows backscattered-to-input pump power ratio as a function of pump power for examined multitone waveforms to find the SBS threshold improvement in each case.

Table 3. Parameters of HNLFs used in Looped PI-FOPA

Length	L	50	m
Cladding diameter		123	um
Loss	α	1.19	dB/km
Dispersion slope	S	0.0407	ps/nm ² /km
Cutoff wavelength		1347	nm
Effective mode area of the fiber	A_{eff}	10.7	um ²
Nonlinearity coefficient	γ	21.4	W ⁻¹ km ⁻¹
Polarization mode dispersion		0.056	ps/ $\sqrt{\text{km}}$
Zero dispersion wavelength	λ_0	1562.9	nm

Figure 42 (b) shows the SBS threshold increase measured for the range of generated in AWG pump waveforms modulated with three ('red') and four ('blue') sine tones with the total bandwidth between 1 and 8 GHz. The total bandwidth was expanded by increasing the spacing between tones, achieved by raising the frequencies of the base tones. It was observed that in the three-tones case the increase in the SBS threshold was from 13.5 dB to 14.7 dB for all pump bandwidths.

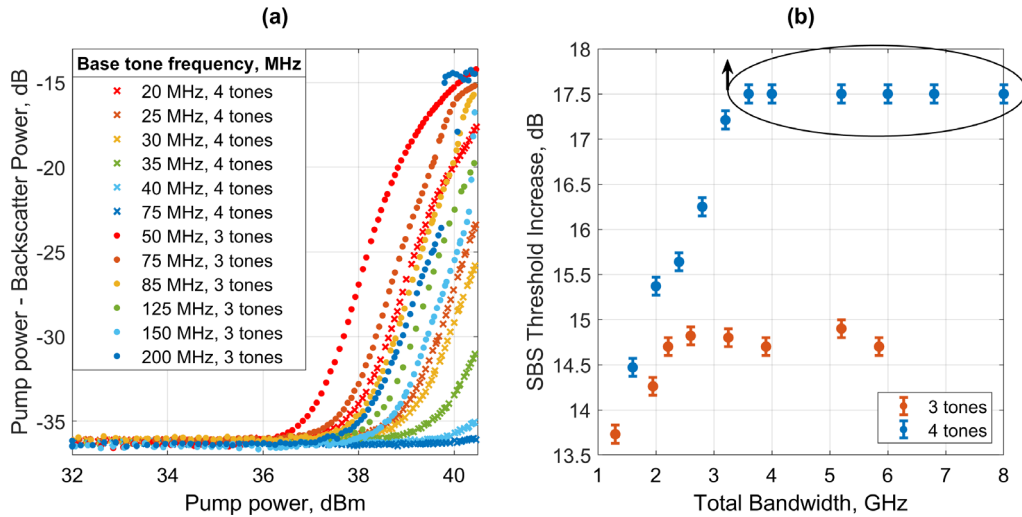


Figure 42. (a) Backscattered-to-input pump power ratio dependence on input Pump power, (b) the SBS threshold increase versus total pump bandwidth.

The latter corresponds to the factor of ~ 27 as the pump was split into 27 lines separated by more than the SBS interaction bandwidth (minimal examined base frequency in this case was 50 MHz). The higher-than-expected SBS threshold increase of 15.5 dB may be attributed to the possible contribution of higher-order harmonics in the pump spectrum, as the modulation amplitude could have been overdriven.

In the four-tones case the SBS threshold increased linearly until pump bandwidth reached 3.5 GHz (base frequency of 45 MHz), and then the maximum EDFA power was not sufficient to induce an observable SBS, so the SBS threshold increase appears flat on the plot, but we expect it to reach ~ 19 dB (factor of 81). In addition, these measurements experimentally confirmed that waveforms with more tones provide higher SBS suppression even for the same pump bandwidth because more tones allow for more uniform and dense spectral power distribution.

Backscattered-to-power ratio remains flat at 17.5 dB for waveforms with 4 sine tones and base tone frequencies of 45 MHz and higher to the maximum available pump power of 41 dBm, suggesting that the SBS threshold is higher than that. This is consistent with theory, as the SBS threshold increase is expected to be 19 dB when four sine tones are applied, producing 81 first-order harmonics in the optical domain. For other curves the SBS threshold was defined as the pump power when the backscattered-to-input power ratio reaches -35.5 dB to evaluate the SBS threshold enhancement in each case.

The backscattered-to-pump power ratio was approximately 4.5 dB higher, and the observed SBS threshold was 1 dB higher when using tones with a non-integer

multiplication factor ($m=3.05$) compared to an integer multiplication factor ($m=3$). This improvement is due to the enhanced flatness achieved by avoiding interference with higher-order harmonics (Figure 43). It should be noted that the results shown in Figure 43 were measured using a different setup from the one in Figure 39, although the same procedure was followed.

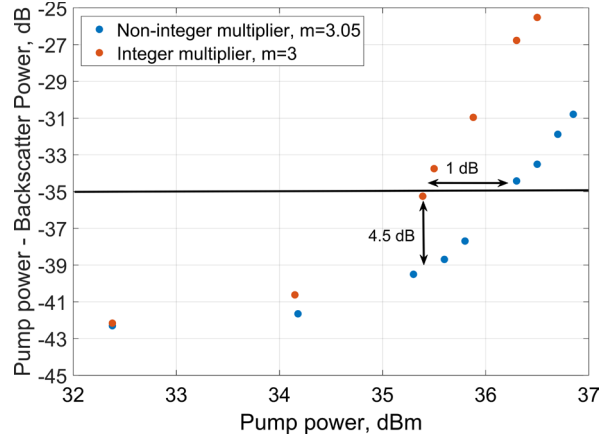


Figure 43. (a) Backscattered-to-input pump power ratio dependence on Pump power for modulation waveform with 4 tones with $f_{\text{base tone}} = 25$ MHz and an integer and non-integer multiplier between tones.

The 1 dB increase of pump power allows for a 25% higher nonlinear phase shift γPL . If the γPL will be increase from 3 to 3.75, the maximum FOPA gain increases from 20 dB to 26.6 dB according to Eq.(2.7) and Figure 6.

4.2 Impact of pump phase modulation with different multi-sinusoidal waveforms on a coherently detected 16-QAM signal

4.2.1 Methodology of rOSNR measurements

Figure 44 shows the experimental setup for evaluation of the rOSNR penalty in the PI-FOPA and different pump phase modulation parameters.

A commercial transponder was used to generate a 35GBaud 200G PDM-16-QAM signal in the wavelength range from 1530 nm to 1547 nm covering the 3 dB FOPA gain bandwidth.

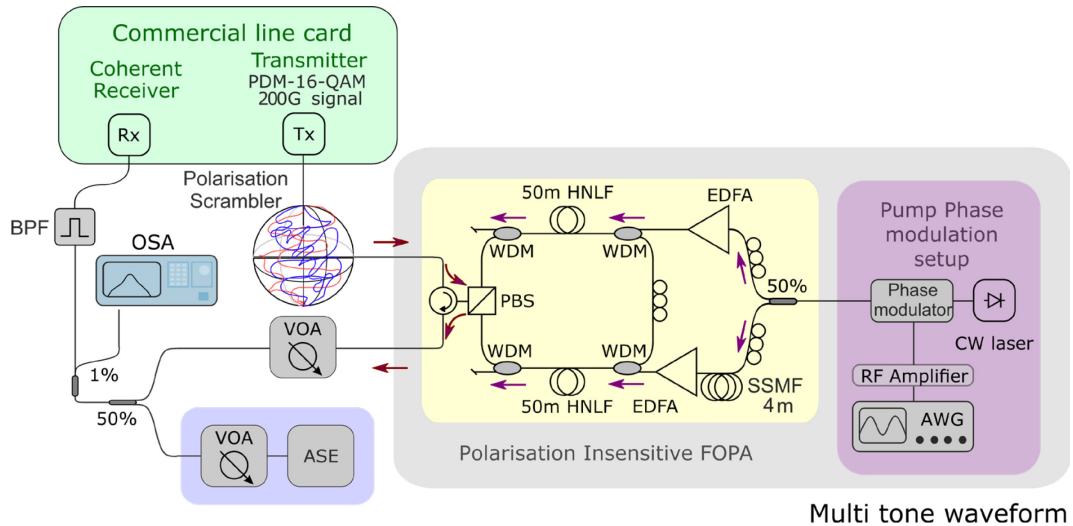


Figure 44. Experimental setup: OSA – Optical spectrum analyser, ASE – amplified spontaneous emission, BPF – bandpass filter, AWG – arbitrary waveform generator, VOA – variable optical attenuator, PC – polarization controller.

The signal was passed through a polarization scrambler to provide a random change of polarization in time to compare results with simulation. The polarization scrambling speed was 20 krad/s to allow for penalty-free operation of the employed transponder in back-to-back configuration. Then, the signals were amplified by the PI-FOPA with net gain in the range from 12 ± 0.5 dB to 15 ± 0.5 dB across the examined wavelength range (corresponding on/off gain of 17 ± 0.5 and 20 ± 0.5 dB), with polarization-dependent gain (PDG) of less than 0.2 dB across all measurements. For B2B measurements used as a reference, the PI-FOPA has been bypassed. The signal was then passed through a variable optical attenuator (VOA) to ensure that the detected signal power was -7 dBm for all BER measurements including B2B. Then, the signal was combined with an ASE noise, which power was varied with another VOA to sweep the OSNR. Then, the signal OSNR was measured through a 1% tap coupler with an optical spectral analyzer (OSA). Finally, the signal was passed through a band pass filter (BPF) and then detected by a coherent receiver which measured BER via counting errors for 1 s.

The PI-FOPA architecture was as explained in sections 2.3 and 3.3. The PI-FOPA pump was sourced from a 100 kHz linewidth laser at the wavelength 1566.2 nm. The pump was then phase modulated with a range of multi tone waveforms to examine their impact on an amplified signal. The phase modulation setup is explained in 4.1.1.

4.2.2 Evaluation of rOSNR penalty with Real-World receivers

This subsection describes the study of the impact of induced signal phase and amplitude modulation on the BER of a commercial receiver. Inclusion of this data into the simulation model instead of an ideal receiver will improve simulation model and allow for comparison between the simulated and experimental results. The impact of the signal phase and amplitude modulation on performance of a commercial receiver has been investigated by measuring the required received (rRx) power penalty in B2B configuration when a small phase or amplitude modulation with a sine wave was applied to the signal. The rRx penalty was defined as the difference between the required receiver power to achieve BER of 0.01 with and without the sine wave modulation. The measured rRx penalty is assumed to be equivalent to the rOSNR penalty under condition that the received signal SNR is limited by the receiver noise in the former case and by the optical noise in the latter case. Back-to-back measurements were performed with a commercial line card for signal with and without external phase or amplitude modulation. An external phase or amplitude modulation was done by inserting a phase or amplitude modulator prior to the transmitter IQ modulator (Figure 45).

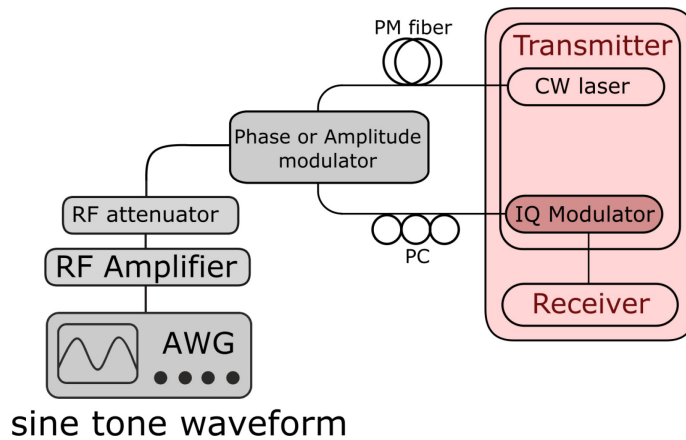


Figure 45. Setup for characterization receiver penalty. AWG – arbitrary waveform PC – polarization controller, PM fiber – polarization maintaining fiber [108].

A polarization controller was added after the external modulator to set correct polarization for the IQ modulator. The external phase or amplitude modulator was driven with a single sine tone from an AWG. Its electrical power was adjusted with RF amplifier and RF attenuator. The depth of the induced signal phase and amplitude modulation has been varied and the required Rx power penalty to achieve BER of 0.01 has been measured for the 35 Gbaud PDM-16-QAM signal. First, the sine tone frequency was varied from 100 MHz to 4 GHz to assess its impact on the results. Figure 46 presents the measurements,

where each point represents the average of five measurements, and the error bars indicate the standard deviation. The relatively large error bars and the absence of a clear trend in rRx penalty with increasing sine tone frequency confirm that the penalty is independent of the sine tone frequency.

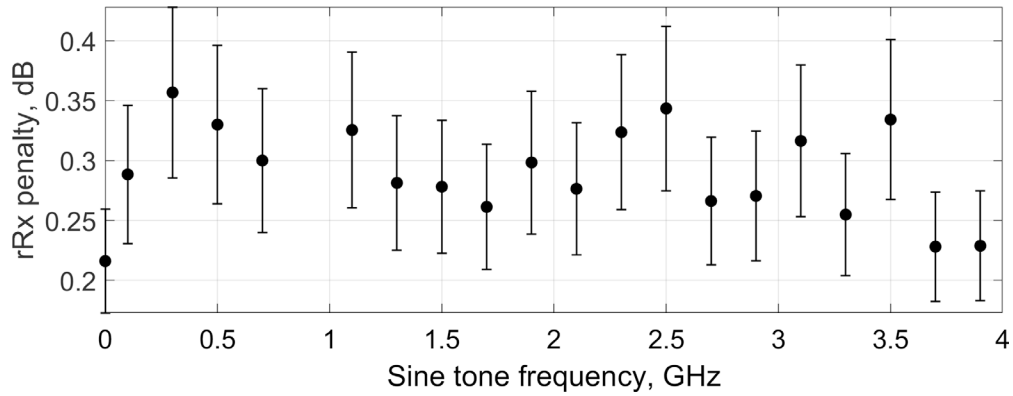


Figure 46. Required received penalty versus sine tone frequency for phase modulation amplitudes ranging from 0.002 to 0.008 radians.

Figure 47 shows the linecard rRx penalty depending on the induced (a) phase modulation and (b) amplitude modulation penalty with linear approximation. The rRx power was increased by 0.2 dB compared to the back-to-back case after the phase/amplitude modulator and polarization controller were inserted into the setup, even without any modulation applied. This implementation penalty was subtracted from the results. Error bars were calculated as for results (Figure 46).

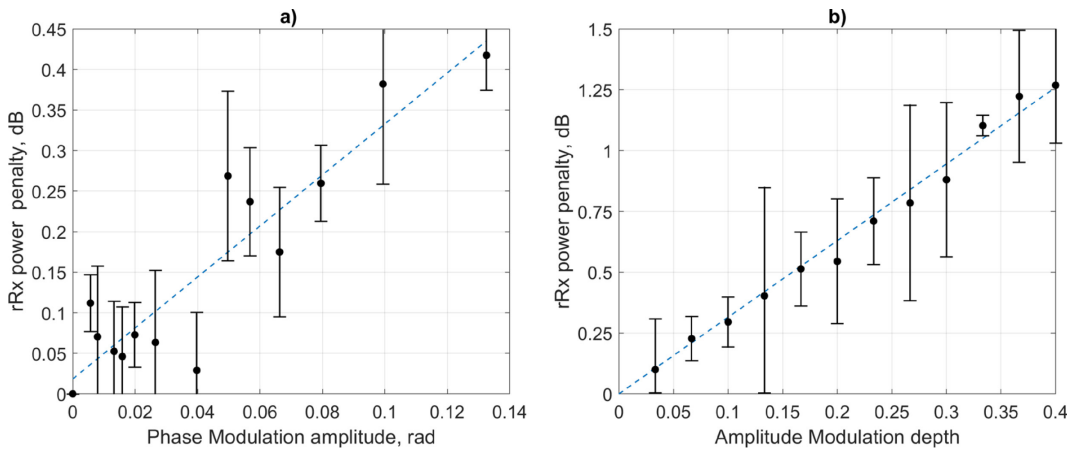


Figure 47. (a) required Rx power penalty vs phase modulation amplitude, (b) required Rx power penalty vs amplitude modulation depth. Modulation frequency is 100 MHz. Blue dashed line is linear fit after a 0.2 dB implementation penalty had been subtracted [108].

The best fitting line shows that penalties grow linearly with an increase of modulation amplitude in both cases. The rRx penalty scaling factor was approximated to be 3.145 dB/rad for phase modulation and 0.0315 dB per percent of amplitude modulation depth, which indicates the magnitude of changes in signal amplitude when amplitude modulation is applied. Both signal phase amplitude and amplitude modulation depth were multiplied by introduced scaling factors and summed up to simulate rOSNR penalty considering residual dithering on the receiver.

4.2.3 The rOSNR penalty as a function of pump bandwidth

The required-OSNR penalty was experimentally measured and determined at the BER level of 0.01 for each examined pump phase modulation waveform compared to back-to-back case for signal wavelengths between 1530 and 1547 nm. The OSNR penalty increases with the total pump bandwidth (see Figure 48) along the same trend for both three and four tones. The rOSNR penalty is linearly scaled with the pump bandwidth rather than with the number of tones or base frequencies.

The impact of pump dithering on the required-OSNR penalty experimentally measured across several signal wavelengths as a function of total pump bandwidth and compared the results with simulation to confirm simulation model of Looped PI-FOPA described in sections 3.2 and 3.3.

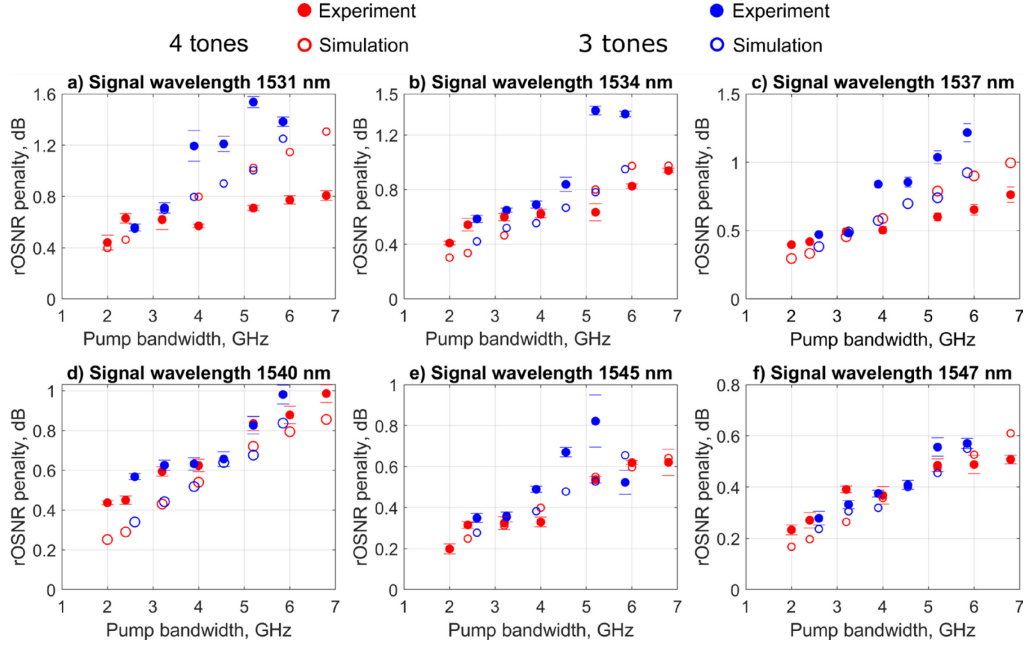


Figure 48. rOSNR penalty versus total pump bandwidth for 6 wavelengths across the 3 dB FOPA gain bandwidth. Red: experiment (dots) and simulation (circles) with 4 tones, 25–85 MHz base tone. Blue: experiment (dots) and simulation (circles) with 3 tones, 100–225 MHz base tone. Tones generated with $m = 3$. FOPA parameters from Figure 5, including real receiver performance.

In simulation FOPA parameters were taken from Figure 5 and description of experimental setup from subsection 4.2.1 to fit the experimental gain spectrum. Both the signal phase and amplitude modulation depth, derived from the output signal complex amplitudes in simulations, were multiplied by the scaling factors introduced in Figure 47 and summed to obtain the rOSNR penalty, accounting for residual dithering at the receiver.

Figure 48 demonstrates rOSNR penalty versus total pump bandwidth for 6 wavelengths across the 3 dB FOPA gain bandwidth. Experimental results shown with red dots and blue dots follow the same trend of the rOSNR penalty increase with pump bandwidth demonstrated in Figure 28(b), although experimental points show some scattering.

The linear slope increases with the signal wavelength detuning from the pump in accordance with the Figure 28(b). The rOSNR penalty are about 0.2–0.4 dB at the 2 GHz pump bandwidth and increase up to 0.5–1 dB at 6.8 GHz. Therefore, the pump bandwidth must be kept as low as possible for the best performance and then rOSNR penalties of signals amplified by a PI-FOPA can be kept low in the range of 0.2–0.4 dB even without dithering cancellation.

4.2.4 rOSNR penalty as a function of the pump modulation base tone frequency

In the PI-FOPA, the phase-modulated pump was split into two arms via 3 dB coupler and amplified by high-power EDFAs. The delay between pumps was measured by amplifying a 10 Gbit/s OOK signal with a (2^7-1) PRBS pattern in for each arm in turn, measuring the rising edge of the longest string of consecutive one symbols on Tektronix Oscilloscope. The delay between pumps was determined by comparing PRBS patterns saved from the two arms (Figure 49).

The measured delay between PRBS patterns was 20.56 ± 0.02 ns, corresponding to an optical path difference between the pumps of $4.1\text{m} \pm 4\text{mm}$. The pump powers launched into HNLf were approximately 38 dBm, and the HNLfs were 50 m long. Required-OSNR penalty were measured by varying the base tone frequency with a step of 250 kHz to confirm this approach described in section 3.4.

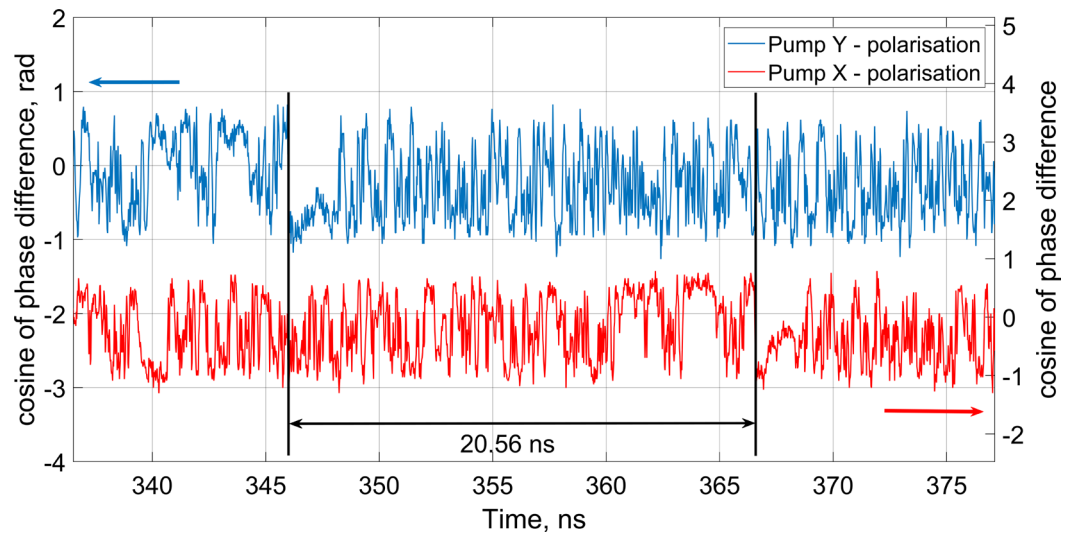


Figure 49. Measured delay between pumps of 20.56 ± 0.02 ns by comparing PRBS patterns saved from the two FOPA arms.

Figure 50 shows rOSNR penalty versus pump base tone frequency for two examined signal wavelengths of 1531 nm and 1545 nm. Experimental data point (depicted in black with error bars) represents an average obtained from an ensemble that includes all potential signal polarization states measured over a period of ~ 10 minutes. This period was the same for each base tone frequency within the range of 22 MHz to 27 MHz.

The two lowest experimentally measured penalties were observed at base tone frequencies of 23.5 MHz and 25.25 MHz as predicted by our simulation. Although experimental results might look like a random scatter, they are averaged across a number of measurements taken at different times, and the minimum penalty for both signal

wavelengths occur exactly at the frequency where we expect the best cancellation for the measured delay between the pump paths.

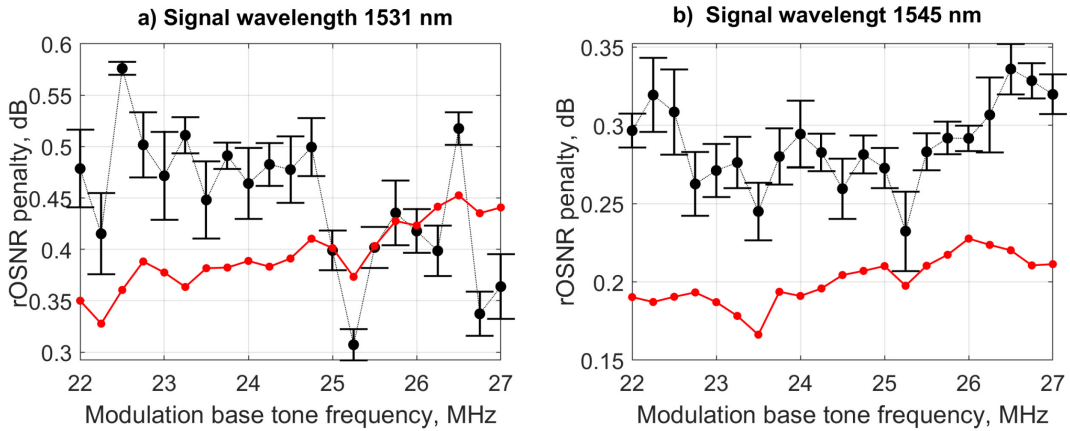


Figure 50. rOSNR penalty vs Pump base tone frequency for signal wavelength of (a) 1531 nm and (b) 1545 nm. Black – experimental data with error bars, Red –simulation using the FOPA parameters from Figure 5, $K =$ random, and including performance of real receivers [108].

Therefore, this is confirmation that reduction of the required-OSNR penalty by $\sim 32\%$ can be achieved by matching the pump phase modulation frequency with the time delay between pumps. The discrepancy between simulations and experiments, such as increased penalties being generally higher than theoretical ones, can be explained by impact of other penalty sources, such as nonlinear distortion.

4.2.5 rOSNR penalty distribution across the FOPA gain spectrum

Figure 51 illustrates the rOSNR penalty as a function of signal wavelength for 4 scenarios. The pumps were phase modulated with a combination of 4 sine tones, whereas the base tone was 25.25 MHz, and higher frequencies were obtained via multiplication by 3.05, 3.05^2 , 3.05^3 . Blue curve represents an ideal receiver which penalties could be below 0.1 dB between 1530 nm and 1545 nm.

However, experimental results (black) show a larger penalty, as the receiver adds more penalty to the signals with residual phase and amplitude modulation, as shown in subsection 4.2.2. The penalty due to the induced signal amplitude modulation (green) exhibits a minimum at the FOPA gain peak of ~ 1534 nm, where gain spectrum is flat and so the induced amplitude gain fluctuation is the lowest as was shown in [35]. Similarly, the rOSNR penalty is the highest at the gain spectrum slope (Figure 28(b), i.e., 1530 nm. Amplitude modulation is more pronounced at the spectrum edges of 1530 nm and 1548 nm leading to an increase in rOSNR penalty.

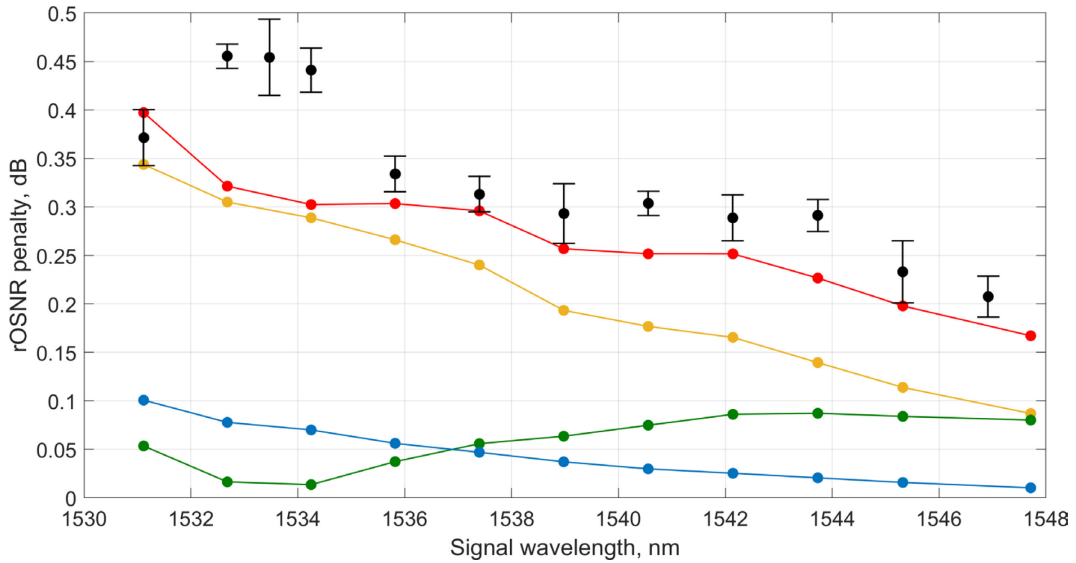


Figure 51. rOSNR penalty vs signal wavelength. Red - simulated real receiver, Yellow – simulated real receiver considering only induced phase modulation, Green – simulated real receiver with only induced amplitude modulation, Blue – simulation of ideal receiver, Black – experiments. Simulation using the FOPA parameters from Figure 5, $K = \text{random}$ and including data scaling from Figure 47 [108].

The yellow curve shows how the commercial receiver adds penalty due to the transferred phase modulation to the signals: the penalty increases monotonically with the distance from the pump wavelength until the FOPA gain slope becomes negative. Penalties at wavelengths closer to pump wavelength are mostly caused by residual signal amplitude modulation, while the distant wavelengths are exposed to the inherited signal phase modulation. The red curve summarizes the effect of both modulations and matches the experimental results shown by black dots very well although with a small additional penalty not reflected in the simulation.

The measurement error of ~ 0.05 dB in the required-OSNR penalty fluctuation is caused by several reasons, such as the OSNR measurement error, FOPA gain drifts with 1 dB, and polarization variations.

4.3 Summary

This chapter experimentally demonstrates the relationship between pump phase modulation, SBS mitigation effectiveness, and induced signal phase modulation in polarization-diverse FOPAs.

Increasing the number of tones and reducing the spacing between them enhances SBS mitigation. Specifically, using four tones instead of three with a spacing of 25 MHz, compared to 100 MHz, increased the SBS threshold by 2.5dB, as shown by the measurements. The use of tones with a non-integer multiplication factor prevents Bessel function harmonics from overlapping, resulting in a flatter pump spectrum, as observed in the optical spectra measurements. It additionally raised the SBS threshold by 1 dB.

The induced signal phase modulation caused by pump phase modulation was estimated through rOSNR penalty measurements, which revealed that the penalty scales linearly with the total pump bandwidth rather than the number of tones or base frequencies. The total pump bandwidth should be minimized to reduce the required-OSNR penalty, while without compromising the SBS mitigation by using a larger number of tones. The required-OSNR penalty distribution across the FOPA gain spectrum has been experimentally shown to match the simulation. The rOSNR penalty increases monotonically with the distance from the pump wavelength until the FOPA gain slope becomes negative. Polarization-diverse PI-FOPA architecture allows to mitigate the impact of pump phase modulation. The rOSNR penalty reduction by third by adjusting the pump phase modulation frequencies and/or mismatch between the pump's optical paths has been demonstrated.

The receiver DSP significantly contributes to penalties due to challenges in handling residual signal amplitude and phase modulation. Added penalties at wavelengths closer to pump wavelength are mostly caused by residual signal amplitude modulation, while the distant wavelengths are exposed to the inherited signal phase modulation.

5 PERFORMANCE EVALUATION OF PI-FOPA IN RECIRCULATION LOOP ENVIRONMENT

In this chapter, I investigate the performance of polarization-insensitive FOPA for amplifying WDM signals in a long-haul transmission experiment with a recirculating loop. Polarization-insensitive MZ-FOPA architecture was employed to enable performance improvement by allowing to mitigate nonlinear FWM crosstalk between WDM channels [68] [69]. Pump phase modulation optimization achieved in section 4.2 was applied and examined in a recirculating loop setup. The resulted transmitted record number of WDM channels was more than 30 at a record per channel rate (200 Gbit/s PM-16-QAM) over the record distance (for PI-FOPA) of 540km. By evaluating the impact of nonlinear crosstalk and pump phase modulation, it was shown that FOPA performance is primarily limited by pump phase modulation rather than nonlinear crosstalk.

5.1 WDM transmission in a recirculating loop with MZ-FOPA

5.1.1 Experimental setup

The experimental arrangement of the recirculation loop transmission testbed with a polarization insensitive MZ-FOPA are shown in Figure 52. The setup includes a WDM signal emulator (left red box), MZ-FOPA (green box), recirculation loop (yellow box), and a receiver (right red box).

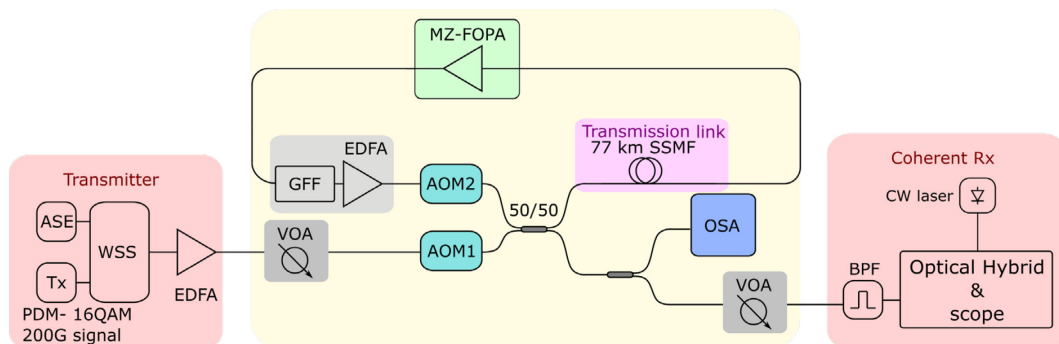


Figure 52. Experimental setup for recirculating loop transmission to investigate WDM signal amplification using cascaded MZ-FOPA.

The WDM signal emulator produced 38 x 50-GHz spaced channels between 1527 nm and 1543 nm, whereas the data channel was tuned between 1530 nm and 1542 nm. The data channel as the 35 Gbaud polarization-multiplexed 16-QAM signal sourced from a Ciena WaveLogic3 transponder, and other channels were obtained by shaping an ASE. The signal channel at 1534 nm was omitted in some measurements to estimate noise and nonlinear crosstalk level at the FOPA output. The power per channel was tuned by an EDFA and a VOA.

The receiver comprised a band pass filter (BPF), a commercial integrated coherent receiver with analogue to digital conversion achieved using an 256GSa/s, 72GHz bandwidth real-time oscilloscope and offline DSP for bit error counting. The signal power at the receiver was fixed at -14 dBm, where optimal receiver performance has been observed.

The WDM channels were gated in the recirculating loop via an acousto-optical modulator (AOM) and a 3dB coupler. The loop consisted of a 77 km length of a standard SMF (loss of 15.4 dB), the MZ-FOPA under test, a gain flattening filter (GFF) and a supplementary EDFA followed by another AOM for gating the signals out of the loop. The total loss insertion loss of the loop without amplifiers was 25 dB.

The polarization insensitive MZ-FOPA is shown in detail at Figure 53 [68], [69].

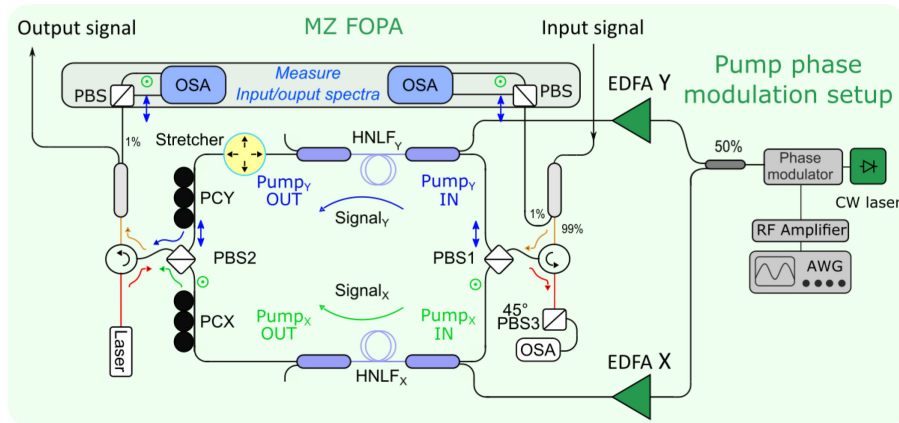


Figure 53. The polarization-insensitive MZ-FOPA setup [68].

The signal components split into the first PBS with an extinction ratio of 20 dB. Co-propagated pumps are coupled to and decoupled from the HNLs via WDM filters. HNLs are ~100 m long with $\lambda_0 \sim 1551$ nm, $\gamma \sim 14$ W⁻¹km⁻¹. The pump wavelength was 1553.43 nm. The delay between the optical path length of the two MZ arms was adjusted to be <1 ps (~0.2 mm) by tuning a fiber stretcher in the shortest arm. This delay is substantially

lower than the polarization mode dispersion tolerance of ~ 150 ps of the commercial receivers. The small signal noise figure of the MZ-FOPA was ~ 4.5 dB [69].

Figure 54 shows optical power spectra of 38 WDM channels at the input and output of the MZ-FOPA and MZ-FOPA gain spectra for both polarizations (X and Y) and PDG calculated from the input and output MZ-FOPA spectra for both polarizations.

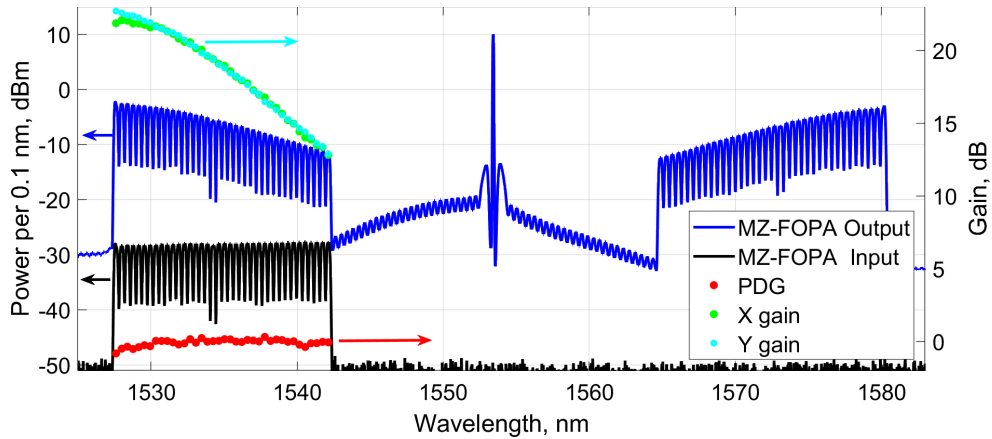


Figure 54. Optical power spectra at the input and output of the MZ-FOPA (left), MZ-FOPA gain spectra for two polarizations (labelled as X and Y) and PDG (right).

These spectra were monitored by an OSA through calibrated polarization-maintaining 1% tap couplers at MZ-FOPA input and output. MZ-FOPA gain per each polarization was from 22.3 ± 0.4 dB at 1527.6 nm (the shortest WDM wavelength) to 13.3 ± 0.4 dB at the 1541.8 nm (the longest WDM wavelength). PDG was < 0.8 dB across the range of 38 channels (14 nm).

5.1.2 Results and Discussion

Figure 55 shows the input optical power spectra of the WDM signal to the recirculation loop after the VOA and before AOM1, as well as the spectra after a number of recirculations, saved on the OSA (Figure 52).

The power level of input signals and signals after propagation in recirculation loop are the same indicating that losses from 77 km of SSMF were compensated by MZ-FOPA and supplementary EDFA. The 38 channels powers were maintained within 1 dB by Gain Flattering filter. However, the channel with data at 1534 nm stands out slightly of emulated channels due to its sharper peak edges. The total power launched to transmission fiber was varied from 5.8 dBm to 17.8 dBm and the power per channel was between -10 dBm to 2 dBm.

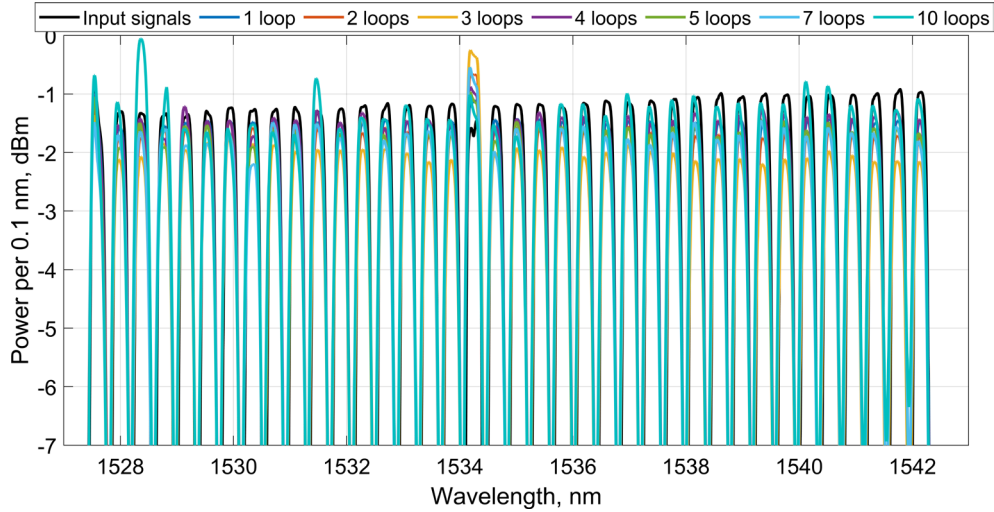


Figure 55. Optical power spectra of WDM signal at the input of recirculation loop (black) and output after 1 to 10 recirculations.

Figure 56 shows optical power spectra at the output of MZ-FOPA before GFF with 3 channels removed to assess in-band nonlinear crosstalk for different number of recirculations.

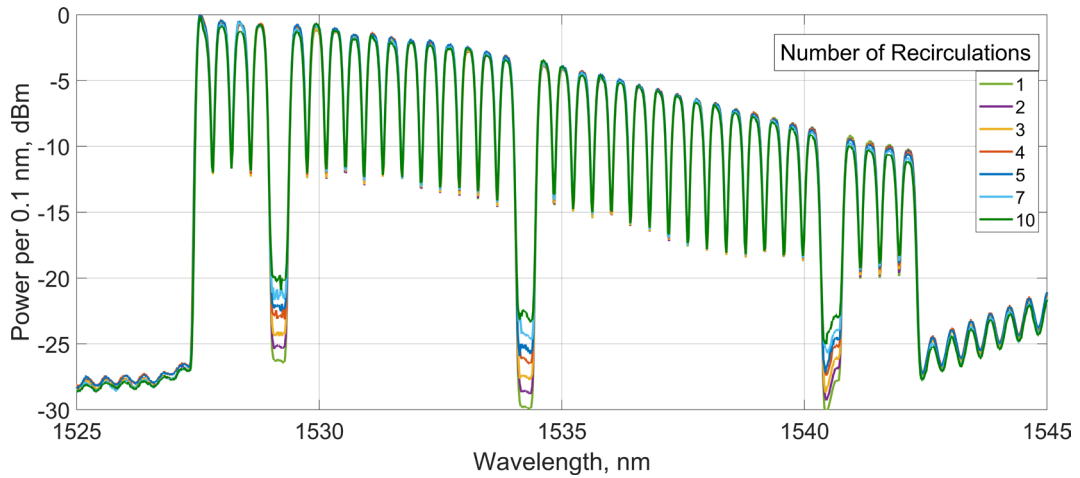


Figure 56. Optical power spectra at the output of MZ-FOPA (before GFF and supplementary EDFA) with 3 omitted channels for 1 to 10 recirculations. Pump wavelength 1553.43 nm [112].

The input power per channel at the MZ-FOPA was -16.6 dBm. The combined power of noise and nonlinear crosstalk is highest at the omitted channel at the 1529.2 nm, the OSNR (defined as the ratio of the total channel power to noise power at 0.1 nm) reaches 31.8 dB after 1 recirculation and reduced to 26.9 dB after 7 recirculations. The OSNR of 32.7 dB is observed for the omitted middle channel after 1 recirculation and degraded to 27.2 dB after

7 recirculations. Difference between pump wavelength and the closest to it channel wavelength or guard-band width $\Delta\omega_{Guard}$ is 11.25 nm or 1.41 THz, where total signal bandwidth is 14 nm (1.85 THz). Since the guard band is less than the signal band, therefore the 1st-order unwanted FWM products overlap with signals. Their power scales as $\sim \frac{P_{signal\ out}^2}{P_{pump}}$. The ripple at the longer wavelength side of the signal band indicates notable inner nonlinear crosstalk, and it is likely responsible for the relatively low OSNR at 1540.5nm measured to be 30.8 dB after 1 recirculation and 22.3 dB after 7 recirculations. The outer 1st-order FWM are generated from 1502 nm to 1530 nm, partially covering signals. However, the inner FWM products have higher power than the outer FWM products. Low SNR starting from 1540 nm indicates that the expected signal performance, expressed as BER, would be worse than that of the left neighbouring channels.

The BER against the number of recirculations for the channel at 1534 nm is plotted on Figure 57(a). Figure 57(b) shows the trend of calculated BER against optical power per same channel launched to the transmission fiber for 2, 5, 7 and 10 recirculations, which correspond to 154 km, 385 km, 539 km, and 770 km respectively.

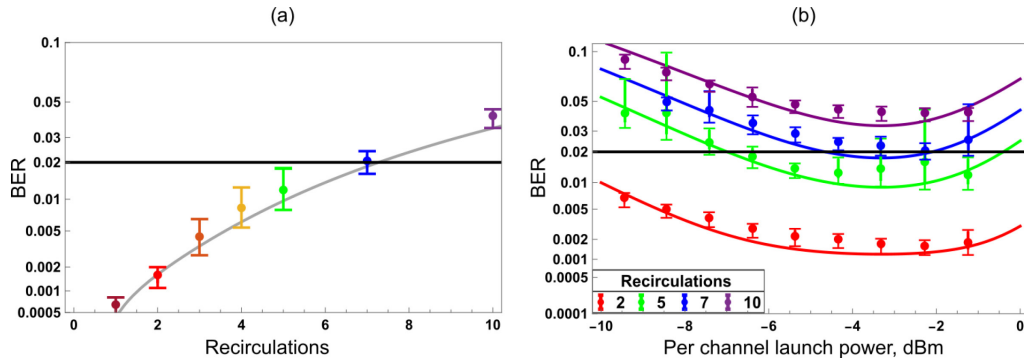


Figure 57. (a) BER versus number of recirculations, (b) BER versus launched power to transmission fiber per channel for 2 (red), 5 (green), 7 (blue) and 10 (purple) recirculations. The points are experimentally measured, and lines are fittings based on Eq.(5.1), (5.2) [112].

The data were fitted with theoretical BER calculated as a function of nonlinear SNR_{NL} (Eq. (5.1)) [53], where BER_{PN} represents the power-independent error floor due to phase noise induced by pump phase modulation.

$$BER = BER_{PN} + \frac{1}{2} \left(1 - \operatorname{erfc} \left(\sqrt{\frac{SNR_{NL}}{2.5}} \right) \right) \quad (5.1)$$

The theoretical nonlinear SNR_{NL} was calculated from Eq.(5.2), where s and n_s are the signal power and number of recirculations. SNR_0 , ASE , and NL are fitting parameters determining the transceiver noise, the amplifier noise and the intra channel nonlinear effects respectively:

$$\frac{1}{SNR_{NL}} = \frac{\frac{s}{SNR_0} + n_s \cdot ASE + n_s \cdot NL \cdot s^3}{s}. \quad (5.2)$$

After 10 recirculations 16-QAM constellation of amplified signal reaches the point where DSP was not able to recover the data for BER calculation. Maximum 7 recirculations or 539 km were detected with the BER below the FEC threshold of 0.02. Figure 57(b) indicates that the experimental BER degrades when the per channel output signal power is below -3 dBm for all measured recirculations. The optimal signal power does not depend on transmission distance and reaches a plateau at optical power at \sim -2 dBm. While BER is limited by noise at low signal power and by nonlinear crosstalk at high signal power, observing the plateau suggests that the performance is constrained by induced phase noise from pump phase modulation. Indeed, the impact of ASE noise reduces with signal power, and the impact of nonlinear crosstalk increases with signal power. At the same time the impact of pump dithering is independent of signal power.

Then, performance was compared at several different wavelengths across the amplified WDM channels (Figure 58). The channels at 1530 nm and 1534 nm have very similar performance: the same optimal launched power after 2 recirculations with same the same BER floor of $1-1.5e-4$ (Figure 58(a)). However, after 5 recirculations (Figure 58(b)), the signal at 1530 nm is more degraded at the low launched power compared to the channel at 1534 nm, as it, being close to the left side of WDM spectrum, experiences larger total gain from MZ-FOPA and larger attenuation from GFF with every recirculation. However, the BER floor at the optimal power remains the same, indicating that the performance of both channels may be limited by pump dithering. The channel at 1540 nm is significantly degraded after 2 recirculations, with its optimal signal power shifting to -5 dBm, after which nonlinear behavior becomes apparent. Such signal degradation is in accordance with significant nonlinear crosstalk observed at the MZ-FOPA output spectrum at \sim 1540 nm on the Figure 56. After 5 recirculations, its BER exceeds the FEC threshold of 0.02, which means that the signal is no longer detectable (Figure 58 (b)).

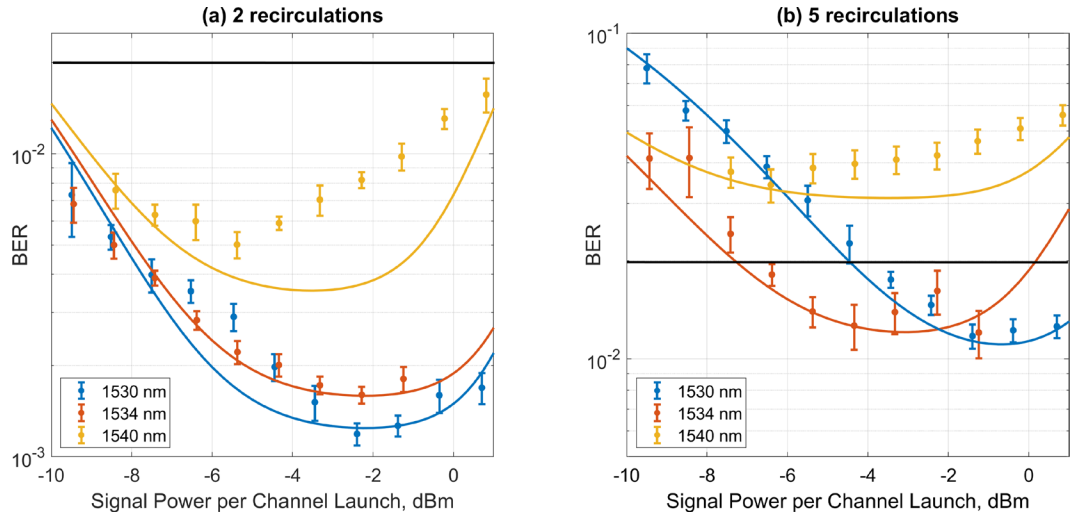


Figure 58. BER versus launched power to transmission fiber per channel for 1530, 1534, 1540 nm for (a) 2 recirculations and (b) 5 recirculations.

Finally, performance of WDM channels was estimated as a function of signal wavelength for the number of recirculations (Figure 59). The observed similar behavior of channel between 1530 nm and 1538 nm suggests that at the optimal launched signal power, their performance was limited by the same source of degradation—pump dithering. Only for channels with wavelengths longer than 1538 nm did the impact of nonlinear crosstalk dominate over pump dithering, as expected from Figure 56.



Figure 59. BER versus wavelength for number of recirculations.

5.2 Pump dithering characterization in recirculation loop transmission with MZ-FOPA

To investigate the impact of pump dithering in the recirculation loop, the experimental setup shown in Figure 52, was simplified by removing the WDM system and supplementary EDFA, leaving only the 35 Gbaud polarization-multiplexed 16-QAM signal sourced from a Ciena WaveLogic3 transponder at the MZ-FOPA's gain peak of 1530 nm (see Figure 54).

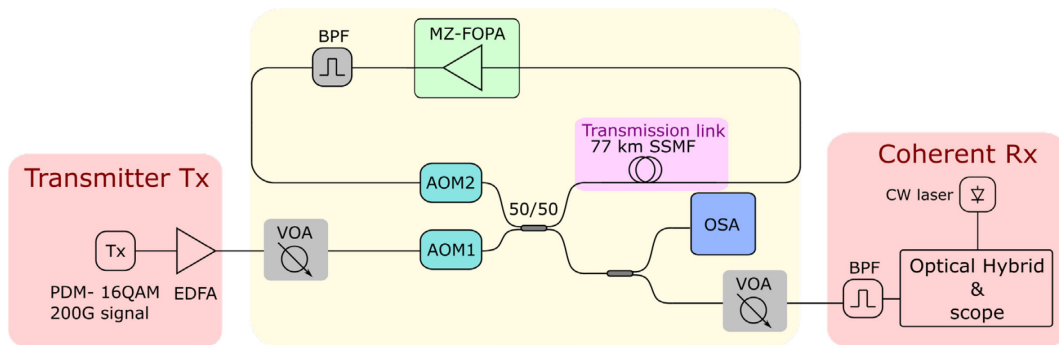


Figure 60. Experimental setup of recirculating loop transmission arrangement to examine impact of pump dithering MZ-FOPA.

The total insertion loss of the loop decreased to 25 dB after replacing the GFF with a BPF. MZ-FOPA's net gain of 25 dB was sufficient to fully compensate for the total loop loss.

The AWG was used to vary the pump phase modulation waveforms for examination of impact of pump dithering. The pump phase waveform consisted of 4 sine tones, where the base tone frequency was varied between 22 and 40 MHz, and other frequencies were obtained via multiplication by 3.05 , 3.05^2 , 3.05^3 .

Figure 61(a) shows the BER versus the number of recirculations for single channel, where base tone frequency was 30 MHz. The experimental data were fitted with (5.1) and (5.2). Figure 61(a) additionally shows experimental data obtained for the same channel in the setup from the previous section with 38 WDM channels. Notably, the performance of a single channel is very close to that of 38 channels, although the latter employed an additional GFF and an EDFA to compensate for its loss and had much larger total MZ-FOPA output signal power. This indicates that neither nonlinear interchannel crosstalk arising from interaction between multiple channels nor noise from an additional EDFA have been the limiting factors in the WDM case. This observation is further reinforced with Figure 61(b) showing BER vs power per channel launched into transmission fiber for a

single and 38 WDM channels after 2 recirculations. Indeed, Figure 61(b) shows an expected BER vs signal power behavior at low and high signal powers, whereas performance is limited by amplifier noise and nonlinear crosstalk respectively, but also shows the same BER floor for both single channel and WDM transmission experiments around optimal launch signal power.

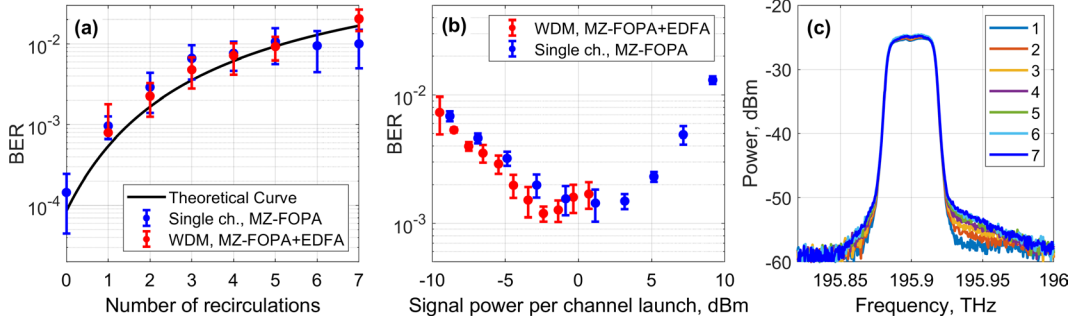


Figure 61. (a) BER versus a number of recirculations, (b) BER versus signal power per channel launch after 2 recirculations for two scenarios, (c) Optical power spectra of the received signal after a varied number of recirculations.

Figure 61(c) additionally shows optical power spectra of the received signal for different number of recirculations and demonstrates the received signal OSNR of 26 dB after 7 spans which rules out BER limitations due to broadband noise. Indeed, the MZ-FOPA noise figure is measured to be ~5 dB at 1530 nm [69], on par with commercial EDFAs, so it is not the limiting factor. Therefore, the remaining source of signal degradation should be the pump phase modulation. It suggests the pump phase modulation as a key limiting factor for the BER at the optimal signal launch power.

Consequently, the impact of pump phase modulation on the signal performance was examined by varying the pump phase modulation frequency. Figure 62(a) shows BER vs power per channel launched into transmission fiber after 2 recirculations for a single channel and for variations of pump phase modulation frequency. It clearly shows that BER is limited by noise at low signal power, by nonlinear crosstalk at high signal power and has a flat BER floor in the middle, which level is defined by the pump phase modulation frequency. This confirms that the pump phase modulation is the key factor limiting the minimum signal BER.

Additionally, the experimental data were fitted using the same equation as above, with BER_{pN} varying for different modulation frequencies. The black curve uses the same fitting parameters, but $BER_{pN} = 0$, and it shows the potential BER without pump phase

modulation. Figure 62(b) summarizes the BER floor observed at Figure 62(a) versus the base tone frequency (and corresponding total pump bandwidth).

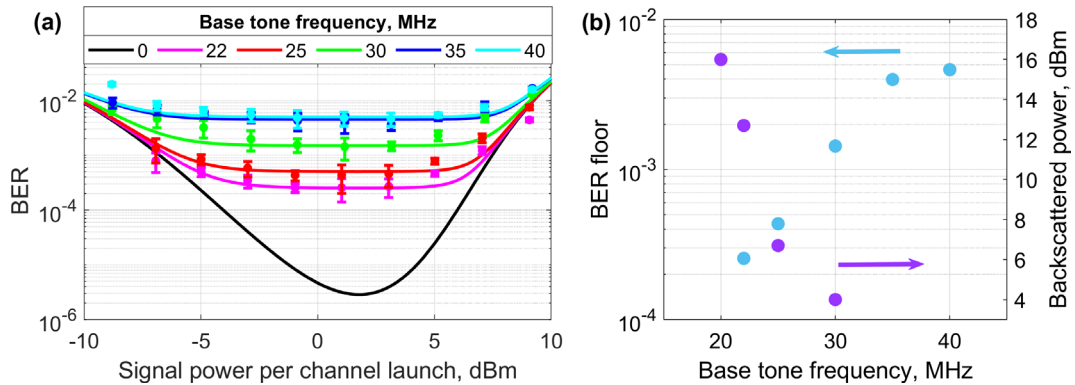


Figure 62. (a) BER versus versus signal power launched into transmission fiber after 2 recirculations for a range of pump phase modulation frequencies (dots – experiment, lines – fitting with Eq.(5.1),(5.2)), (b) BER floor (left) and Backscattered power (right) versus base tone frequency.

BER worsens steadily with the base tone frequency (blue), which shows there is great potential to decrease the impact of pump phase modulation via decrease of the pump phase modulation bandwidth. However, Figure 62(b) also shows that the backscattered power due to the SBS growing rapidly with the base tone frequency decrease. The BER measurements were not performed for the base tone frequency below 22 MHz as backscattered power reached 16 dBm and I didn't risk damaging the high power EDFA with the power backscattered into it. However, there is a room for further BER improvement by reducing the pump phase modulation base tone frequency despite an increase of the backscattered power. Consequently, the SBS threshold should be redefined for FOPAs as the point where SBS starts degrading the amplified signal BER, although there was no opportunity to achieve this point. This result also shows that employment of any SBS mitigation techniques which allow to reduce the required level of pump phase modulation (e.g. employment of Al-doped HNLF or isolators), would drastically improve the FOPA performance.

5.3 Summary

The performance of amplified 38x50GHz channels including 200G PDM-16-QAM data carrier channel amplified by polarization insensitive MZ-FOPA in recirculation loop has been examined. Maximum 7 recirculations with BER under 0.02 have been achieved

resulting in a total transmission distance of 539 km. This implies that comparing with the previous work [56] the improved MZ-FOPA along with optimized pump phase modulation scheme has allowed for transmission of same number of channels (30) with more advanced modulation format (16-QAM vs QPSK) over comparable distance (453.6 km vs 604.8 km).

By isolating the single channel from interchannel nonlinear crosstalk, pump phase modulation was shown to be a primary source of signal degradation and had a significant impact on the BER. The performance improved steadily as the pump bandwidth decreased, despite the large backscattered power induced by SBS. This indicates that induced phase noise from pump phase modulation plays a key role in limiting FOPA performance.

6 CONCLUSION AND FUTURE WORK

6.1 Conclusion

In this thesis, SBS mitigation, a major challenge in enhancing the state-of-the-art FOPA performance in optical communications, has been revisited. Various well-studied SBS mitigation techniques were analyzed to identify the most efficient solution that meets the demands of high FOPA performance in modern optical communications, such as achieving high net gain (up to 20 dB) and broad amplification bandwidth. The primary focus has been on identifying an optimal SBS mitigation method that, when employed in FOPA, delivers high performance with minimal signal degradation, specifically minimizing the induced phase noise that reduces signal SNR. A comparison of these methods revealed that pump phase modulation is the only technique capable of providing the necessary SBS suppression levels (up to 20 dB) for high-gain FOPA while not directly affecting HNLf dispersion, allowing for broadband amplification.

This thesis has also reviewed phase modulation schemes and provided optimization recommendations: using a higher number of tones with smaller spacing between first-order harmonics results in a dense, flat pump spectrum. At the same time, the total pump bandwidth should remain narrow, as pump phase modulation-induced signal phase noise is proportional to the pump bandwidth. The optimal phase modulation involves four sine tones, with the base tone frequency matching the Brillouin linewidth of the chosen HNLf (around 20-30 MHz for silica HNLf). The tone multiplier should be a non-integer value close to 3, ensuring equal spacing between the first-order harmonics. The effectiveness of this phase modulation scheme in suppressing SBS and flattening the pump spectrum was experimentally verified.

A numerical model was developed to estimate 16-QAM signal degradation through OSNR penalty in optical communication systems with coherent detection. Coherent detection of QAM signals reduces the impact of signal amplitude modulation induced by pump phase modulation, but QAM signals are highly susceptible to induced signal phase modulation. The results in this thesis, along with comparisons to previous studies, confirmed that phase noise is the primary source of degradation for coherently detected QAM signals. Experiments have also confirmed that the required OSNR penalty

distribution across the FOPA gain spectrum differs from previously reported results for OOK keying signals.

The predicted rOSNR penalty for 16-QAM signals was less than 0.5 dB to achieve a BER of 0.01 with the suggested optimal phase modulation. However, the induced phase and amplitude modulation on a commercial receiver increased the penalty. The receiver DSP plays a significant role in contributing to penalties, as an ideal simulated receiver could result in much lower penalties.

Additionally, the state-of-the-art PI-FOPA, employing polarization-diverse Looped or Mach-Zehnder architectures, was shown to reduce the rOSNR penalty below 0.1 dB by controlling pump optical path lengths, dithering frequencies, and signal polarization where possible. Experiments confirmed that the rOSNR penalty could be reduced by ~30% through pump dithering frequency adjustments. This finding has implications for other SBS-limited parametric devices, such as wavelength converters and optical phase conjugators, by enabling pump dithering compensation while using a single pump.

Finally, the state-of-the-art polarization-insensitive MZ-FOPA architecture, combined with the optimized pump phase modulation scheme, was examined in a long-haul transmission experiment using a recirculating loop. The experiment successfully transmitted more than 30 channels, including a 200 Gb/s 16QAM channel, over a record distance of 539 km, staying below the FEC limit of 0.02. However, the transmission distance is still limited by pump phase dithering, requiring further improvements to enhance FOPA performance.

Overall, the techniques proposed in this thesis represent significant progress in mitigating induced signal noise in FOPA.

6.2 Future work

This thesis demonstrated the estimation of induced phase noise in amplified 16-QAM signals using optimized pump phase modulation in FOPA. The level of phase noise is more pronounced in higher-order modulation formats, such as 64-QAM and beyond, making the requirements for pump phase modulation even stricter. In these cases, it may be necessary to further reduce the phase-modulated pump bandwidth below 1 GHz, and as was shown in last section can cause large backscattered power due to SBS. Therefore, future work should explore hybrid SBS mitigation approaches that combine pump phase modulation with passive methods, such as strain, temperature distribution, or the use of Al-doped

HNLf, which inherently reduces SBS. This could further increase the SBS threshold while minimizing signal degradation.

Even if standard HNLf is replaced with Al-doped fiber from [88], the nonlinear phase shift will be doubled, and the phase modulation waveform can be reduced to 3 sine tones, which will decrease the pump bandwidth below 1 GHz. As a result, the rOSNR penalty will drop below 0.2 dB. If standard HNLf is replaced with a perfectly manufactured Al-doped HNLf with a loss of < 0.8 dB and a reduction of g_B by 7 dB, the expected $\gamma P L_{eff}$ will be four times higher. This enhancement in the nonlinear phase shift will provide FOPA gain < 10 dB without any phase dithering. Adding strain distribution with precise dispersion control over the fiber length will introduce an additional factor of 2 to nonlinear phase shift, making it possible to achieve a gain of 20 dB. A dithering-free FOPA adds no phase noise to signals, making the FOPA performance comparable to EDFA performance in the C-band and enhancing its performance in the S and L bands.

Another very promising approach is the use of the polarization-diverse FOPA architecture described in Section 3.4. By upgrading the setup with a polarization tracker to maintain a 50/50 polarization splitting ratio between the two arms, it is possible to effectively cancel out the inherited signal phase modulation. With this approach, very high FOPA gain > 30 dB can be achieved while keeping the rOSNR penalty below 0.05 dB, offering the potential for higher data capacity and longer reach in multi-span transmissions.

Both approaches establish FOPA as a powerful wideband amplifier for optical communications. Its performance can be comparable to that of an EDFA in the C-band, achieving BER levels of $10^{-6} \dots 10^{-5}$ for 16-QAM signals in multi-span transmission, while also offering enhanced performance in the S and L bands.

In dynamic optical networks, varying conditions such as temperature changes, power fluctuations, and specific gain requirements demand adaptive FOPA control. Research could focus on real-time pump phase modulation techniques that adjust the pump waveform to optimize gain and increase the SBS threshold. For instance, reducing FOPA gain by 2–3 dB can be achieved by narrowing the pump bandwidth through sine tone adjustments. Machine learning can further enhance this adaptability by analyzing real-time transmission data to predict optimal modulation parameters, helping to mitigate system impairments and maximize performance, particularly in complex and flexible WDM transmission systems.

REFERENCES

- [1] Y. Niu, X. Yan, J. Chen, Y. Ma, Y. Zhou, H. Chen, Y. Wu, and Z. Bai, "Research progress on periodically poled lithium niobate for nonlinear frequency conversion," *Infrared physics & technology*, vol. 125, pp. 104243, 2022.
DOI: [10.1016/j.infrared.2022.104243](https://doi.org/10.1016/j.infrared.2022.104243)
- [2] R. Stolen, "Phase-matched-stimulated four-photon mixing in silica-fiber waveguides," *IEEE Journal of Quantum Electronics*, vol. 11, no. 3, pp.100-103, 1975. DOI: [10.1109/JQE.1975.1068571](https://doi.org/10.1109/JQE.1975.1068571)
- [3] G. P. Agrawal, "Four-Wave Mixing," in *Nonlinear Fiber Optics*, 5th ed., Elsevier, 2013, pp. 397–457.
- [4] M. E. Marhic, "Scalar OPA theory", in *Fiber Optical Parametric Amplifiers, Oscillators and Related Devices*, New York: Cambridge University Press, 2008, pp. 31-75.
- [5] M. E. Marhic, "The optical gain spectrum in Fiber Optical Parametric Amplifiers, Oscillators and Related Devices, New York: Cambridge University Press, 2008, pp. 31-75.
- [6] T. Torounidis, P.A. Andrekson, B.E. Olsson, "Fiber-optical parametric amplifier with 70-dB gain," *IEEE Photonics Technol. Letters*, vol. 18, no.10, pp.1194–1196, 2006.
DOI: [10.1109/LPT.2006.874714](https://doi.org/10.1109/LPT.2006.874714)
- [7] R. Malik, Rohit, and M.E. Marhic, "High-power continuous-wave operation of a fiber optical parametric oscillator in L and U bands," *Optical Fiber Technology*, vol. 20, no. 6, pp. 694-701, 2014. DOI: [10.1016/j.yofte.2014.08.006](https://doi.org/10.1016/j.yofte.2014.08.006)
- [8] M. E. Marhic, Y. Park, F. S. Yang, and L. G. Kazovsky, "Broadband fiber-optical parametric amplifiers and wavelength converters with low-ripple Chebyshev gain spectra," *Optics Letters*, vol. 21, no 17, pp.1354-1356, 1996.
DOI:[10.1364/OL.21.001354](https://doi.org/10.1364/OL.21.001354)
- [9] A.D. Ellis, M. A. Z. Al Khateeb, and M. E. McCarthy, "Impact of optical phase conjugation on the nonlinear Shannon limit," *Journal of Lightwave Technology*, vol. 35, no. 4, pp. 792-798, 2016. DOI: [10.1109/JLT.2016.2606548](https://doi.org/10.1109/JLT.2016.2606548)
- [10] A.D. Ellis, M. Tan, M. A. Iqbal, M. A. Z.Al-Khateeb, V. Gordienko, G. S. Mondaca, S. Fabbri et al, "4 Tb/s transmission reach enhancement using 10×400

- Gb/s super-channels and polarization insensitive dual band optical phase conjugation," *Journal of Lightwave Technology*, vol. 34, no. 8, pp.1717-1723, 2016.
- [11] H. Zhou, Y. Duan, M. Ramakrishnan, Z. Jiang, X. Su, K. Zou, A. T. Heiniger, M. Tur, and A. E. Willner, "Demonstration of an Optical Parametric Oscillator (OPO)-Based High-Power Data Transmitter for a 10-Gbit/s QPSK Mid-IR Coherent Free-Space Link Through Fog," *Journal of Lightwave Technology*, vol. 42, no. 11, pp. 3989-3996, 2024.
- [12] E. Agrell, M. Karlsson, F. Poletti, S. Namiki, X. V. Chen, L. A. Rusch, B. Puttnam et al, "Roadmap on optical communications," *Journal of Optics*, vol. 26, no. 9, pp. 093001, 2024. DOI:[10.1088/2040-8986/ad261f](https://doi.org/10.1088/2040-8986/ad261f)
- [13] Cisco Annual Internet Report (2018–2023), Cisco Systems, San Jose, CA, 2023.
- [14] Global Network Traffic 2030 Report, Nokia, Espoo, Finland, 2024.
- [15] D. Uzunidis, E. Kosmatos, C. Matrakidis, A. Stavdas and A. Lord, "Strategies for Upgrading an Operator's Backbone Network Beyond the C-Band: Towards Multi-Band Optical Networks," *IEEE Photonics Journal*, vol. 13, no. 2, pp. 1-18, 2021. DOI: [10.1109/JPHOT.2021.3054849](https://doi.org/10.1109/JPHOT.2021.3054849).
- [16] N. Deng, L. Zong, H. Jiang, Y. Duan and K. Zhang, "Challenges and Enabling Technologies for Multi-Band WDM Optical Networks," *Journal of Lightwave Technology*, vol. 40, no. 11, pp. 3385-3394, 2022. DOI: [10.1109/JLT.2022.3162725](https://doi.org/10.1109/JLT.2022.3162725).
- [17] N. Sambo, V. Curri, G. Shen, M. Cantono, J. Pedro and E. Pincemin, "Guest Editorial: Multi-Band Optical Networks," *Journal of Lightwave Technology*, vol. 40, no. 11, pp. 3360-3363, 2022. DOI: [10.1109/JLT.2022.3172875](https://doi.org/10.1109/JLT.2022.3172875).
- [18] L. Rapp and M. Eiselt, "Optical amplifiers for multi-band optical transmission systems," *Journal of Lightwave Technology*, vol. 40, no. 6, pp. 1579-1589, 2021. DOI: [10.1109/JLT.2021.3120944](https://doi.org/10.1109/JLT.2021.3120944)
- [19] G. Vladimir, "BROADBAND FIBRE PARAMETRIC AMPLIFIERS VLADIMIR GORDIENKO Broadband fibre parametric amplifiers," 2018.
- [20] M. Jamshidifar, A. Vedadi, and M. E. Marhic, "Continuous-wave one-pump fiber optical parametric amplifier with 270 nm gain bandwidth," in *European Conference on Optical Communication (ECOC 2009)*, p. 1.1.4.
- [21] T. Kobayashi, S. Shimizu, M. Nakamura, T. Umeki, T. Kazama, R. Kasahara, F. Hamaoka, M. Nagatani, H. Yamazaki, H. Nosaka, and Y. Miyamoto, "Wide-band inline-amplified WDM transmission using PPLN-based optical parametric

- amplifier," *Journal of Lightwave Technology*, vol. 39, no. 3, pp. 787-794, 2021.
DOI: [10.1109/JLT.2020.3039192](https://doi.org/10.1109/JLT.2020.3039192)
- [22] S. Shimizu, T. Kobayashi, T. Kazama, T. Umeki, M. Nakamura, K. Enbutsu, T. Kashiwazaki, R. Kasahara, K. Watanabe, and Y. Miyamoto, "PPLN-based optical parametric amplification for wideband WDM transmission," *Journal of Lightwave Technology*, vol. 40, no. 11, pp. 3374-3384, 2022. DOI: [10.1109/JLT.2022.3142749](https://doi.org/10.1109/JLT.2022.3142749)
- [23] N. Kuznetsov, A. Nardi, A. Davydova, M. Churaev, J. Riemensberger, P. Seidler, and T. J. Kippenberg, "An ultra-broadband photonic-chip-based traveling-wave parametric amplifier," arXiv preprint arXiv:2404.08609 (2024).DOI:[10.48550/arXiv.2404.08609](https://doi.org/10.48550/arXiv.2404.08609)
- [24] P. Zhao, V. Shekhawat, M. Girardi, Z. He, V. Torres-Company, and P.A. Andrekson, "Single-mode Dispersion-engineered Nonlinear Integrated Waveguides for Ultra-broadband Optical Amplification and Wavelength Conversion," arXiv preprint arXiv:2409.15845 (2024).DOI:[10.21203/rs.3.rs-5153136/v1](https://doi.org/10.21203/rs.3.rs-5153136/v1)
- [25] G. P. Agrawal, "Stimulated Brillouin Scattering," in *Nonlinear Fiber Optics*, 5th ed., Elsevier, 2013, pp. 353–396.
- [26] V. Gordienko, A. D. Szabó, M. F. C. Stephens, V. Vassiliev, C. B. Gaur, and N. J. Doran, "Limits of broadband fiber optic parametric devices due to stimulated Brillouin scattering," *Optical Fiber Technology*, vol. 66, no., pp. 2–6, 2021. DOI: [10.1016/j.yofte.2021.102646](https://doi.org/10.1016/j.yofte.2021.102646)
- [27] K. Shiraki, M. Ohashi, and M. Tateda, "Suppression of stimulated Brillouin scattering in a fibre by changing the core radius," *Electronics Letters*, vol. 31, no. 8, pp. 668–669, 1995. DOI:[10.1049/el:19950418](https://doi.org/10.1049/el:19950418)
- [28] MJ. Li, X. Chen, J. Wang, S. Gray, A. Liu, J. A. Demeritt, A. B. Ruffin, A. M. Crowley, D.T. Walton, and L.A. Zenteno. "Al/Ge co-doped large mode area fiber with high SBS threshold." *Optics Express*, vol. 15, no. 13, pp.8290-8299, 2007. DOI:[10.1364/OE.15.008290](https://doi.org/10.1364/OE.15.008290)
- [29] M. Takahashi, M. Tadakuma, and T. Yagi, "Dispersion and Brillouin managed HNLFs by strain control techniques," *Journal of lightwave technology*, vol. 28, no. 1, pp. 59-64, 2010. DOI: [10.1109/JLT.2009.2035824](https://doi.org/10.1109/JLT.2009.2035824)
- [30] J. Hansryd, F. Dross, M. Westlund, P. A. Andrekson, and S. N. Knudsen, "Increase of the SBS threshold in a short highly nonlinear fiber by applying a temperature distribution," *Journal of lightwave technology*, 19, no. 11, pp. 1691, 2001. DOI: [10.1109/50.964069](https://doi.org/10.1109/50.964069)

- [31] Y. T. T. Okoshi, "Suppression of simulated Brillouin scattering using optical isolators," *Electronics Letters*, vol. 28, no. 12, pp. 1155–1157, 1992.
DOI: [10.1049/el:19920729](https://doi.org/10.1049/el:19920729)
- [32] X. Tian, X. Zhao, M. Wang, and Z. Wang, "Suppression of stimulated Brillouin scattering in optical fibers by tilted fiber Bragg gratings," *Optic Letters*, vol. 45, no. 17, pp. 4802, 2020, DOI:10.1364/ol.401433.
- [33] A. Mussot, A. Durecu-Legrand, E. Lantz, C. Simonneau, D. Bayart, H. Maillotte, and T. Sylvestre, "Impact of pump phase modulation on the gain of fiber optical parametric amplifier," *IEEE Photonics Technology Letters*, vol. 16, no. 5, pp.1289–1291, 2004. DOI: [10.1109/LPT.2004.826123](https://doi.org/10.1109/LPT.2004.826123)
- [34] A. Legrand, S. Lanne, C. Simonneau, D. Bayart, A. Mussot, T. Sylvestre, E. Lantz, and H. Maillotte, "System impact of pump phase modulation for fiber optical parametric amplifiers," In *Optical Fiber Communication Conference (OFC 2004)*, p. TuK2, 2004.
- [35] J. M. C. Boggio, A. Guimaraes, F. A. Callegari, J. D. Marconi, and H. L. Fragnito, "Q penalties due to pump phase modulation and pump RIN in fiber optic parametric amplifiers with non-uniform dispersion," *Optic Communications*, vol. 249, pp. 451–472, 2005. DOI: [10.1016/j.optcom.2005.01.056](https://doi.org/10.1016/j.optcom.2005.01.056)
- [36] M.F.C. Stephens, A. Redyuk, S. Sygletos, I. D. Phillips, P. Harper, K. J. Blow, and N. J. Doran, "The impact of pump phase-modulation and filtering on WDM signals in a fibre optical parametric amplifier," In *Optical Fiber Communication Conference (OFC 2015)*, pp. W2A-43, 2015. DOI: [10.1364/OFC.2015.W2A.43](https://doi.org/10.1364/OFC.2015.W2A.43)
- [37] M.E. Marhic, P.A. Andrekson, P. Petropoulos, S. Radic, C. Peucheret, M. Jazayerifar, "Fiber optical parametric amplifiers in optical communication systems," *Laser Photonics Review*, vol. 9, no. 1, pp.50–74, 2015, DOI:[10.1002/lpor.201400087](https://doi.org/10.1002/lpor.201400087).
- [38] J. M. C. Boggio, S. Moro, E. Myslivets, J. R. Windmiller, N. Alic, and S. Radic, "155-nm continuous-wave two-pump parametric amplification," *IEEE Photonics Technol. Letters*, vol. 21, no. 10, pp. 612–614, 2009.
DOI: [10.1109/LPT.2009.2015276](https://doi.org/10.1109/LPT.2009.2015276)
- [39] V. Gordienko, M. F. C. Stephens, A. E. El-Taher, and N. J. Doran, "Ultra-flat wideband single-pump Raman-enhanced parametric amplification," *Optics Express*, vol. 25, no. 5, pp. 4810–4818, 2017. DOI:[10.1364/OE.25.004810](https://doi.org/10.1364/OE.25.004810)

- [40] V. Gordienko, M. F. C. Stephens, and N. J. Doran, "Towards wide-bandwidth ultra-flat FOPAs," in *International Conference on Transparent Optical Networks (ICTON 2017)*, p. We.D5.1. DOI: [10.1109/ICTON.2017.8025079](https://doi.org/10.1109/ICTON.2017.8025079)
- [41] V. Gordienko, M. F. C. Stephens and N. J. Doran, "Raman-Generated Pump and Its Use for Parametric Amplification and Phase Conjugation," in *European Conference on Optical Communication (ECOC 2018)*, pp. 1-3, DOI: [10.1109/ECOC.2018.8535241](https://doi.org/10.1109/ECOC.2018.8535241)
- [42] T. Torounidis, H. Sunnerud, P. O. Hedekvist, and P. A. Andrekson, "Amplification of WDM signals in fiber-based optical parametric amplifiers," *IEEE Photonics Technology Letters*, vol. 15, no. 8, pp. 1061-1063, 2003. DOI: [10.1109/LPT.2003.815334](https://doi.org/10.1109/LPT.2003.815334)
- [43] J.M.C. Boggio, E. A. M. Fagotto, M. E. Marhic, F. A. Callegari, and H. L. Fragnito, "Amplification of 12×10 Gb/s WDM signals with negligible FWM crosstalk in a double-pumped fiber optical parametric amplifier," *Optics communications*, vol. 280, no. 2, pp.468-471. 2007. DOI:[10.1016/j.optcom.2007.08.033](https://doi.org/10.1016/j.optcom.2007.08.033)
- [44] M. F. C. Stephens, V. Gordienko, and N. J. Doran, "20 dB net-gain polarization-insensitive fiber optical parametric amplifier with >2 THz bandwidth," *Optic Express*, vol. 25, no. 9, pp. 10597-10609, 2017. DOI:[10.1364/OE.25.010597](https://doi.org/10.1364/OE.25.010597)
- [45] A. Supe, K. Zakis, L. Gegere, D. Redka, J. Porins, S. Spolitis, and V. Bobrovs, "Raman assisted fiber optical parametric amplifier for S-band multichannel transmission system," *Fibers*, vol. 9, no. 2, pp. 9, 2021. DOI:[10.3390/fib9020009](https://doi.org/10.3390/fib9020009)
- [46] C.B. Gaur, V. Gordienko, P. Hazarika, and N. J. Doran, "Polarization insensitive fiber optic parametric amplifier with a gain bandwidth of 22 nm in S-band," In *Optical Fiber Communication Conference (OFC 2022)*, pp. W4J-1, 2022. DOI: [10.1364/OFC.2022.W4J.1](https://doi.org/10.1364/OFC.2022.W4J.1)
- [47] H. Hu, R. M. Jopson, A. H. Gnauck, M. Dinu, S. Chandrasekhar, Chongjin Xie, and Sebastian Randel, "Parametric Amplification, Wavelength Conversion, and Phase Conjugation of a 2.048-Tbit/s WDM PDM 16-QAM Signal," *Journal Lightwave Technology*, vol. 33, pp. 1286-1291. 2015
- [48] V. Gordienko, C. B. Gaur, F. Bessin, A. D. Ellis, and N.J. Doran, "Automated Polarization-Insensitive C & L Band Fiber Optical Parametric Amplifier for Bidirectional Long-Reach Access Networks," *Journal of Lightwave Technology*, 2024. DOI: [10.1109/JLT.2024.3434580](https://doi.org/10.1109/JLT.2024.3434580).

- [49] C. B. Gaur, V. Gordienko, F. Ferreira, V. Ribeiro, and N. J. Doran, "Fibre optic parametric amplifier for high capacity burst-mode access networks," *Optics Express*, vol. 29, no. 14, pp. 21190-21198, 2021. DOI: [10.1364/OE.422990](https://doi.org/10.1364/OE.422990)
- [50] P.A. Andrekson and M. Karlsson, "Fiber-based phase-sensitive optical amplifiers and their applications," *Advances in Optics and Photonics*, vol. 1, no. 2, pp. 367-428, 2020 DOI:[10.1364/AOP.382548](https://doi.org/10.1364/AOP.382548)
- [51] R. Kakarla, J. Schröder, and P. A. Andrekson, "One photon-per-bit receiver using near-noiseless phase-sensitive amplification," *Light: science & applications*, vol. 9, no. 1, pp. 153, 2020.
- [52] S.L. Olsson, H. Eliasson, E. Astra, M. Karlsson, and P. A. Andrekson, "Long-haul optical transmission link using low-noise phase-sensitive amplifiers," *Nature communications*, vol. 9, no. 1, pp. 2513, 2018. DOI:[10.1038/s41467-018-04956-5](https://doi.org/10.1038/s41467-018-04956-5)
- [53] A. D. Ellis, M. E. McCarthy, M. A. Z. Al Khateeb, M. Sorokina, and N. J. Doran, "Performance limits in optical communications due to fiber nonlinearity," *Advances in Optics and Photonics*, vol. 9, no. 3, pp 429-503, 2017. DOI:[10.1364/AOP.9.000429](https://doi.org/10.1364/AOP.9.000429)
- [54] V. Gordienko, F. Ferreira, J. R. Lamb, A. Szabo, and N. Doran, "Phase-sensitive amplification of 11 WDM channels across bandwidth of 8 nm in a fibre optic parametric amplifier," in *European Conference Optical Communication. (ECOC 2020)*, pp. 2–5, 2020. DOI: [10.1109/ECOC48923.2020.9333194](https://doi.org/10.1109/ECOC48923.2020.9333194).
- [55] Z. Lali-Dastjerdi, O. Ozolins, Y.A., V. Cristofori, F. Da Ros, N. Kang, H. Hu et al, "Demonstration of cascaded in-line single-pump fiber optical parametric amplifiers in recirculating loop transmission," In *European Conference on Optical Communication (ECOC2012)*, pp. Mo-2, 2012. DOI:[10.1364/ECEOC.2012.Mo.2.C.5](https://doi.org/10.1364/ECEOC.2012.Mo.2.C.5)
- [56] M. F. C Stephens, M. Tan, V. Gordienko, P. Harper, and N. J. Doran, "In-line and cascaded DWDM transmission using a 15dB net-gain polarisation-insensitive fiber optical parametric amplifier," *Optics express*, vol. 25, no. 20, pp.24312-24325, 2017. DOI:[10.1364/OE.25.024312](https://doi.org/10.1364/OE.25.024312)
- [57] J.B. Coles, B.P.P. Kuo, N. Alic, S. Moro, C.S. Bres, J.M.C. Boggio, P.A. Andrekson, M. Karlsson, "Bandwidth-efficient phase modulation techniques for Stimulated Brillouin Scattering suppression in fiber optic parametric amplifiers," *Optic Express*, vol. 18, no. 17, p. 18138, 2010. DOI:[10.1364/OE.18.018138](https://doi.org/10.1364/OE.18.018138)
- [58] L. H. Nguyen, S. Boscolo, and S. Sygletos, "Online digital compensation of pump dithering induced phase and amplitude distortions in transmission links with

- cascaded fiber-optical parametric amplifiers," *Optics Express*, vol. 32, pp. 13467-13477, 2024. DOI:[10.1364/OE.516840](https://doi.org/10.1364/OE.516840)
- [59] A. Sobhanan, V. Gordienko, C. B. Gaur, and A. Ellis, "All-optical any-to-any wavelength conversion across 36nm range," In *European Conference on Optical Communication (ECOC)*, pp. 1-4, 2022.
- [60] H.N. Tan, T. Inoue, K. Solis-Trapala, S. Petit, Y. Oikawa, K. Ota, S. Takasaka, T. Yagi, M. Pelusi, and S. Namiki, "On the cascability of all-optical wavelength converter for high-order QAM formats," *Journal of Lightwave Technology*, vol. 34, no. 13, pp. 3194-3205, 2016. DOI: [10.1109/JLT.2016.2545246](https://doi.org/10.1109/JLT.2016.2545246)
- [61] V. Gordienko, S. Boscolo, M. Bastamova, A. D. Ellis, and N. J. Doran, "Record bandwidth waveband-shift-free optical phase conjugation in nonlinear fiber optical loop mirror," *Optics Express*, vol. 32, no. 16, pp. 27894-27905. 2024. DOI:[10.1364/OE.527800](https://doi.org/10.1364/OE.527800)
- [62] I. Sackey, C. Schmidt-Langhorst, R. Elschner, T. Kato, T. Tanimura, S. Watanabe, T. Hoshida, and C. Schubert, "Waveband-Shift-Free Optical Phase Conjugator for Spectrally Efficient Fiber Nonlinearity Mitigation," *Journal of Lightwave Technology*, vol. 36, no. 6, pp. 1309-1317, 2018. DOI: [10.1109/JLT.2018.2790799](https://doi.org/10.1109/JLT.2018.2790799)
- [63] M. E. Marhic, "Nonlinear crosstalk in fiber OPAs", in *Fiber Optical Parametric Amplifiers, Oscillators and Related Devices*, New York: Cambridge University Press, 2008, pp. 281–302.
- [64] K. K. Y. Wong, M. E. Marhic, K. Uesaka and L. G. Kazovsky, "Polarization-independent two-pump fiber optical parametric amplifier," *IEEE Photonics Technology Letters*, vol. 14, no. 7, pp. 911-913, 2002, DOI: [10.1109/LPT.2002.1012382](https://doi.org/10.1109/LPT.2002.1012382).
- [65] K. K. Y. Wong, M. E. Marhic, K. Uesaka and L. G. Kazovsky, "Polarization-independent one-pump fiber optical parametric amplifier," *IEEE Photonics Technology Letters*, vol. 14, no. 11, pp. 1506-1508, 2002, DOI: [10.1109/LPT.2002.803372](https://doi.org/10.1109/LPT.2002.803372)
- [66] S. Takasaka, and S. Ryuichi, "Polarization insensitive fiber optical parametric amplifier using a SBS suppressed diversity loop," In *Optical fiber communication conference (OFC 2016)*, pp. M3D-4., 2016. DOI:[10.1364/OFC.2016.M3D.4](https://doi.org/10.1364/OFC.2016.M3D.4)
- [67] V. Gordienko, F.M. Ferreira, C.B. Gaur, N.J. Doran, "Looped Polarisation-insensitive fiber optical Parametric amplifiers for broadband high gain applications,"

Journal of Lightwave Technology, vol. 39, no.19, pp. 6045–6053, 2021.

DOI: [10.1109/JLT.2021.3099441](https://doi.org/10.1109/JLT.2021.3099441)

- [68] F. Bessin, V. Gordienko, F. M. Ferreira, and Nick Doran, "First experimental Mach-Zehnder FOPA for polarization-and wavelength-division-multiplexed signals," in *European Conference on Optical Communication (ECOC 2021)*, pp. 1-3, 2021.

DOI: [10.1109/ECOC52684.2021.9605811](https://doi.org/10.1109/ECOC52684.2021.9605811)

- [69] F. Bessin, V. Gordienko, F. M. Ferreira, and N. J. Doran, "Demonstration of a stable, high-performance Mach-Zehnder Polarization-Insensitive Fiber Optical Parametric Amplifier," in *Optical Fiber Communications Conference (OFC2024)*, pM1B1, 2024. DOI:[10.1364/OFC.2024.M1B.1](https://doi.org/10.1364/OFC.2024.M1B.1)

DOI: [10.1364/OFC.2024.M1B.1](https://doi.org/10.1364/OFC.2024.M1B.1)

- [70] V. Gordienko, M. A. Z. Al-Khateeb, F. M. Ferreira, A. D. Ellis, and N. J. Doran, "Unwanted four-wave mixing in fibre optical parametric amplifiers," In *International Conference on Transparent Optical Networks (ICTON 2019)*, pp. 1-4, 2019. DOI: [10.1109/ICTON.2019.8840198](https://doi.org/10.1109/ICTON.2019.8840198)

DOI: [10.1109/ICTON.2019.8840198](https://doi.org/10.1109/ICTON.2019.8840198)

- [71] M. Jamshidifar, A. Vedadi and M. E. Marhic, "Reduction of Four-Wave-Mixing Crosstalk in a Short Fiber-Optical Parametric Amplifier," *IEEE Photonics Technology Letters*, vol. 21, no. 17, pp. 1244-1246, 2009.

DOI: [10.1109/LPT.2009.2025051](https://doi.org/10.1109/LPT.2009.2025051)

- [72] M.F.C. Stephens, V. Gordienko, and N. J. Doran, "Reduced crosstalk, polarization insensitive fiber optical parametric amplifier (PI FOPA) for WDM applications," In *Optical Fiber Communication Conference (OFC 2018)*, pp. W3D-4, 2018.

DOI: [10.1364/OFC.2018.W3D.4](https://doi.org/10.1364/OFC.2018.W3D.4)

- [73] V. Gordienko, F. M. Ferreira, V. Ribeiro, and N. Doran, "Suppression of nonlinear crosstalk in a polarization insensitive FOPA by mid-stage idler removal," In *Optical Fiber Communications Conference (OFC 2019)*, pp. 1-3, , 2019.

- [74] X. Guo, C. Shu, "Investigation of Raman-Assisted Crosstalk Reduction in Multi-Wavelength Fiber Optical Parametric Amplification," *Journal of Lightwave Technology*, vol. 33, no. 23, pp. 4746-4751, 2015, DOI: [10.1109/JLT.2015.2480858](https://doi.org/10.1109/JLT.2015.2480858).

DOI: [10.1109/JLT.2015.2480858](https://doi.org/10.1109/JLT.2015.2480858)

- [75] A. Redyuk, M.F.C. Stephens, and N.J. Doran, "Suppression of WDM four-wave mixing crosstalk in fibre optic parametric amplifier using Raman-assisted pumping," *Optic Express*, vol. 23, no. 21, pp. 27240-27249, 2015. DOI: [10.1364/OE.23.027240](https://doi.org/10.1364/OE.23.027240)

DOI: [10.1364/OE.23.027240](https://doi.org/10.1364/OE.23.027240)

- [76] A. Kobaykov, M. Sauer, and D. Chowdhury. "Stimulated Brillouin scattering in optical fibers," *Advances in optics and photonics*, vol. 2, no. 1, pp. 1-59, 2010.

DOI: [10.1364/AOP.2.000001](https://doi.org/10.1364/AOP.2.000001)

- [77] D. Cotter, "Stimulated Brillouin Scattering in Monomode Optical Fiber," *Journal of Optical Communications*, vol. 4, no.1, pp. 10 - 19, 1983.
DOI:[10.1515/JOC.1983.4.1.10](https://doi.org/10.1515/JOC.1983.4.1.10)
- [78] E. P. Ippen and R. H. Stolen, "Stimulated Brillouin scattering in optical fibers," *Apply Physic Letters.*, vol. 21, no. 11, pp. 539–541, 1972, DOI:[10.1063/1.1654249](https://doi.org/10.1063/1.1654249).
- [79] Y. Aoki, T. Kazuhito, and M. Ikuo, "Input power limits of single-mode optical fibers due to stimulated Brillouin scattering in optical communication systems," *Journal of Lightwave Technology*, vol. 6, no. 5, pp. 710-719, 1988. DOI: [10.1109/50.4057](https://doi.org/10.1109/50.4057)
- [80] M. Deroh, J.-C. Beugnot, K. Hammani, C. Finot, F. Julien Fatome, H.M. Smektala, T. Sylvestre, B. Kibler, "Comparative analysis of stimulated Brillouin scattering at 2 μ m in various infrared glass-based optical fibers," *J. Opt. Soc. Am. B*, vol. 37, no. 12, pp.3792–3800, 2020. DOI:[10.1364/JOSAB.401252](https://doi.org/10.1364/JOSAB.401252).
- [81] M. Horowitz, A.R. Chraplyvy, R.W. Tkach, J.L. Zyskind, Broad-band transmitted intensity noise induced by Stokes and anti-Stokes Brillouin scattering in singlemode fibers, *IEEE Photonics Technology Letters*, vol.9, no. 1, pp. 124–126, 1997.
DOI: [10.1109/68.554530](https://doi.org/10.1109/68.554530)
- [82] J. Zhang, M. R. Phillips, "Modeling intensity noise caused by stimulated Brillouin scattering in optical fibers," in *Conference on Lasers and Electro-Optics (CLEO 2005)*, p. CMH6. DOI: [10.1109/CLEO.2005.201703](https://doi.org/10.1109/CLEO.2005.201703)
- [83] R.G. Smith, "Optical power handling capacity of low loss optical fibers as determined by stimulated Raman and Brillouin scattering," *Applied optics*, vol.11, no. 11, pp. 2489-2494, 1972. DOI:[10.1364/AO.11.002489](https://doi.org/10.1364/AO.11.002489)
- [84] D. A. Fishman and J. A. Nagel, "Degradations due to stimulated Brillouin scattering in multigigabit intensity-modulated fiber-optic systems," *Journal of Lightwave Technology*, vol. 11, no. 11, pp. 1721–1728, 1993. DOI: [10.1109/50.251167](https://doi.org/10.1109/50.251167)
- [85] P. Narum, A. L. Gaeta, M. D. Skeldon, and R. W. Boyd, "Instabilities of laser beams counterpropagating through a Brillouin-active medium," *J. Opt. Soc. Am. B*, vol. 5, no. 3, pp. 623–628, 1988. DOI:[10.1364/JOSAB.5.000623](https://doi.org/10.1364/JOSAB.5.000623)
- [86] K. Tsujikawa, K. Nakajima, Y. Miyajima, and M. Ohashi, "New SBS suppression Fiber with uniform chromatic dispersion to enhance four-wave mixing," *IEEE Photonics Technology Letters*, vol. 10, no. 8, pp. 1139–1141, 1998.
DOI: [10.1109/68.701528](https://doi.org/10.1109/68.701528)

- [87] M. Ohashi, and M. Tateda, "Design of strain-free-fiber with nonuniform dopant concentration for stimulated Brillouin scattering suppression," *Journal of Lightwave Technology*, vol. 11, no. 12, pp. 1941-1945, 1993. DOI: [10.1109/50.257954](https://doi.org/10.1109/50.257954)
- [88] L. Grüner-Nielsen, S. Dasgupta, M. D. Mermelstein, D. Jakobsen, S. Herstrøm, M. EV Pedersen, E. L. Lim et al, "A silica based highly nonlinear fibre with improved threshold for stimulated Brillouin scattering," in *European Conference on Optical Communication (ECOC 2010)*, pp. Tu 4D3. DOI: [10.1109/ECOC.2010.5621232](https://doi.org/10.1109/ECOC.2010.5621232)
- [89] J. Ballato and P. Dragic, "Materials approaches to mitigating parasitic effects in optical networks: Towards the perfect optical fiber," in *18th International Conference on Transparent Optical Networks (ICTON)*, pp. 1-4, 2016. DOI: [10.1109/ICTON.2016.7550711](https://doi.org/10.1109/ICTON.2016.7550711)
- [90] M. Tuggle, C. Kucera, T. Hawkins, D. Sligh, A. F. J. Runge, A. C. Peacock, P. Dragic, and J. Ballato, "Highly nonlinear yttrium-aluminosilicate optical fiber with a high intrinsic stimulated Brillouin scattering threshold," *Optics Letters*, vol. 42, no. 23, pp. 4849-4852, 2017. DOI: [10.1364/OL.42.004849](https://doi.org/10.1364/OL.42.004849)
- [91] R. Slavík, F. Parmigiani, J. Kakande, et al., "All-optical phase and amplitude regenerator for next-generation telecommunications systems," *Nature Photonics*, vol. 4, pp. 690–695, 2010. DOI: [10.1038/nphoton.2010.203](https://doi.org/10.1038/nphoton.2010.203)
- [92] N. Yoshizawa, and T. Imai, "Stimulated Brillouin scattering suppression by means of applying strain distribution to fiber with cabling," *Journal of Lightwave Technology*, vol. 11, no. 10, pp. 1518-1522, 1993. DOI: [10.1109/50.249889](https://doi.org/10.1109/50.249889)
- [93] J. M. Chavez Boggio, J. D. Marconi, and H. L. Fragnito, "Experimental and numerical investigation of the SBS-threshold increase in an optical fiber by applying strain distributions," *Journal of Lightwave Technology*, vol. 23, no. 11, pp. 3808–3814, 2005, DOI: [10.1109/JLT.2005.856226](https://doi.org/10.1109/JLT.2005.856226).
- [94] R. Engelbrecht, "Analysis of SBS gain shaping and threshold increase by arbitrary strain distributions," *Journal of Lightwave Technology*, vol. 32, no. 9, pp. 1689-1700, 2014.
- [95] E. Myslivets, C. Lundstrom, J. M. Aparicio, S. Moro, A. OJ Wiberg, C.S. Bres, N. Alic, P. A. Andrekson, and S. Radic, "Spatial equalization of zero-dispersion wavelength profiles in nonlinear fibers," *IEEE Photonics Technology Letters*, vol. 21, no. 24, pp. 1807-1809, 2009. DOI: [10.1109/LPT.2009.2033462](https://doi.org/10.1109/LPT.2009.2033462)
- [96] C. Lundström, E. Myslivets, A. O. Wiberg, N. Alic, S. Radic, M. Karlsson, and P. A. Andrekson, "Tension-optimized highly nonlinear fiber for parametric applications,"

- In *European Conference on Optical Communication, (ECOC 2012)*, pp. We1F2, 2012. DOI: [10.1364/ECEOC.2012.We.1.F.2](https://doi.org/10.1364/ECEOC.2012.We.1.F.2)
- [97] C. Guo, M. Vasilyev, Y. Akasaka, P. Palacharla, S. Takasaka, and R. Sugizaki, "Temperature-tuned two-segment highly-nonlinear fiber with increased stimulated Brillouin scattering threshold," In *Optical Fiber Communications Conference (OFC2023)*, pp. 1-3, 2023. DOI: [10.1364/OFC.2023.Th1B.2](https://doi.org/10.1364/OFC.2023.Th1B.2)
- [98] H. Rabbani, C. Guo, and M. Vasilyev, "Positive (> 0 dB) Wavelength Conversion Efficiency in Temperature-Tuned Five-Segment Highly-Nonlinear Fiber Without Pump Dithering," In *Optical Fiber Communication Conference (OFC 2024)*, pp. M1B-5, 2024. DOI: [10.1364/OFC.2024.M1B.5](https://doi.org/10.1364/OFC.2024.M1B.5)
- [99] C. Lundstrom, R. Malik, L. Gruner-Nielsen, B. Corcoran, S. LI Olsson, M. Karlsson, and P. A. Andrekson, "Fiber optic parametric amplifier with 10-dB net gain without pump dithering," *IEEE Photonics Technology Letters*, vol. 25, no. 3, pp.234-237. 2012. DOI: [10.1109/LPT.2012.2230160](https://doi.org/10.1109/LPT.2012.2230160)
- [100] S. Olsson, H. Eliasson, E. Astra, M. Karlsson, and P. A. Andrekson, "Long-haul optical transmission link using low-noise phase-sensitive amplifiers", *Nature communications*, vol. 9, no. 1, pp.2513, 2018. DOI: [10.1038/s41467-018-04956-5](https://doi.org/10.1038/s41467-018-04956-5)
- [101] M. Mccarthy, S. Fabbri, and A. Ellis, "Signal Processing Using Opto-Electronic Devices," In *All-Optical Signal Processing: Data Communication and Storage Applications*, pp. 291-323. 2015.
- [102] J. Coles. Advanced phase modulation techniques for stimulated Brillouin scattering suppression in fiber optic parametric amplifiers. University of California, San Diego, 2009.
- [103] K. K.Y. Wong, K. Shimizu, K. Uesaka, G. Kalogerakis, M. E. Marhic, and L. G. Kazovsky, "Continuous-wave fiber optical parametric amplifier with 60-dB gain using a novel two-segment design," *IEEE Photonics Technology Letters*, vol. 15, no. 12, pp. 1707-1709, 2003. DOI: [10.1109/LPT.2003.819706](https://doi.org/10.1109/LPT.2003.819706)
- [104] C. Zeringue, I. Dajani, S. Naderi, G. T. Moore, and C. Robin, "A theoretical study of transient stimulated Brillouin scattering in optical fibers seeded with phase-modulated light," *Optic Express*, vol. 20, no. 19, pp. 21196, 2012. DOI: [10.1364/OE.20.021196](https://doi.org/10.1364/OE.20.021196)
- [105] A. Mussot, M. Le Parquier, and P. Szriftgiser, "Thermal noise for SBS suppression in fiber optical parametric amplifiers," *Optic Communications*, vol. 283, no. 12, pp. 2607–2610, 2010, DOI: [10.1016/j.optcom.2010.02.007](https://doi.org/10.1016/j.optcom.2010.02.007).

- [106] M. Lorenzen, D. Noordegraaf, C.V. Nielsen, O. Odgaard, L. Grüner-Nielsen, and K. Rottwitt, "Brillouin suppression in a fiber optical parametric amplifier by combining temperature distribution and phase modulation", In *Optical Fiber Communication Conference (OFC 2008)*, p. OML1, 2008.
- [107] A. Vedadi, A. Mussot, E. Lantz, H. Maillotte, and T. Sylvestre, "Theoretical study of gain distortions in dual-pump fiber optical parametric amplifiers," *Optics communications*, vol. 267, no. 1, pp. 244-252, 2006.
DOI:[10.1016/j.optcom.2006.05.074](https://doi.org/10.1016/j.optcom.2006.05.074)
- [108] M. Bastamova, V. Gordienko, N. J. Doran, and A. D. Ellis, "Impact of pump phase modulation on QAM signals in polarization-insensitive fiber optical parametric amplifiers," *Optical Fiber Technology*, vol. 84, pp.103758, 2024.
DOI:[10.1016/j.yofte.2024.103758](https://doi.org/10.1016/j.yofte.2024.103758)
- [109] J.R. Barry, E. A. Lee, *Digital communication*. Springer Science & Business Media, 2012.
- [110] B. Koch, R. No'e, D. Sandel, V. Mirvoda, "Versatile endless optical polarization controller/tracker/demultiplexer", *Optic Express*, vol. 22, no.7, pp.8259–8276, 2014.
DOI:[10.1364/OE.22.008259](https://doi.org/10.1364/OE.22.008259)
- [111] K. Sankar, "Symbol Error Rate (SER) for 16 QAM",
<https://dsplog.com/2007/12/09/symbol-error-rate-for-16-qam/>, accessed on 20 March 2022.
- [112] M. Bastamova, V. Gordienko, S.s Sygletos, T. Mingming, A. Donodin, L. Nguyen, F. Bessin, S. Boscolo, N. J. Doran, and A. D. Ellis, "Performance evaluation of a polarisation insensitive Mach-Zehnder fiber parametric amplifier with 38 channel transmission," In *European Conference on Optical Communication (ECOC 2024)*, pp. W2A.1, 2024.
- [113] IDPhotonics, *CoBrite DX1 Tunable Laser datasheet*. [Online]. Available: <https://id-photonics.com/products-solutions/cobrite-tunable-laser/cobrite-dx1/>. Accessed: Sep. 6, 2024.